Dissertation
submitted to the
Combined Faculties for the Natural Sciences and for Mathematics
of the Ruperto-Carola University of Heidelberg, Germany
for the degree of
Doctor of Natural Sciences

presented by
Diplom-Physiker Mario Verschl
born in Schwäbisch Gmünd

Oral examination: July 18, 2007

Dispersion in laser-driven relativistic quantum systems

Referees: **Prof. Dr. C. H. Keitel**
Prof. Dr. O. Nachtmann

Abstract

The wave packet dynamics of electrons driven by strong laser fields is examined with the objective to both describe and manipulate the spreading dynamics. Having established analytical methods based on either classical or quantum mechanics, the quantum approach is first applied to free, laser-driven electrons. Intuitive results are found for both the relativistic and the nonrelativistic regime beyond the dipole approximation. In order to generalize the concept of recollisions to relativistic energies where magnetic field effects are important, the electron dynamics in standing laser fields with linear and circular polarization are analyzed and compared. Furthermore, a novel scheme of two consecutive laser pulses is introduced, which allows for recollisions with the maximum electron energy accessible in propagating laser fields. In this scheme, the Lorentz drift is employed both to separate electrons from atoms or molecules and to drive them back for recollisions. Aiming to increase the reaction probabilities of recollisions, two methods to inverse wave packet spreading are introduced. Both approaches, i.e. refocusing with a harmonic potential and magnetic refocusing, can be implemented in the scheme with two consecutive laser pulses to enable effective, relativistic recollisions.

Zusammenfassung

Es wird die Wellenpaketdynamik von Elektronen in starken Laserfeldern untersucht mit dem Ziel, das Zerfließen von Wellenpaketen sowohl zu beschreiben als auch zu beeinflussen. Nach der Einführung analytischer Methoden, die entweder auf der klassischen Mechanik oder der Quantenmechanik beruhen, wird die quantenmechanische Beschreibung zuerst auf freie, lasergetriebene Elektronen angewandt. Es werden einfach zu interpretierende Ergebnisse sowohl für den relativistischen Fall als auch für den nichtrelativistischen gefunden, der über die Dipolnäherung hinaus geht. Um das Konzept der Rekollisionen auf relativistische Energien zu erweitern, bei denen Magnetfeldseffekte nicht vernachlässigt werden können, wird die Dynamik der Elektronen in stehenden Feldern mit entweder linearer oder zirkularer Polarisation analysiert und verglichen. Außerdem wird ein neues Modell mit zwei aufeinander folgenden Laserpulsen eingeführt, welches Rekollisionen mit der höchsten Energie ermöglicht, die Elektronen in einem propagierenden Laserfeld erreichen können. In diesem Modell wird die Driftbewegung ausgenutzt, um Elektronen von Atomen oder Molekülen zuerst zu separieren und dann zur Kollision zu bringen. Mit dem Ziel, die Reaktionswahrscheinlichkeit von Rekollisionen zu erhöhen, werden zwei Methoden vorgestellt, mit denen das Zerfließen von Wellenpaketen wieder rückgängig gemacht werden kann. Beide Methoden, die magnetische Refokussierung und die Refokussierung mit harmonischen Potentialen, können in das Rekollisionsmodell mit zwei Laserpulsen integriert werden, was effektive, relativistische Rekollisionen ermöglicht.

In connection with the present work, the following articles have been published in refereed journals:

- M. Verschl and C. H. Keitel,
  Analytical Approach to Wave-Packet Dynamics of Laser-Driven Particles beyond the Dipole Approximation
  Laser Physics **15**, 529 (2005)

- M. Verschl and C. H. Keitel,
  Relativistic classical and quantum dynamics in intense crossed laser beams of various polarizations
  Phys. Rev. ST AB **10**, 024001 (2007)

- M. Verschl and C. H. Keitel,
  Relativistic recollisions with two consecutive laser pulses
  J. Phys. B **40**, F69 (2007)

- M. Verschl and C. H. Keitel,
  Refocussed relativistic recollisions
  Europhys. Lett **77**, 64004 (2007)

Contents

Introduction

Since the first laser has been built in 1960, the achievable intensity of laser light has increased by many orders of magnitude up to $10^{22}\,\mathrm{W/cm^2}$ at present. Therefore, the interaction of laser light with matter comprises different regimes from linear to highly nonlinear optics, including the case of relativistic electron dynamics. Typical nonlinear effects in the nonrelativistic regime are the ionization of atoms via tunneling or multiphoton absorption, where possibly more photons are absorbed than necessary for ionization [*above threshold ionization* (ATI)]. For reviews of the physics of atoms in laser fields see [1, 2, 3, 4, 5, 6].

Many applications of laser-matter interactions are based on the important concept of recollisions. First, an atom or molecule is ionized by a laser field, then the electron is accelerated, and finally, when the laser phase has reversed, it is driven back to the core. The recolliding electron can, for instance, be scattered, further ionize the atom or molecule (*nonsequential double ionization* [7, 8]) or it can give rise to the emission of radiation which is dominated by high harmonics of the laser frequency [*high harmonic generation* (HHG)]. In the process of HHG [1, 9], a small fraction of the bound wave packet tunnels out of the barrier which is formed by the superposition of the laser electric field and the binding Coulomb potential. Then, it gains energy in the laser field, and the superposition of the returning wave with the bound wave packet creates a radiating charge oscillation. As this process repeats every half laser period, the emitted light of odd high harmonics of the laser frequency interferes constructively and therefore produces a discrete spectrum. In this way, coherent radiation can be created with frequencies several hundred times higher than the laser frequency. The emission of radiation can also be considered as the energy which is released by the recombination of the electron with the atom or molecule. The maximum frequency of the emitted light is therefore given by the sum of the ionization energy plus the maximum kinetic energy which the electron can gain in the laser field from the instant of tunneling ionization to recollision. Besides employing this process for a coherent, ultraviolet light source [10, 11], the radiation offers various other applications. For example, the information on atomic orbitals or the nuclear distance of molecules are encoded in the radiation spectrum, which enables probing the nuclear dynamics of simple molecules [12, 13] (a different approach based on the analysis of recollisions is shown in [14]) or the tomographic imaging of molecular orbits [15]. Furthermore, the superposition of parts of the high-frequency spectrum can be employed to create attosecond pulses [16, 17, 18] which are much shorter than a single cycle of visible laser light. Thus, the time scale of atomic and molecular physics is reached, which is a major requirement for analyzing the dynamics of electronic processes such as chemical reactions.

The maximum energy of recollisions depends on the laser intensity. However, if the fields are too intense (i.e., more than about $10^{17}\,\mathrm{W/cm^2}$ for optical laser frequencies),

the motion of the electron becomes relativistic and recollisions are suppressed because of the laser magnetic field, which is perpendicular to the motion in the polarization direction and therefore exerts a force on the electron. The electron is then pushed in the laser propagation direction (*Lorentz drift*) and consequently returns with a certain distance to the core [3, 6]. As for this scheme, effective recollisions are limited to the nonrelativistic regime. For recollisions with relativistic energies, which allow for probing dynamics of nuclear processes [19], high-energetic γ-radiation or muon-antimuon pair creation [20], other recollision schemes are required.

Various methods have been proposed to circumvent the problem of the Lorentz drift. To some extent, additional electric fields pointing in the laser propagation direction can be applied to cancel the drift [21]. Another option is to preaccelerate the ions such that the laser light is Doppler-shifted to higher frequencies in the accelerated system [22, 23]. Consequently, the laser periods are shorter and thus the drifting time of the electrons is reduced. Furthermore, working with antisymmetric molecular states has been proposed [24]. In this case, parts of the wave packet possess an initial momentum after the ionization which partly cancels the Lorentz drift. If positronium is employed for recollisions, both the electron and the positron are subject to the same drift such that recollisions can occur [25, 26]. Another method is to employ counterpropagating waves to eliminate the Lorentz drift [19, 27, 28, 29]. Finally, the drift can be minimized if the laser pulse is tailored in such a way that ionization and recollision are initiated by short and intense peaks with vanishing electromagnetic fields in between [30].

Today, laser intensities are available which can accelerate electrons to highly relativistic energies [31, 32]. The interaction of such intense laser pulses with solid targets creates plasmas in which other effects such as electron-positron pair creation, electrostimulated nuclear fission, or nuclear excitation by means of electron impact can occur [33, 34, 35, 36, 37, 38, 39]. As opposed to controlled recollisions, those are random processes in plasmas which are not suitable to drive coherent processes. In the relativistic regime, the electronic motion in the laser fields is dominated by the drift in the laser propagation direction. This effect can be employed to create strong electric fields. For example, an intense laser pulse penetrating a thin foil separates electrons from the heavier ions and thus creates an electric field which can be employed for the acceleration of ions [40, 41, 42, 43] [*target normal sheath acceleration* (TNSA)]. A further possible process is the production of energetic electrons by means of *wakefield acceleration* [44, 45] in gases in which the separation of electrons and ions creates a plasma wave which can efficiently accelerate electrons. The generation of monoenergetic electron beams of up to 1 GeV based on wakefield acceleration has been demonstrated [46, 47]. Compared to conventional accelerators, the advantage of particle acceleration by means of laser beams is the compact dimensions of the facilities often fitting in usual laboratories. Further applications of high-energetic laser pulses are the nuclear fusion from explosions of laser-heated deuterium clusters [48] and the direct interaction of intense laser fields with nuclei [49].

In order to create such intense laser pulses, the light has to be focused on a small spot and the pulse length needs to be short. The limits for the size of the focus and the pulse length are both given by the wave length of the laser. Presently, the shortest pulses are a few cycles long (see e.g. [50, 51]). The amplification of short pulses to high energies in a laser medium has been enabled with the implementation of *chirped pulse amplification* (CPA) [31, 39, 52, 53] where the pulses are first stretched by dispersive systems to reduce the intensity significantly in order to avoid damaging of the laser

medium. After the amplification, the pulse is compressed again by another dispersive system. With this method, intensities of $10^{22}\,\mathrm{W/cm^2}$ have been achieved [32]. A large-scale implementation of CPA may even allow to raise intensities up to $10^{28}\,\mathrm{W/cm^2}$ in the future [54].

A different concept to achieve higher laser intensities is to employ high-order harmonics which are efficiently created by irradiating a solid surface with intense laser pulses [55]. If the radiation is focused, extremely short pulses with intensities of $10^{29}\,\mathrm{W/cm^2}$ might be obtained [18, 56], which is close to the Schwinger limit of $2.3 \times 10^{29}\,\mathrm{W/cm^2}$ where spontaneous electron-positron pair creation is expected.

This thesis—*Dispersion in laser-driven relativistic quantum systems*—deals with the wave packet dynamics of laser-driven electrons, mainly in the relativistic regime. Analytical methods are developed to describe the spreading dynamics of wave packets. As opposed to previous numerical approaches, these allow for intuitive understanding of relativistic wave packet dynamics over a vast range of parameters. First, one of the formalisms is employed to construct analytical solutions of electrons driven by a propagating laser field, where effects of the laser magnetic field and relativity are recovered and described quantitatively. The methods are then applied to compare two standing wave configurations allowing for recollisions in the relativistic regime. By means of analytical results, effects are identified which give rise to different behaviors of electrons in the two configurations. Thus, it is seen which configuration is more favorable for an implementation of recollisions. For other problems where analytical solutions are not available, a fast numerical approach is at hand for the description of wave packet dynamics.

Furthermore, a novel relativistic scheme is introduced implying the new feature that recollisions can be enforced at the highest electron energy achievable in propagating laser fields. For example, collision energies in standing laser fields scale differently with the laser intensity and therefore yield lower energies in the relativistic regime.

A general problem of recollisions is the dispersion of wave packets since spreading reduces the reaction probabilities. Here, two methods are developed which can be employed to reverse spreading, i.e., electron wave packets can thus be refocused to their initial width. These ideas are then incorporated into the new recollision scheme to combine refocusing with energetic recollisions. In this way, new schemes allowing for effective relativistic recollisions are established.

The methods of describing wave packets include an analytical implementation of *phase-space averaging* which is a classical Monte-Carlo method based on the uncertainty of the initial conditions of the particle. Since the dynamics is deduced from classical equations of motion, this method allows for an intuitive understanding of (relativistic) wave packet dynamics, especially due to the analytical implementation. This formalism of describing wave packets can as well be employed for a fast numerical implementation. The second, fully quantum mechanical approach considered here can be applied to a certain class of solutions of wave equations such as the quantum mechanical states describing free, laser-driven particles (*Volkov states*). Both methods are described in detail in Chapter 1.

In Chapter 2, the quantum mechanical approach is applied to construct wave packets of free electrons driven by intense laser fields. Different regimes are considered where magnetic fields and relativistic effects are important. This problem has been addressed previously by numerically solving the Dirac equation [57, 58, 59, 60, 61, 62], the Schrödinger equation beyond the dipole approximation (see e.g. [63, 64]) or by su-

perimposing a set of Volkov-states on a computer [65, 66]. However, there is no detailed understanding of the occurring spreading and deformation dynamics of wave packets, as computers are needed to evaluate the final results. In this thesis, analytical solutions for the charge density are established and interpreted. One calculation is carried out for the nonrelativistic regime beyond the dipole approximation in order to include magnetic field effects (see also [67]). The second calculation concerns the relativistic regime where effects like Lorentz contraction and time dilation are observed.

The dynamics of electrons in intense, crossed laser fields is examined in Chapter 3 (see also [68]). Two standing-wave configurations with different laser polarizations are compared which have in common that they possess axes on which electrons can oscillate without experiencing any Lorentz force. Due to this feature, these configurations are suitable for recollisions in the relativistic regime. For the case of linearly polarized, counterpropagating laser fields with equal polarization direction (see [27, 28, 29]), the standing wave has nodes where the magnetic field vanishes and the electric field amplitude is maximal. For circularly polarized standing waves, the magnetic field is antiparallel to the electric field [19], i.e., the Lorentz force vanishes if the electron oscillates in the direction of the electric field. This means that the magnetic fields are different for the two configurations which gives rise to different electron dynamics in the vicinity of the axes of vanishing Lorentz force, with consequences for the stability of the motion.

In Chapter 4, a novel recollision scheme for the relativistic regime is introduced (see also [69]). The displacement due to the Lorentz drift which is responsible for the suppression of recollisions in propagating laser fields is canceled by a second, time-delayed counterpropagating pulse. With suitable pulse shapes, recollisions can occur with maximal kinetic energy. As also shown in that chapter, the recollision energy scales differently with the laser intensity and can be much higher than in the discussed approaches with standing waves or positronium.

Spreading of the electron wave packet reduces the efficiency of recollisions in the model with two consecutive laser pulses. To address this general problem of spreading, two methods are presented in Chapter 5 showing that the spreading of free wave packets can be reversed. This can be achieved by applying a suitably strong and short magnetic field pulse. The wave packet then refocuses in the plane perpendicular to the magnetic field. The second method is the application of a harmonic potential for a certain time. It is shown that such a potential can be realized by means of the ponderomotive potential of a laser field run in the TEM01 mode. The electron is then shown to move in an effective parabolic potential. In this case, laser fields can be crossed to implement refocusing in all three spatial dimensions.

Finally, in Chapter 6, those ideas of refocusing wave packets are applied to the relativistic recollision scheme of Chapter 4. The pulses which initiate refocusing, i.e., either the magnetic field pulse or the harmonic potential, are inserted in between the two counterpropagating laser pulses. It is demonstrated that the wave packets refocus and reach minimal widths at the instant of recollision. Thus, effective recollisions can be achieved at highly relativistic energies (for magnetic refocusing see also [70]).

In Appendix A, the derivation of the analytical solutions for an electron driven by a plane laser field with otherwise arbitrary vector potential is reviewed, for both the classical and the quantum mechanical case. The electron trajectories are only slightly influenced by the electron spin [6, 71]. For the case the spin vector is parallel to the magnetic field direction of the laser field, there is no effect on the trajectory at all

[72]. For these reasons, spin effects are not considered here and quantum mechanical solutions for the problem of laser-driven particles are therefore derived from the Klein-Gordon equation for spinless particles.

All equations in this thesis are given in atomic units, i.e., Gaussian units are employed with Planck's constant $\hbar$, the electron mass m and the unit charge e equal to unity. This system of units is discussed in Appendix B, where also a table is given to restore constants and to convert results to SI units.

Chapter 1

Classical and quantum description of wave packets

The description of localized wave packets needed in the following chapters is based on two approaches. The first one—*phase-space averaging*—is a classical method where spreading is considered as a consequence of uncertain initial conditions of the particle.

Whereas this method has previously been implemented by numerical Monte-Carlo simulations [73, 74, 75, 76, 77, 78], here, an analytical approach is developed. An analytical integral expression for the probability density is established which often can be integrated for Gaussian distributions of the initial conditions if the classical equations of motion are known. Since this approach is based on the classical equations of motion, it is very intuitive, and it allows for insight into the wave packet dynamics in both the relativistic and the nonrelativistic regime.

In some cases, solutions of quantum mechanical wave equations are known which have to be superimposed to yield localized wave packets. For the common case where only the phase of the solution depends on the initial momentum and the modulus is constant, a Gaussian superposition can often be carried out analytically. As opposed to phase-space averaging, this is a fully quantum mechanical method.

In both approaches, it is employed that the dependence of the initial momentum can be expanded, which then allows for an analytical description. This simplification is justified if the width of the distribution of the initial velocity is small compared to the speed of light. The results of this chapter are the basis for determining the wave packet dynamics of the subsequent chapters.

1.1 Phase-space averaging

The method of phase-space averaging is a classical Monte-Carlo approach to describe wave packets. It has first been applied in the year 1978 to describe the ionization of Rydberg atoms by microwaves [79, 80]. From that time on, it has been employed successfully in describing various laser-atom processes [73, 74, 75]. The approach has also been applied in the relativistic regime [76, 77, 78].

The basic idea is to represent the probability distribution of a particle by an ensemble of particles which move on classical trajectories, whereas the initial conditions are varied. The probability to find the particle in a certain volume can then be determined from the number of classical particles found in this volume.

This classical approach requires much less computational power than numerically solving wave equations on grids. Numerical codes are available to solve the time-dependent Schrödinger equation (see e.g. [63, 64]) for nonrelativistic and the Dirac equation for relativistic problems [57, 58, 59, 60, 61, 62]. In the relativistic regime, high electron energies require extremely small spacing in the time domain. Limited computing power therefore restricts the range of parameters. So far, energies have been limited to the lower MeV-regime and calculations have been restricted to one particle in two spatial dimensions. The solution of classical equations of motion required for phase-space averaging is less time consuming and it can be implemented for more general parameters.

Phase-space averaging cannot describe intrinsic quantum mechanical effects like tunneling or interferences, but it is suitable to describe spreading of wave packets because this can as well be understood in classical terms. For a classical particle, the probability density is a moving delta-peak if the initial conditions are known exactly. However, if the initial momentum is subject to an uncertainty, the location of the particle usually becomes more and more unclear, i.e., the probability distribution of its position spreads. According to Heisenberg's uncertainty principle there is always an uncertainty in momentum space for a localized initial state which consequently causes spreading.

1.1.1 Analytical implementation

Usually, this approach is implemented by propagating the ensemble of classical particles with different initial conditions numerically. Here, it is shown how this scheme can be implemented in a different way allowing for an analytical treatment if the classical equations of motion can be solved. This method can also be implemented if analytical solutions of the equations of motion are not available. In this case, they need to be solved numerically only for a small set of different initial conditions.

Probability density

The first step of a quantitative description consists in calculating the probability of a classical particle to propagate from the initial position to some other point at a certain time, where the initial momentum $\vec{p}_0$ is subject to a probability distribution $\tilde{\rho}(\vec{p}_0)$. The classical equations of motion need to be solved for the initial momentum $\vec{p}_0 = \vec{g}(\vec{x}, \vec{x}_0, t)$, i.e., $\vec{g}$ denotes the function which gives the initial momentum needed for the classical trajectory to run from the initial position $\vec{x}_0$ through the point $\vec{x}$ at time t. Now, the probability $\rho'(\vec{x}, \vec{x}_0, t)d^3x$ to find the particle at the point $\vec{x}$ within the volume element d^3x is equal to the probability that the required initial momentum $\vec{p}_0$ is within the volume element d^3p_0 of momentum space:

$$\rho'(\vec{x}, \vec{x}_0, t)\, d^3x = \tilde{\rho}(\vec{g}(\vec{x}, \vec{x}_0, t))\, d^3p_0\,. \tag{1.1}$$

The volume elements are related via the Jacobi determinant. The probability density is then given by

$$\rho'(\vec{x}, \vec{x}_0, t) = \tilde{\rho}(\vec{g}(\vec{x}, \vec{x}_0, t)) \left| \frac{\partial \vec{g}(\vec{x}, \vec{x}_0, t)}{\partial \vec{x}} \right|\,. \tag{1.2}$$

This expression still depends on the initial position which is subject to some probability distribution $\rho_0(\vec{x}_0)$. The next step is to sum up the probabilities ρ' for different

initial positions, i.e., the following weighted integral has to be carried out to yield the probability density of the particle:

$$\rho(\vec{x},t) = \iiint \rho'(\vec{x},\vec{x}_0,t)\rho_0(\vec{x}_0)\,d^3x_0 = \iiint \tilde{\rho}(\vec{g}(\vec{x},\vec{x}_0,t))\left|\frac{\partial\vec{g}(\vec{x},\vec{x}_0,t)}{\partial\vec{x}}\right|\rho_0(\vec{x}_0)\,d^3x_0\,. \tag{1.3}$$

Current density

In the same way, a term for the current density can be derived which is based on classical trajectories. First, consider the initial position of the particle to be fixed. The current density $\vec{j}'(\vec{x},\vec{x}_0,t)$ is then given by the product of the probability density $\rho'(\vec{x},\vec{x}_0,t)$ and the velocity $\vec{v}(\vec{x},\vec{x}_0,t)$ at which the particle travels if it is found at the position $\vec{x}$ at time t, because the current is given by the probability per unit time that the particle flows through the surface perpendicular to its velocity. The velocity at some point $\vec{x}$ at the instant t is not unique, because it depends on the initial position $\vec{x}_0$ of the particle as well. The current density $\vec{j}'(\vec{x},\vec{x}_0,t)$ therefore needs to be summed over the different initial positions according to the initial probability density ρ_0 in order to obtain the current density $\vec{j}(\vec{x},t)$:

$$\vec{j}(\vec{x},t) = \iiint \vec{j}'(\vec{x},\vec{x}_0,t)\rho_0(\vec{x}_0)\,d^3x_0 = \iiint \rho'(\vec{x},\vec{x}_0,t)\vec{v}(\vec{x},\vec{x}_0,t)\rho_0(\vec{x}_0)\,d^3x_0\,. \tag{1.4}$$

Generally, the velocity depends on the initial momentum which is determined by the classical trajectories via $\vec{p}_0 = \vec{g}(\vec{x},\vec{x}_0,t)$, but in the relativistic case, this dependence usually becomes very weak. This is seen if the absolute value of the velocity v is expressed by the relativistic γ-factor according to

$$\gamma = \frac{1}{\sqrt{1-\frac{v^2}{c^2}}} \quad\Leftrightarrow\quad v = c\sqrt{1-\gamma^{-2}}\,, \tag{1.5}$$

where c is the speed of light. The relative variation of the velocity with respect to the initial momentum is given by

$$\frac{\vec{\nabla}_{\vec{p}_0} v}{v} = \frac{\frac{\vec{\nabla}_{\vec{p}_0}\gamma}{\gamma}}{\gamma^2(1-\gamma^{-2})}\,, \tag{1.6}$$

which scales like γ^{-2} in the relativistic case. This becomes a small number already for moderately relativistic values of the order $\gamma \sim 10$. The weak dependence on the initial momentum is simply understood, because once the particle is accelerated to high energies, its velocity is always similar to the speed of light. Equation (1.6) also depends on the relative variation of the γ-factor on the initial momentum. Usually, this is not a big number but it needs to be checked once a specific term is given. With the weak dependence of the velocity on the initial momentum, it is justified to neglect the initial momentum. The intuitive interpretation of this approximation is to neglect the current due to wave packet spreading with respect to the current of the relativistically moving particle, because in this case, the velocities of the different trajectories which form the wave packet are considered to be equal.

There is another approximation which is very useful. The initial wave packets are usually very small compared to the laser wave length. Typical values are several atomic

units for the spatial widths of the initial wave packet as compared to 15000 a.u. for the wave length of 800 nm. This means that the particles of the ensemble see almost the same laser phase and the dependence of the particle velocity on the initial position is therefore very small. In this case, the velocity can be pulled out of the integral in Eq. (1.4) and with Eq. (1.3) the current density simplifies to

$$\vec{j}(\vec{x},t) = \vec{v}(\vec{x},t) \cdot \rho(\vec{x},t)\,. \tag{1.7}$$

Linearization and numerical implementation

As already discussed in connection with particle velocities, the initial position for a particle which is localized on an atomic scale is of minor importance for the dynamics in a laser field with wave lengths in the visible regime. Therefore, it is sufficient to work with classical solutions which are linearized with respect to the initial position. A linearization can also be applied with respect to the initial momentum whose variations are responsible for spreading. With variations of the order of a few atomic units or less, quadratic terms of initial momentum deviation over the velocity of light ($c \approx 137$ a.u.) can usually be neglected. In this case, the equations of motion simplify to

$$\vec{x}(\vec{p}_0,\vec{x}_0,t) \approx \mathbf{G}(t)\frac{\vec{p}_0-\vec{p}_m}{c} + \mathbf{H}(t)\frac{\vec{x}_0-\vec{x}_m}{\lambda} + \vec{m}(t)\,. \tag{1.8}$$

Here $\mathbf{G}(t)$ and $\mathbf{H}(t)$ are 3×3-matrices, $\vec{p}_m$ and $\vec{x}_m$ are the points about which the series is expanded and λ is the laser wave length. The vector $\vec{m}(t)$ describes the motion for vanishing deviations of the initial momentum and position, which can be considered as the motion of the center of the wave packet. Now, the linearized expression for the particle position can easily be solved for the initial momentum in order to obtain the function $\vec{g}(\vec{x},\vec{x}_0,t) = \vec{p}_0$ and the corresponding Jacobian which are needed to construct the probability density and current:

$$\vec{g}(\vec{x},\vec{x}_0,t) = c\mathbf{G}^{-1}(t)\left(\vec{x}(\vec{p}_0,\vec{x}_0,t) - \mathbf{H}(t)\frac{\vec{x}_0-\vec{x}_m}{\lambda} - \vec{m}(t)\right) + \vec{p}_m\,, \tag{1.9a}$$

$$\left|\frac{\partial\vec{g}(\vec{x},\vec{x}_0,t)}{\partial\vec{x}}\right| = \frac{c^3}{\det\mathbf{G}}\,. \tag{1.9b}$$

These general expressions in Eqs. (1.8) and (1.9) can simplify considerably for specific applications. For example, $\mathbf{H}(t)$ can reduce to the unit matrix when a different initial position effects only a spatial shift of the trajectory, or $\mathbf{G}(t)$ becomes (partly) diagonal if the motion in different dimensions are independent of each other. This is important once the integrals in Eqs. (1.3) and (1.4) need to be carried out.

If the equations of motion are not known explicitely, the coefficients of $G(\tilde{t})$, $H(\tilde{t})$ and $m(\tilde{t})$ can easily be determined numerically for any instant of time $\tilde{t}$. After numerically calculating the position for several times with different initial conditions, the coefficients are fixed. For example, by setting $\vec{p}_0 = \vec{p}_m$ and $\vec{x}_0 = \vec{x}_m$ one finds $\vec{m}(\tilde{t}) = \vec{x}(\tilde{t})$. Then, with $\vec{p}_0 - \vec{p}_m = (1,0,0)$ and $\vec{x}_0 = \vec{x}_m$ the first column of $G(\tilde{t})$ is determined, etc. In this way, wave packets can be propagated with rather little computational effort by determining the coefficients (21 at the most) and solving the integrals in Eq. (1.3).

Initial states

In order to construct the wave packet or the current density, the initial momentum distribution $\tilde{\rho}$ and the initial probability distributions ρ_0 are needed. These distributions are often given by a microcanonical ensemble, where the initial electron state is represented by a set of classical trajectories with side conditions, e.g. on the energy or angular momentum to mimic some initial quantum state (for details see e.g. [75]). A further possibility is to derive the probability distributions for the initial conditions from the initial quantum mechanical state. Here, the initial distributions are chosen to be the following spherically symmetric Gaussians with arbitrary widths:

$$\rho_0(\vec{x}_0) = (\sqrt{\pi}\Delta w)^{-3} \exp\left[-\frac{\vec{x}_0 \cdot \vec{x}_0}{\Delta w^2}\right], \tag{1.10a}$$

$$\tilde{\rho}(\vec{p}_0) = (\sqrt{\pi}\Delta p)^{-3} \exp\left[-\frac{\vec{p}_0 \cdot \vec{p}_0}{\Delta p^2}\right]. \tag{1.10b}$$

Δw and Δp are the widths in coordinate and momentum space, respectively. Here, the width of a Gaussian (centered at the origin) is defined by the absolute value of the vectors yielding values which are by the Euler number smaller than the maximum of the distribution. The parameters Δw and Δp can be adapted to mimic the localization of some initial state in both coordinate and momentum space. Choosing Gaussians for the initial distributions has the great advantage that this allows for an analytical description of wave packet dynamics.

As discussed previously, spreading originates from the uncertainty of the initial momentum, i.e., large widths Δp generally imply quick spreading. Due to Heisenberg's uncertainty principle, the widths in momentum and coordinate space cannot both be arbitrarily small. For the widths used here, the uncertainty relation is given by[1] $\Delta w \cdot \Delta p \geq 1$. This means that on an atomic scale, small spatial widths imply large uncertainties in momentum space and thus spreading generally becomes faster for strongly localized particles. The other way round, slow spreading involves large spatial uncertainties.

There is a useful approximation which can be applied to study the long-term behavior of wave packets. Once the wave packet has spread to a size much bigger than the initial wave packet, small variations of the initial position of the classical trajectories often become insignificant. In this case, the initial probability density can be approximated by a delta-function $\rho_0(\vec{x}_0) \approx \delta(\vec{x}_0)$. The integrals in Eqs. (1.3) and (1.4) can then be carried out and one finds simplified expressions for the current and probability density:

$$\rho(\vec{x},t) \approx \rho'(\vec{x},\vec{x}_0=0,t) = \tilde{\rho}(\vec{g}(\vec{x},\vec{x}_0=0,t)) \left|\frac{\partial \vec{g}(\vec{x},\vec{x}_0=0,t)}{\partial \vec{x}}\right|, \tag{1.11a}$$

$$\vec{j}(\vec{x},t) \approx \rho'(\vec{x},\vec{x}_0=0,t)\vec{v}(\vec{x},\vec{x}_0=0,t). \tag{1.11b}$$

Correlations of initial conditions

The distributions of the initial positions and momenta (1.10) are not correlated, i.e., the initial momentum distribution is independent of any given initial position. However, this does not necessarily have to be the case. For instance, consider a wave packet

[1] If a Gaussian $f(x)$ is given via $f(x) \propto \exp\left[-x^2/(2\sigma^2)\right]$, where the width is defined by σ, the uncertainty relation has the common form $\Delta w \cdot \Delta p \geq 1/2$.

which has broadened in the course of time. In the classical picture, where wave packets are mimicked by ensembles of classical trajectories, the particle has some different momentum if it is found at the margin of the wave packet than if it is found at the center. Such a correlation is found as well for quantum mechanical wave packets.

Here, an argument is given to show, under which circumstances the initial position and momentum distributions following from some quantum mechanical initial state are uncorrelated such that the initial distributions (1.10) can be applied.

Consider the following one-dimensional model: First, the particle be in some state $\psi(x)$. Then, it is detected to be at the position x_0 with a spatial uncertainty of Δx. Thus the wave function is projected on the subspace between $x_0 - \Delta x/2$ and $x_0 + \Delta x/2$. Now, the spatial uncertainty be small enough that the collapsed wave function $\psi_p(x)$ can be considered to linear approximation in the interval of interest:

$$\psi_p(x) = n[\psi(x_0) + \psi'(x_0)(x - x_0)][\Theta(x - x_0 + \Delta x/2) - \Theta(x - x_0 - \Delta x/2)]\,. \quad (1.12)$$

Here, Θ is the Heaviside step function and n is a normalization constant. The following calculation is carried out consistently to linear order in $(x - x_0)$. The wave function $\psi_p(x)$ is then found to be normalized for $|n|^2 = (|\psi(x_0)|^2 \Delta x)^{-1}$. The goal is to find an expression for the momentum expectation value $< p >$ of this wave function which is localized in the vicinity of x_0. $< p >$ is the pendant of the classical momentum and it will be seen under which conditions the momentum is independent of the initial position. The expectation value is given by

$$< p >= \int \psi_p^*(x) \left(-i \frac{\partial}{\partial x} \psi_p(x) \right) dx\,. \quad (1.13)$$

Considering that the derivative of the step function is the δ-function, this expression reduces to

$$\begin{aligned} < p >= -i|n|^2 \Big[& \psi^*(x_0)\psi'(x_0)\Delta x \\ & + \int_{-\Delta x/2}^{\Delta x/2} \left[|\psi(x_0)|^2 + (\psi^*(x_0)\psi'(x_0) + \psi(x_0)\psi'^*(x_0))(x - x_0) \right] \\ & \times \left[\delta(x - x_0 + \Delta x/2) - \delta(x - x_0 - \Delta x/2) \right] dx \Big]\,. \end{aligned} \quad (1.14)$$

To carry out the integral, the following property of the δ-function needs to be taken into account:

$$\int_{-\infty}^{\eta} x\delta(x - \eta)dx = \int_{-\infty}^{0} (y + \eta)\delta(y)dy = \eta \int_{-\infty}^{0} \delta(y)dy = \frac{\eta}{2}\,. \quad (1.15)$$

Finally, the following result for the momentum expectation value is found:

$$< p >= \mathrm{Im} \frac{\psi'(x_0)}{\psi(x_0)}\,. \quad (1.16)$$

According to this simple result, the momentum is found to be independent of the initial position if the wave function $\psi(x_0)$ is real. Note, that this result becomes exact in the limit that the particle position is determined exactly since the accuracy of the first order approximation increases as Δx decreases.

The essential result is that the uncorrelated initial probability distributions (1.10) can be employed if the initial quantum mechanical states are real.

Example of a free electron wave packet

It is instructive to apply this analytical formalism of phase-space averaging to a simple example which can be compared with the exact quantum mechanical result. Consider a one-dimensional wave packet of a free electron. The motion of a free particle is given by $x = p_0 \cdot t + x_0$, which can be solved for the initial momentum p_0 to yield the function required to determine the probability density (1.3):

$$g(x, x_0, t) \equiv p_0 = \frac{x - x_0}{t}\,, \tag{1.17a}$$

$$\frac{\partial g(x, x_0, t)}{\partial x} = \frac{1}{t}\,. \tag{1.17b}$$

With the one-dimensional analog of the initial Gaussian distributions[2] (1.10), the probability density is given by

$$\begin{aligned}\rho(\vec{x}, t) &= \int_{-\infty}^{\infty} \frac{\exp\left[-\frac{(x-x_0)^2}{\Delta p^2 t^2}\right]}{\sqrt{\pi}\Delta p\, t} \cdot \frac{\exp\left[-\frac{x_0^2}{\Delta w^2}\right]}{\sqrt{\pi}\Delta w}\, dx_0 \\ &= \frac{1}{\sqrt{\pi}\sqrt{\Delta w^2 + \Delta p^2 t^2}} \exp\left[-\frac{x^2}{\Delta w^2 + \Delta p^2 t^2}\right]\,. \end{aligned} \tag{1.18}$$

The quantum mechanical solution $\psi(x, t)$ is given by a superposition of plane propagating waves with momentum p_0, which solve the free Schrödinger equation:

$$\psi(x, t) = \int_{-\infty}^{\infty} \frac{1}{\sqrt{2\pi}} \exp\left[i(p_0 x - \frac{1}{2} p_0^2 t)\right] \cdot \tilde{\psi}(p_0)\, dp_0\,. \tag{1.19}$$

The initial state in momentum space $\tilde{\psi}(p_0)$ is chosen in a way that the corresponding initial probability distribution $|\tilde{\psi}(p_0)|^2$ matches the one-dimensional version of Eq. (1.10b):

$$\tilde{\psi}(p_0) = \frac{1}{\sqrt{\Delta p \sqrt{\pi}}} \exp\left[-\frac{p_0^2}{2\Delta p^2}\right]\,, \tag{1.20a}$$

$$|\tilde{\psi}(p_0)|^2 = \frac{1}{\Delta p \sqrt{\pi}} \exp\left[-\frac{p_0^2}{\Delta p^2}\right]\,. \tag{1.20b}$$

Then, the following solution for the wave function and the probability distribution $|\psi(x, t)|^2$ is found:

$$\psi(x, t) = \frac{1}{\sqrt[4]{\pi}\sqrt{\Delta p^{-1} - i\Delta p\, t}} \exp\left[-\frac{\frac{\Delta p}{2} x^2}{\Delta p^{-1} - i\Delta p\, t}\right]\,, \tag{1.21a}$$

$$|\psi(x, t)|^2 = \frac{1}{\sqrt{\pi}\sqrt{\Delta p^{-2} + \Delta p^2 t^2}} \exp\left[-\frac{x^2}{\Delta p^{-2} + \Delta p^2 t^2}\right]\,. \tag{1.21b}$$

It can be read off, that the initial spatial width of the probability density associated with the initial state (1.20a) is given by $\Delta w = \Delta p^{-1}$ and the quantum mechanical result (1.21b) is identical to the result (1.18) obtained by phase-space averaging.

[2]Note, that the three-dimensional initial distributions are simple products of one-dimensional Gaussians.

Now, consider the approximation discussed in Sec. 1.1.1 (*Initial states*) where the initial probability density distribution was considered to be point-like as compared to the broadened wave packet. In this case, the probability distribution follows from Eq. (1.11a):

$$\psi(x,t) \approx \frac{1}{\sqrt{\pi}\Delta p\, t} \exp\left[-\frac{x^2}{\Delta p^2 t^2}\right] . \tag{1.22}$$

This result is also obtained from the exact result (1.18) in the limit of long evolution times, i.e. for $t \to \infty$.

As discussed in Sec. 1.1.1 (*Correlations of initial conditions*), it is expected that the particle position and its momentum become correlated as the wave packet evolves. If the particle is detected in the vicinity at some point x_0, then the expectation value for its momentum is given by Eq. (1.16). Applied to the spreading wave packet (1.21a) one obtains

$$< p >= \frac{x_0 t}{\Delta p^{-4} + t^2} = \frac{x_0}{t} \cdot \frac{1}{1 + \frac{1}{\Delta p^4 t^2}} \approx \frac{x_0}{t} . \tag{1.23}$$

The approximation is valid for the long-term behavior. This result can be understood in classical terms: If the particle is found at the point x_0 at time t, the particle must have had the initial momentum of x_0/t to get there. In the long-term behavior, the uncertainty of the initial position can be neglected.

1.2 Superposition of solutions with constant modulus

In many cases, solutions of wave equations, such as the Schrödinger or the Klein-Gordon equation have the simple structure where only the phase depends on some momentum variables, whereas the modulus is constant. The solution ϕ then has the form

$$\phi(\vec{x}, \vec{p}, t) \propto \exp i f(\vec{x}, \vec{p}, t) , \tag{1.24}$$

where f is a real function depending on both the position and the momentum $\vec{p}$. With the linearity and the homogeneity of the corresponding equation of motion, these solutions can be superimposed to construct a wave packet which is a solution of the wave equation as well.

1.2.1 Gaussian wave packets

If the momentum distribution $\tilde{\psi}$ is a Gaussian, the superposition can be carried out analytically. The following Gaussian is chosen:

$$\tilde{\psi}(\vec{p}) = \left(\sqrt{\pi}\Delta p\right)^{-3/2} \exp\left[-\frac{(\vec{p} - \vec{p}_m)^2}{2\Delta p^2}\right] , \tag{1.25}$$

where $\vec{p}_m$ is the maximum of the distribution and Δp is again the width. The distribution is normalized according to

$$\int |\tilde{\psi}(\vec{p})|^2 \, d^3p = 1 . \tag{1.26}$$

The functions $\phi(x, p, \tilde{t})$ be subject to the following normalization condition at some time $\tilde{t}$:

$$\int \phi^*(\vec{x}, \vec{p}, \tilde{t}) \phi(\vec{x}, \vec{p}\,', \tilde{t}) d^3x = \delta^3(\vec{p} - \vec{p}\,') . \tag{1.27}$$

With these conditions, wave packets can be shown to be normalized in coordinate space. The Gaussian superposition is simply given by

$$\psi(\vec{x},t) = \int \phi(\vec{x},\vec{p},t)\tilde{\psi}(\vec{p})d^3p\,, \tag{1.28}$$

where the spatial integral over the modulus squared of this wave function is equal to unity at time $\tilde{t}$ which is seen by means of Eqs. (1.26) and (1.29):

$$\int |\psi(\vec{x},\tilde{t})|^2 d^3x = \int \phi^*(\vec{x},\vec{p},\tilde{t})\phi(\vec{x},\vec{p}\,',\tilde{t})\tilde{\psi}^*(\vec{p})\tilde{\psi}(\vec{p}\,')d^3p\,d^3p'\,d^3x = 1\,. \tag{1.29}$$

In nonrelativistic quantum mechanics, the modulus square of the wave function represents the probability density. With Eq. (1.29) it has been shown that the wave function is normalized at time $\tilde{t}$, but since $\phi(\vec{x},\vec{p},t)$ is the solution of a wave equation which conserves the probability distribution, the normalization holds for all times t. This is not a surprise for the nonrelativistic case, however, the same argument can be employed if $\phi(\vec{x},\vec{p},t)$ is a solution of a relativistic wave equation. In this case, the normalized charge distribution is not given by the modulus square of the wave function. However, if the dynamics is nonrelativistic at the instant $\tilde{t}$, the charge density may reduce to $|\psi(\vec{x},\tilde{t})|^2$. With Eq. (1.35), this will be shown explicitly for the Klein-Gordon equation. This means that the normalization can be shown for an instant $\tilde{t}$ when the dynamics is nonrelativistic and the normalization for arbitrary times t is ensured by charge conservation of the wave equation.

The Gaussian superposition $\psi(\vec{x},t)$, requires a three-dimensional integral to be carried out:

$$\psi(\vec{x},t) \propto \iiint \exp\left[if(\vec{x},\vec{p},t) - \frac{(\vec{p}-\vec{p}_m)^2}{2\Delta p^2}\right] d^3p\,. \tag{1.30}$$

In general, this integral cannot be solved, but for small widths Δp in momentum space, the function $f(\vec{x},\vec{p},t)$ can be expanded to second order about the maximum $\vec{p}_m$ of the momentum distribution, which renders the superposition in Eq. (1.30) a Gaussian integral. The function $f(\vec{x},\vec{p},t)$ reduces to the following quadratic form:

$$f(\vec{x},\vec{p},t) \approx f(\vec{x},\vec{p}_m,t) + (\vec{p}-\vec{p}_m,t)\vec{\nabla}f(\vec{x},\vec{p}_m,t) + \frac{1}{2}\left((\vec{p}-\vec{p}_m,t)\cdot\vec{\nabla}\right)^2 f(\vec{x},\vec{p}_m,t)\,. \tag{1.31}$$

How well this approximation works, depends on both the widths Δp and the function $f(\vec{x},\vec{p},t)$. Generally, the accuracy increases with decreasing widths Δp. The behavior of $f(\vec{x},\vec{p},t)$ can be analyzed when the formalism is applied.

With the expansion of $f(\vec{x},\vec{p},t)$, the integrals in Eq. (1.30) can be solved directly. However, for the applications considered here, it is easier to reduce the problem to three one-dimensional integrals. This is always possible, because with the expansion (1.31) the exponent in Eq. (1.30) is a quadratic form which can be diagonalized by means of a coordinate transformation in momentum space. The wave function $\psi(\vec{x},t)$ can then be written as a product of three one-dimensional integrals and the formalism introduced in the following can be applied.

One-dimensional Gaussian superpositions

The one-dimensional functions be given by

$$\begin{aligned}\phi(x,p,t) &= \frac{1}{\sqrt{2\pi}} \exp if(x,p,t) \\ &\approx \frac{1}{\sqrt{2\pi}} \exp\left[i\left(f(x,p_m,t) + f'(x,p_m,t)(p-p_m) + \frac{1}{2} f''(x,p_m,t)(p-p_m)^2 \right)\right] , \quad (1.32)\end{aligned}$$

where the function $f(x,p,t)$ has been expanded to second order about the momentum p_m as seen in Eq. (1.31) for the three-dimensional case. The Gaussian superposition can then be carried out to yield the wave function of the wave packet, where the momentum distribution is chosen to be the one-dimensional version of Eq. (1.25):

$$\begin{aligned}\psi(x,t) &= \int \phi(x,p,t)(\sqrt{\pi}\Delta p)^{-1/2} \exp\left[-\frac{(p-p_m)^2}{2\Delta p^2} \right] dp \\ &= \frac{\exp if(x,p_m,t)}{\sqrt[4]{\pi}\sqrt{\Delta p^{-1} - i\Delta p f''(x,p_m,t)}} \exp - \frac{\frac{\Delta p}{2} f'(x,p_m,t)^2}{\Delta p^{-1} - i\Delta p f''(x,p_m,t)} . \quad (1.33)\end{aligned}$$

This expression shows that $f'(x,p_m,t)$ determines the maximum of the wave packet, $f''(x,p_m,t)$ affects the width and $f(x,p_m,t)$ appears only in a phase factor[3]. The absolute square of the wave function is found to be

$$|\psi(x,t)|^2 = \frac{1}{\sqrt{\pi}\sqrt{\Delta p^{-2} + \Delta p^2 f''(x,p_m,t)}} \exp - \frac{f'(x,p_m,t)^2}{\Delta^{-2} + \Delta p^2 f''(x,p_m,t)^2} . \quad (1.34)$$

For nonrelativistic quantum mechanics, $|\psi(x,t)|^2$ represents the probability distribution, but this expression will be useful for the relativistic case as well.

Charge density for the Klein-Gordon equation

The charge density $\rho(\vec{x},t)$ of a relativistic particle whose dynamics is described by the Klein-Gordon equation is given by the following expression (e.g., see [81]):

$$\rho(\vec{x},t) = \frac{i}{2c^2}\left[\phi^* \left(\frac{\partial}{\partial t} + \frac{i}{c}\Phi \right)\phi - \phi \left(\frac{\partial}{\partial t} - \frac{i}{c}\Phi \right)\phi^* \right] , \quad (1.35)$$

where $\phi(\vec{x},t)$ is the wave function and $\Phi(\vec{x},t)$ the scalar electromagnetic potential. To show that this expression reduces to the absolute square of the wave function in the nonrelativistic limit, the operator for the particle energy $\hat{E}$ (kinetic energy plus rest energy) is approximated by the rest energy of the particle[4], i.e., the kinetic energy is neglected with respect to c^2:

$$\hat{E} = i\frac{\partial}{\partial t} - \frac{1}{c}\Phi = c^2 \left(1 + \frac{\left(i\frac{\partial}{\partial t} - \frac{1}{c}\Phi \right) - c^2}{c^2} \right) \approx c^2 . \quad (1.36)$$

[3]Note that in the classical approach of the previous section, wave packet spreading is obtained from the terms proportional to the initial momentum, whereas here, quadratic terms are required. For this reason, the second order approximations of the initial momentum dependence in the quantum approach corresponds to the linear approximation of the classical method, i.e., it does not yield higher accuracy.

[4]Note that in the Hamilton-formalism, the particle energy (kinetic energy+rest energy) is given by $H - \Phi/c = (p - A/c)^2/2$ where H is the Hamilton function representing the total energy including the potential energy. The replacement of H by $\partial/\partial t$ yields the operator for the particle energy.

In this nonrelativistic limit, the charge density reduces to the well known form

$$\rho(\vec{x}, t) \approx \phi^* \phi \,. \tag{1.37}$$

As discussed above, this can be employed to ensure the normalization of wave packets (1.30), because the charge density of a laser-driven electron is given by the nonrelativistic expression (1.37) before the (intense) laser pulse hits the electron and gives rise to relativistic dynamics.

Chapter 2

Laser-driven wave packets

The objective of this chapter is to establish analytical expressions for Gaussian wave packets of laser-driven electrons. First, the wave equation has to be solved and second, the solutions need to be superimposed which is accomplished by means of the quantum formalism developed in Sec. 1.2.

In dipole approximation where the spatial dependence of the laser field is neglected, the problem of laser-driven particles can easily be solved (see Sec. 2.1.3). However, in this case, the laser magnetic field is neglected. To include magnetic field effects which are important for strong laser fields, the dependence of the vector potential on the spatial position is considered to first order in an expansion. This analysis is carried out in Sec. 2.1 for the Schrödinger equation, i.e. for the regime where the dynamics is still nonrelativistic but magnetic fields are non-negligible.

For higher intensities which involve relativistic electron dynamics, the solutions of the Klein-Gordon equation need to be superimposed to yield a relativistic wave packet. This case is discussed in Sec. 2.2. As opposed to previous attempts of numerically solving the Schrödinger equation beyond the dipole approximation (see e.g. [63, 64]), the Dirac equation [57, 58, 59, 60, 61, 62] or the computational superposition of Volkov-states [65, 66], the results are completely analytical.

2.1 Nonrelativistic dynamics beyond the dipole approximation

2.1.1 Laser field expansion

In the following, the laser pulse is chosen to propagate in the z direction with linear polarization in the x direction. The laser fields are described by the vector potential:

$$\vec{A} = \hat{x}A(\omega t - kz) \equiv \hat{x}A(\varphi)\,. \tag{2.1}$$

φ is the laser phase, ω the angular laser frequency and k the wave vector. If the region of interest remains close to the plane $z = 0$, i.e., if the electron stays in a region where kz is small, then the spatial dependence of the vector potential can be expanded:

$$\vec{A} \approx \hat{x}\big[A(\omega t) - kz \cdot A'(\omega t)\big]\,. \tag{2.2}$$

The prime denotes the derivative with respect to the laser phase. Often, the spatial dependence can be neglected completely, e.g., an electronic wave packet in an atom

has extensions of the order of several atomic units whereas a laser wave length of 800 nm$\hat{=}$15000 a.u. is much higher. However, the dipole approximation of the vector potential cannot describe magnetic field effects, because the vector potential needs a spatial dependence to yield a nonvanishing magnetic field $\vec{B} = \vec{\nabla} \times \vec{A}$. For example, an important effect caused by the magnetic field is the electron drift in the laser propagation direction which occurs in strong laser fields. To consider magnetic field effects, the expansion (2.2) includes one term more than the dipole approximation. To keep the linear term kz smaller than 10^{-1} at the laser wave length of 800 nm, the z position may reach values of up to a few hundred atomic units.

The electric and magnetic fields follow from the vector potential:

$$\vec{E} = -\frac{1}{c}\dot{\vec{A}} = -\frac{\omega}{c}(A' - kz \cdot A'')\hat{x}\,, \tag{2.3a}$$

$$\vec{B} = \vec{\nabla} \times \vec{A} = -kA'\hat{y}\,. \tag{2.3b}$$

2.1.2 Classical solutions

Before solving the Schrödinger equation, the classical solution is presented. This is interesting for a comparison with the quantum mechanical wave packet dynamics.

The classical equations of motion are given by

$$\ddot{\vec{x}} = \vec{E} + \frac{\dot{\vec{x}}}{c} \times \vec{B}\,, \tag{2.4}$$

which yields the following equations if the fields (2.3) are inserted:

$$\ddot{x} = -\frac{\omega}{c}(A' - kz \cdot A'') + \frac{k}{c}\dot{z}A'\,, \tag{2.5a}$$

$$\ddot{y} = 0\,, \tag{2.5b}$$

$$\ddot{z} = -\frac{\omega}{c^2}\dot{x}A'\,. \tag{2.5c}$$

With $\omega A'(\omega t) = \dot{A}(\omega t)$ and $c = \omega/k$, the equation for the x direction can be integrated. The dynamics in the y direction is simply a free motion. Then, the following equations are found:

$$\dot{x} = -\frac{1}{c}A + \frac{\omega}{c^2}zA' + p_{x_0}\,, \tag{2.6a}$$

$$y = p_{y_0}t + y_0\,, \tag{2.6b}$$

$$\ddot{z} = \frac{\omega}{c^2}\left(\frac{1}{c}A - kz\frac{1}{c}A' - p_{x_0}\right)A'\,. \tag{2.6c}$$

The initial conditions are defined by $\vec{x}(t=0) = \vec{x}_0 = (x_0, y_0, z_0)$ and $\dot{\vec{x}}(t=0) = \vec{p}_0 = (p_{x_0}, p_{y_0}, p_{z_0})$.

From Eq. (2.6a), it is seen that the terms A/c^2 and p_{x_0}/c have to be small ($A/c^2 \sim p_{x_0}/c \lesssim 0.1$) to keep the dynamics nonrelativistic ($\dot{x}/c \ll 1$). Usually, the maximum values of $A(t)$ and $A'(t)$ are of the same order of magnitude which is shown by the following example. For a typical laser pulse of sinusoidal shape with an envelope $R(t)$ one finds

$$A(t) = R(t)\sin(\omega t)\,, \tag{2.7a}$$

$$A'(t) = \frac{\dot{R}(t)}{\omega}\sin(\omega t) + R(t)\cos(\omega t)\,. \tag{2.7b}$$

A laser pulse which is not too short reaches its maximum R_0 only after several quarters of a period T, i.e., the slope of the envelope fulfills the condition $\dot{R}(t) \ll R_0/(T/4) \approx \omega R_0$. By means of Eqs. (2.7), it is seen that the maximum values of $A(t)$ and $A'(t)$ are of the same order of magnitude. Thus, the amplitudes of the vector potential A_0 and the electric field E_0 are related according to Eq. (2.3a): The dimensionless expressions A_0/c^2 and $E_0/(\omega c)$ have similar values and can be used to indicate whether the electron dynamics in laser fields is relativistic ($A_0/c^2 \sim E_0/(\omega c) \gtrsim 1$), weakly relativistic ($A_0/c^2 \sim E_0/(\omega c) \sim 0.5$) or nonrelativistic ($A_0/c^2 \sim E_0/(\omega c) \lesssim 0.1$).

Now, expressions which are higher than second order in the small terms A/c^2, A'/c^2, p_{x_0}/c and kz are neglected. After dividing Eq. (2.6c) by ωc such that the terms become dimensionless, it is seen that the term on the right hand side containing the z position is a third order term which can be neglected. The equation for the z position (2.6c) can then be integrated. The result is inserted into the equation for the x position (2.6a), which can be integrated as well if higher order terms are neglected. Finally, the following solutions of the classical equations of motion are found:

$$x = -\frac{1}{c}\left(1 + \frac{p_{z_0}}{c}\right)\int A dt + \frac{1}{c^2}(p_{z_0}t + z_0)A + p_{x_0}t + x_0\,, \tag{2.8a}$$

$$y = p_{y_0}t + y_0\,, \tag{2.8b}$$

$$z = \frac{1}{2c^3}\int A^2 dt - \frac{p_{x_0}}{c^2}\int A dt + p_{z_0}t + z_0\,. \tag{2.8c}$$

2.1.3 Quantum dynamics

The quantum mechanical solutions are determined by Schrödinger's equation. For the vector potential (2.2), it reads:

$$i\frac{\partial}{\partial t}\psi = \frac{1}{2}\left[-i\vec{\nabla} - \frac{1}{c}\vec{A}\right]^2\psi = \frac{1}{2}\left[-\vec{\nabla}^2 + \frac{2i}{c}(A - kz\cdot A')\frac{\partial}{\partial x} + \frac{1}{c^2}A^2 - \frac{2}{c^2}AA'\right]\psi\,. \tag{2.9}$$

To solve this equation, the electron is assumed to be found in the vicinity of the plane $z = 0$, as employed in the classical solution. This means that terms of second order in kz are assumed to be small. In the following ansatz, the dependence on the z position appears only to linear order in the exponential:

$$\psi = (2\pi)^{-3/2}\exp i\left[\vec{p}_0\cdot(\vec{x} - \vec{x}_0) + u(t)\cdot kz + w(t)\right]\,. \tag{2.10}$$

With this ansatz, the Schrödinger equation is solved separately for each order of kz. That way, the partial differential equation reduces to two ordinary differential equations, one for each order of kz:

$$\dot{u} = -\frac{p_{x_0}}{c}A' + \frac{1}{c^2}AA'\,, \tag{2.11a}$$

$$\dot{w} = -\frac{1}{2}\left[\vec{p}_0^{\,2} + 2kp_{z_0}u + k^2u^2 - \frac{2p_{x_0}}{c}A + \frac{1}{c^2}A^2\right]\,. \tag{2.11b}$$

These equations are easily integrated. The small terms of fourth order in p_{x_0} and A/c^2 then are neglected, and the solution is found to be

$$\psi = (2\pi)^{-3/2}\exp i\left[\vec{p}_0\cdot(\vec{x} - \vec{x}_0) - \frac{1}{2}\vec{p}_0^{\,2}t + \left(-\frac{p_{x_0}}{\omega c}A + \frac{1}{2\omega c^2}A^2\right)kz \right.$$
$$\left. + \frac{p_{x_0}}{c}\left(1 + \frac{p_{z_0}}{c}\right)\int A dt - \frac{1}{2c^2}\left(1 + \frac{p_{z_0}}{c}\right)\int A^2 dt\right]\,. \tag{2.12}$$

These solutions are only valid for small values of kz, but they can be superimposed to construct wave packets which are localized in the valid area. Due to the mixed term $p_{x_0}p_{z_0}$, the exponential function cannot be separated to assume the form $\psi(p_{x_0}, p_{y_0}, p_{z_0}) = \exp f_1(p_{x_0}) \exp f_2(p_{y_0}) \exp f_3(p_{z_0})$ where the functions $f_{1,2,3}$ depend on one momentum variable only. This form is needed to apply the one-dimensional formulas in Eqs. (1.33) and (1.34). However, such a separation can be accomplished by means of a coordinate transformation. The sum of the terms E_q in the exponent of Eq. (2.12) which are quadratic in p_{x_0} and p_{z_0} can be written in the following form:

$$E_q = -\frac{1}{2} \begin{pmatrix} p_{x_0} \\ p_{z_0} \end{pmatrix}^{\mathrm{T}} \begin{pmatrix} t & -\frac{1}{c^2}\int A dt \\ -\frac{1}{c^2}\int A dt & t \end{pmatrix} \begin{pmatrix} p_{x_0} \\ p_{z_0} \end{pmatrix}, \tag{2.13}$$

where T denotes the transpose of a matrix. The 2×2-matrix in Eq. (2.13) has the following eigenvalues $\lambda_{1,2}$ with the corresponding eigenvectors $v_{1,2}$:

$$\begin{aligned} v_1 &= \frac{1}{\sqrt{2}}\begin{pmatrix} 1 \\ 1 \end{pmatrix}, & \lambda_1 &= t - \frac{1}{c^2}\int A dt\,, \\ v_2 &= \frac{1}{\sqrt{2}}\begin{pmatrix} -1 \\ 1 \end{pmatrix}, & \lambda_2 &= t + \frac{1}{c^2}\int A dt\,. \end{aligned} \tag{2.14}$$

The eigenvectors immediately yield the following transformation law, which diagonalizes the quadratic form E_q:

$$\begin{aligned} \tilde{x} &= \frac{1}{\sqrt{2}}(x+z)\,, & x &= \frac{1}{\sqrt{2}}(\tilde{x}-\tilde{z})\,, \\ \tilde{z} &= \frac{1}{\sqrt{2}}(-x+z)\,, & z &= \frac{1}{\sqrt{2}}(\tilde{x}+\tilde{z})\,. \end{aligned} \tag{2.15}$$

This transformation is a rotation of the coordinate system about the y axis by 45 degrees. It is applied to both the momentum and the spatial coordinates. The solutions (2.12) can then be separated:

$$\begin{aligned} \psi = (2\pi)^{-3/2} &\exp i\left[p_{y_0}(y-y_0) - \frac{1}{2}p_{y_0}^2 t - \frac{1}{2c^2}\int A^2 dt\right] \\ &\times \exp i\left[\tilde{p}_{x_0}\left(\tilde{x} - \tilde{x}_0 - \frac{1}{2c^2}A(\tilde{x}+\tilde{z}) + \frac{1}{\sqrt{2}c}\int A dt - \frac{1}{2\sqrt{2}c^3}\int A^2 dt\right)\right] \\ &\times \exp i\left[\tilde{p}_{z_0}\left(\tilde{z} - \tilde{z}_0 + \frac{1}{2c^2}A(\tilde{x}+\tilde{z}) - \frac{1}{\sqrt{2}c}\int A dt - \frac{1}{2\sqrt{2}c^3}\int A^2 dt\right)\right] \\ &\times \exp i\left[-\frac{1}{2}\tilde{p}_{x_0}^2\left(t - \frac{1}{c^2}\int A dt\right) - \frac{1}{2}\tilde{p}_{z_0}^2\left(t + \frac{1}{2c^2}\int A dt\right)\right]. \end{aligned} \tag{2.16}$$

Now, the probability density for a Gaussian wave packet can be determined by means of Eq. (1.34). The following result is found:

$$
\begin{aligned}
&|\psi(x,y,z,t)|^2 = \pi^{-3/2}(\Delta w_+ \Delta w_y \Delta w_-)^{-1} \exp\left[-\frac{f_x'^2}{\Delta w_+^2} - \frac{f_y'^2}{\Delta w_y^2} - \frac{f_z'^2}{\Delta w_-^2}\right], \\
&f_x' \equiv \tilde{x} - \tilde{x}_0 - \frac{1}{2c^2}A(\tilde{x}+\tilde{z}) + \frac{1}{\sqrt{2}c}\int A dt - \frac{1}{2\sqrt{2}c^3}\int A^2 dt - \tilde{p}_{m_x}\left(t - \frac{1}{c^2}\int A dt\right), \\
&f_y' \equiv y - y_0 - p_{m_y} t, \\
&f_z' \equiv \tilde{z} - \tilde{z}_0 + \frac{1}{2c^2}A(\tilde{x}+\tilde{z}) - \frac{1}{\sqrt{2}c}\int A dt - \frac{1}{2\sqrt{2}c^3}\int A^2 dt - \tilde{p}_{m_z}\left(t + \frac{1}{c^2}\int A dt\right), \\
&\Delta w_y \equiv \sqrt{\Delta p^{-2} + \Delta p^2 t^2}, \qquad \Delta w_\pm \equiv \sqrt{\Delta p^{-2} + \Delta p^2\left(t \mp \frac{1}{c^2}\int A dt\right)^2}.
\end{aligned}
\tag{2.17}
$$

The initial momenta p_{m_x}, p_{m_y} and p_{m_z} are the maxima of the momentum distributions. The motion of the wave packet maximum is given by $f_x' = f_y' = f_z' = 0$. If these equations are rewritten with the original coordinates by means of Eqs. (2.15), the classical equations of motion (2.8) are recovered. The equations have to be solved for x, y and z, and third order terms of A/c^2 and p_{m_x}/c are neglected as in the classical analysis. As expected, the maximum of the wave packet moves like a classical particle.

To further analyze the wave packet dynamics, the spatial widths and the directions of its principle axes will be determined. First, the wave packet is shifted such that the maximum is located at the origin. One then finds

$$
\begin{aligned}
|\psi(x,y,z,t)|^2 &= \pi^{-3/2}(\Delta w_+ \Delta w_y \Delta w_-)^{-1} \\
&\exp\left[-\frac{\left(\tilde{x} - \frac{1}{2c^2}A(\tilde{x}+\tilde{z})\right)^2}{\Delta w_+^2} - \frac{y^2}{\Delta w_y^2} - \frac{\left(\tilde{z} + \frac{1}{2c^2}A(\tilde{x}+\tilde{z})\right)^2}{\Delta w_-^2}\right].
\end{aligned}
\tag{2.18}
$$

The distribution with respect to the y coordinate is a Gaussian, whereas the dependence on $\tilde{x}$ and $\tilde{z}$ cannot be written as a product of two Gaussians because mixed terms $\tilde{x}\tilde{z}$ occur. Therefore, the quadratic form QF in the exponent

$$
QF \equiv \frac{\left(\tilde{x} - \frac{1}{2c^2}A(\tilde{x}+\tilde{z})\right)^2}{\Delta w_+^2} + \frac{\left(\tilde{z} + \frac{1}{2c^2}A(\tilde{x}+\tilde{z})\right)^2}{\Delta w_-^2}
\tag{2.19}
$$

needs to be diagonalized. This can be rewritten in matrix-form:

$$
\begin{aligned}
QF &= \begin{pmatrix} \tilde{x} \\ \tilde{z} \end{pmatrix}^{\mathrm{T}} \begin{pmatrix} a & b \\ b & d \end{pmatrix} \begin{pmatrix} \tilde{x} \\ \tilde{z} \end{pmatrix}, \\
a &= \frac{1 - \frac{1}{c^2}A + \frac{1}{4c^4}A^2}{\Delta w_+^2} + \frac{\frac{1}{4c^4}A^2}{\Delta w_-^2}, \quad d = \frac{1 + \frac{1}{c^2}A + \frac{1}{4c^4}A^2}{\Delta w_-^2} + \frac{\frac{1}{4c^4}A^2}{\Delta w_+^2}, \\
b &= \frac{1}{2c^2}A\left[\left(\Delta w_-^{-2} - \Delta w_+^{-2}\right) + \frac{1}{2c^2}A\left(\Delta w_-^{-2} + \Delta w_+^{-2}\right)\right].
\end{aligned}
\tag{2.20}
$$

The symmetric matrix in this equation is diagonalized by the orthogonal transformation

$$
\begin{pmatrix} \tilde{x} \\ \tilde{z} \end{pmatrix} = \frac{1}{\sqrt{(a-\lambda_-)^2 + b^2}} \begin{pmatrix} a - \lambda_- & -b \\ b & a - \lambda_- \end{pmatrix} \begin{pmatrix} X \\ Z \end{pmatrix},
\tag{2.21}
$$

where the columns of the transformation matrix are the normalized eigenvectors. X and Z are the new coordinates, and λ_- is one of the two eigenvalues

$$\lambda_\pm = \frac{a+d}{2} \pm \frac{a-d}{2}\sqrt{1+\frac{4b^2}{(a-d)^2}}\,. \tag{2.22}$$

The new coordinate system is related to the old one by a rotation about the y axis with the rotation angle α. To make this structure more explicit, it is convenient to rewrite the transformation (2.21) in the following form:

$$\begin{pmatrix} \tilde{x} \\ \tilde{z} \end{pmatrix} = \begin{pmatrix} \cos\alpha & \sin\alpha \\ -\sin\alpha & \cos\alpha \end{pmatrix} \begin{pmatrix} X \\ Z \end{pmatrix}, \quad \tan\alpha = -\frac{b}{a-\lambda_-}\,. \tag{2.23}$$

If the off-diagonal terms b in Eq. (2.20) vanish, the rotation angle approaches zero, i.e., the quadratic form is already diagonal. For this reason, the eigenvalue λ_- is needed in the above expressions rather than λ_+ which ensures that the denominator $a-\lambda_-$ in the expression for the angle (2.23) does not vanish as the numerator approaches zero.

With the new coordinates, the quadratic form QF is diagonal and the probability density (2.18) reduces to a product of three Gaussian distributions:

$$|\psi(x,y,z,t)|^2 = \pi^{-3/2}(\Delta w_X \Delta w_y \Delta w_Z)^{-1} \exp\left[-\frac{X^2}{\Delta w_X^2} - \frac{y^2}{\Delta w_y^2} - \frac{Z^2}{\Delta w_Z^2}\right]. \tag{2.24}$$

The widths are related to the eigenvalues via $w_X^2 = 1/\lambda_+$ and $w_Z^2 = 1/\lambda_-$.

If the term $b/(a-d)$ is small such that quadratic orders can be neglected with respect to one, the eigenvalues reduce to $\lambda_+ \approx a$ and $\lambda_- \approx d$. The widths can then be further simplified if only linear terms in A/c^2 are considered:

$$w_X \approx \left(1+\frac{1}{2c^2}A\right) w_+\,, \quad w_Z \approx \left(1-\frac{1}{2c^2}A\right) w_-\,. \tag{2.25}$$

Furthermore, with the simplified eigenvalues, the formula for the rotation angle becomes

$$\tan\alpha \approx -\frac{b}{a-d}\,. \tag{2.26}$$

With the expressions in Eq. (2.20), one finds

$$\frac{b}{a-d} = -\frac{1}{4c^2}A\left[1+\frac{w_-^2-w_+^2}{w_-^2-w_+^2-\frac{1}{c^2}A(w_-^2+w_+^2)}\right], \tag{2.27a}$$

$$w_-^2 - w_+^2 = 4t\frac{\Delta p^2}{c^2}\int A dt\,, \tag{2.27b}$$

$$w_-^2 + w_+^2 = 2\left[\Delta p^{-2} + \Delta p^2\left(t^2 + \left(\frac{1}{c^2}\int A dt\right)^2\right)\right]. \tag{2.27c}$$

In most cases, the term $b/(a-d)$ is small because it is proportional to A/c^2 which is a small number in the nonrelativistic regime considered here. The rotation angle then turns out to be

$$\alpha \approx \tan\alpha = \frac{1}{4c^2}A\left[1+\frac{t\frac{\Delta p^2}{c^2}\int A dt}{t\frac{\Delta p^2}{c^2}\int A dt - \frac{1}{2c^2}A(\Delta p^{-2}+\Delta p^2 t^2)}\right], \tag{2.28}$$

where quadratic terms of A/c^2 are again neglected with respect to one.

However, for certain times when $a = d$ and $b \neq 0$, the term $b/(a-d)$ becomes infinite. In this case, one has to deal with the exact expressions (2.22) and (2.23). The eigenvalues (2.22) then reduce to $\lambda_\pm = a \pm b$ and according to Eq. (2.23) the rotation angle becomes $\alpha = -\pi/4$. With Eq. (2.20) and considering that $a = d$, one finds for the eigenvalues

$$\lambda_\pm = a \pm \frac{1}{4c^2} A \frac{w_+^2 - w_-^2}{w_-^2 w_+^2} \approx a \mp \frac{1}{4c^2} A \frac{4t\frac{\Delta p^2}{c^2} \int A dt}{(\Delta p^{-2} + \Delta p^2 t^2)^2} \approx a \,. \tag{2.29}$$

Here, quadratic terms of A/c^2 have been considered to be small again. Since the two eigenvalues reduce to the same value, the wave packet is spherically symmetric at the instant when $a = d$, i.e., there is no unique direction for the principal axes. The value for the rotation angle α therefore becomes meaningless. Note that the eigenvalues and thus the widths have the same limit $\lambda_+ = \lambda_- = a = d$ as for the previously discussed case where $b/(a-d)$ is small. This means, nothing special happens to the wave packet as $b/(a-d)$ becomes infinite, except that it becomes symmetric.

The results simplify for the case that the widths w_+ and w_- become equal. From the definitions in Eq. (2.17), it is read off that this occurs for the following limits:

$$\begin{aligned} w_\pm &= \Delta p^{-1} \,, && \text{for } \Delta p^{-2} \gg \Delta p^2 \left(t \mp \tfrac{1}{c^2} \textstyle\int A dt\right)^2 \,, \\ w_\pm &= \sqrt{\Delta p^{-2} + \Delta p^2 t^2} \,, && \text{for } t \gg \tfrac{1}{c^2} \textstyle\int A dt \,. \end{aligned} \tag{2.30}$$

The upper limit is valid for short times. The lower limit applies to the long-term behavior because the steadily growing time t becomes much greater than the integral over the vector potential which usually is an oscillating function with a small amplitude in the nonrelativistic regime. It is possible, e.g., if Δp is small, that the two regimes overlap such that $w_+ = w_-$ holds for all times. Of course, equal widths are found as well at the instants when the integral over the vector potential becomes zero. For these cases, when $w_+ = w_-$, Eq. (2.27a) simplifies and the rotation angle given in Eq. (2.26) reduces to the very simple result [compare Eq. (2.28)]

$$\alpha = \frac{1}{4c^2} A \,. \tag{2.31}$$

Together with the previous coordinate transformation [see (2.15)], the angle $\tilde{\alpha}$ between the principle axes and the axes of the original coordinate system is given by

$$\tilde{\alpha} = -\frac{\pi}{4} + \frac{1}{4c^2} A \,. \tag{2.32}$$

Furthermore, the ratio of the widths in Eq. (2.25) turns out to be

$$\frac{w_X}{w_Z} = 1 + \frac{1}{c^2} A \,. \tag{2.33}$$

Example

In the following example, a Gaussian-shaped laser pulse of a few cycles with the wavelength of 800 nm is considered (see FIG. 2.1). It is given by

$$\begin{aligned} A(t) &= Rc^2 \sin(\omega t - \varphi_0) \exp\left[- \left(\frac{\omega t - \varphi_0}{\Delta z} \right)^2 \right] \,, \\ R = 0.25 \,, \quad \Delta z = 6 \,, \quad \varphi_0 &= 3.5 \cdot \Delta z \,, \quad \omega = 0.057 \,. \end{aligned} \tag{2.34}$$

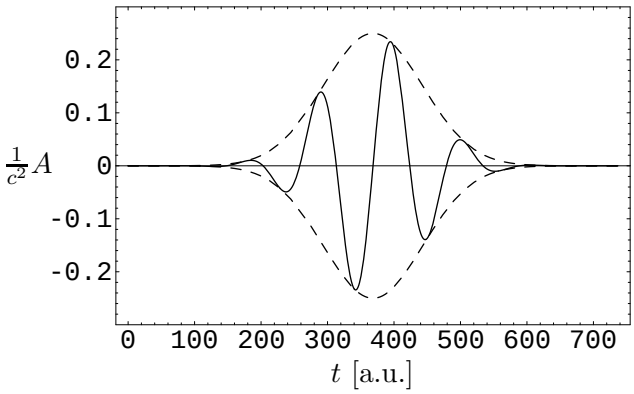

Figure 2.1: The vector potential in the dimensionless form A/c^2 is shown, which represents the laser pulse shape. Except for a factor of four, this curve also represents the time-dependent angle between the principle axes of the electron wave packet in the x-z plane and the diagonals of the coordinate system ($x = \pm z$).

The dynamics of the particle in the x and z direction is depicted in FIG. 2.2, where part (a) shows the motion of the maximum of the wave packet according to Eqs. (2.8). The initial conditions are chosen such that the particle rests at the origin, at the beginning. The width in momentum space is chosen to be $\Delta p = 0.05$ a.u. The wave packet is shown in (b) for the times when the maximum is located at the positions marked in (a). These correspond to the times $t_i = 0$, $\omega t_{ii,vi} - \varphi_0 = \pm\pi$, $\omega t_{iii,v} - \varphi_0 = \pm\pi/2$ and $\omega t_{iv} = \varphi_0$, where φ_0 determines the maximum of the envelope [see Eq. (2.34)]. It is seen that the wave packet, while spreading, deforms according to Eq. (2.33).

Dipole approximation

It is instructive to compare the results of this approach to the corresponding results if the dipole approximation is applied. In this case, the spatial dependence of the vector potential is neglected and it is approximated by [compare Eq. (2.2)]

$$\vec{A} \approx \hat{x} A(\omega t)\,. \tag{2.35}$$

The vector potential describes a homogeneous oscillating electric field. It is clear, that the magnetic field vanishes for this vector potential because there is no spatial dependence [compare Eq. (2.3b)].

The Schrödinger equation has the form

$$i\frac{\partial}{\partial t}\psi = \frac{1}{2}\left[-\vec{\nabla}^2 + \frac{2i}{c}A\frac{\partial}{\partial x} + \frac{1}{c^2}A^2\right]\psi\,, \tag{2.36}$$

and it is solved by

$$\psi = (2\pi)^{-3/2}\exp i\left[\vec{p}_0\cdot(\vec{x}-\vec{x}_0) - \frac{1}{2}\vec{p}_0{}^2 t + \frac{p_{x_0}}{c}\int A dt - \frac{1}{2c^2}\int A^2 dt\right]. \tag{2.37}$$

Employing Eq. (1.34), one arrives at the probability density which is a three-dimensional,

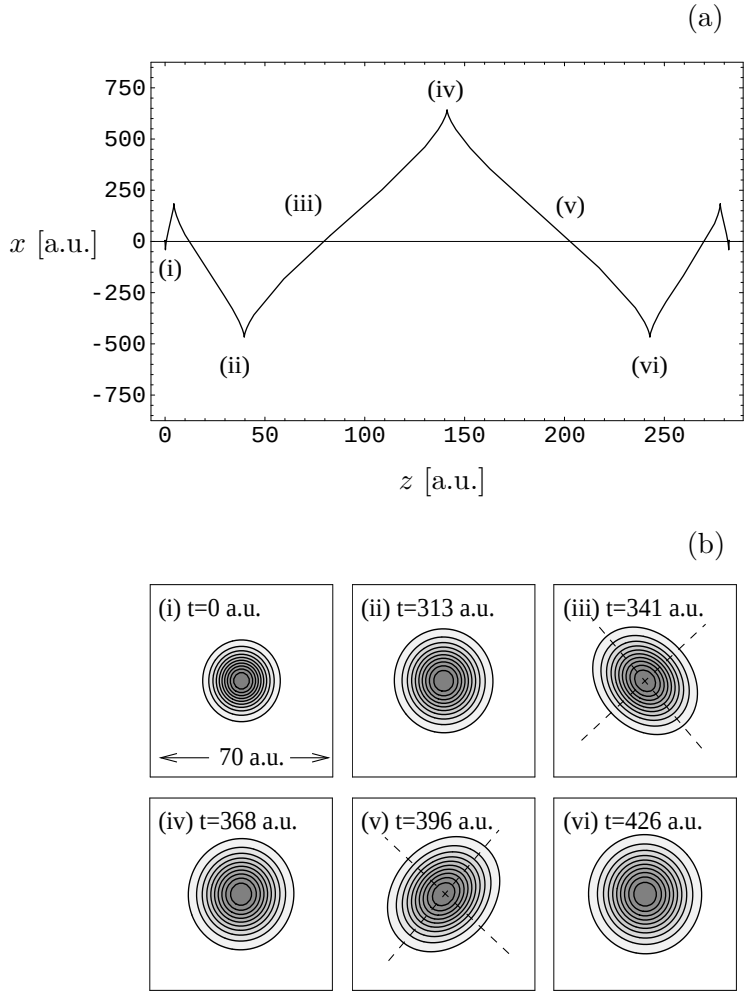

Figure 2.2: Part (a) shows the trajectory of the maximum of the wave packet. The labels (i) to (vi) mark the positions for which the wave packets are plotted in (b). The sides of each of the squares have a width of 70 a.u. In the pictures (iii) and (v), the principle axes of the wave packets are shown. The directions deviate from the diagonals by an angle of $A(t_{iii,v})/(4c^2)$. The other wave packets in (b) are axially symmetric.

spherically symmetric Gaussian distribution:

$$|\psi(x,y,z,t)|^2 = \pi^{-3/2}\left(\Delta p^{-2} + \Delta p^2 t^2\right)^{-3/2} \times \exp - \frac{\left(x - x_0 - p_{m_x} t + \frac{1}{c}\int A dt\right)^2 + \left(y - y_0 - p_{m_y} t\right)^2 + \left(z - z_0 - p_{m_z} t\right)^2}{\Delta p^{-2} + \Delta p^2 t^2}\,. \quad (2.38)$$

The maximum of this wave packet moves like a classical particle, and the spreading dynamics is identical to a free, symmetric Gaussian wave packet [see Eq. (1.21b)].

In dipole approximation, there is no drift in the laser propagation direction because of the vanishing magnetic field. Furthermore, there are no shearing effects which deform the wave packet. The probability distribution remains spherically symmetric.

2.2 Relativistic wave packets

For the case, the driving laser fields become so intense that the charged particles move relativistically, one needs to work with a relativistic wave equation such as the Dirac- or the Klein-Gordon equation. Electrons are particles with spin 1/2, i.e., they are described by the Dirac equation. However, if spin dynamics is not considered, it is sufficient to work with the simpler case of the Klein-Gordon equation for spinless particles.

2.2.1 Gaussian superpositions

In Sec. A.2, the solution of the Klein-Gordon equation for a laser-driven particle has been derived. For a laser wave which is linearly polarized in the x direction and propagates in the z direction, the solution reads

$$\phi(x^\mu) = (2\pi)^{-3/2} \exp i \left[-p_\mu x^\mu + (k_\mu p^\mu)^{-1} \left(\frac{p_{x_0}}{c} \int A \, d\varphi - \frac{1}{2c^2} \int A^2 \, d\varphi \right) \right] . \quad (2.39)$$

The dynamics becomes relativistic due to the laser fields, i.e., the initial momenta $\vec{p}_0$ are nonrelativistic. This is exploited to simplify Eq. (2.39) by expanding terms with respect to p_{x_0}/c, p_{y_0}/c and p_{z_0}/c to quadratic order:

$$p_\mu x^\mu = c^2 t \sqrt{1 + \frac{\vec{p}_0^{\,2}}{c^2}} - \vec{p}_0 \cdot \vec{x} \approx c^2 t + \frac{1}{2} \vec{p}_0^{\,2} t - \vec{p}_0 \cdot \vec{x} \, , \quad (2.40a)$$

$$(k_\mu p^\mu)^{-1} = \frac{1}{\omega} \left(\sqrt{1 + \frac{\vec{p}_0^{\,2}}{c^2}} - \frac{p_{z_0}}{c} \right)^{-1} \approx \frac{1}{\omega} \left(1 + \frac{p_{z_0}}{c} + \frac{p_{z_0}^2}{c^2} - \frac{\vec{p}_0^{\,2}}{2c^2} \right) . \quad (2.40b)$$

With these expansions, the wave function simplifies to the following form where the dependence on the momenta is only of quadratic order:

$$\phi(\vec{x}, t) = (2\pi)^{-3/2} \exp i \left[-c^2 t + \vec{p}_0 \cdot \vec{x} - \frac{1}{2} \vec{p}_0^{\,2} t + \frac{p_{x_0}}{\omega c} \left(1 + \frac{p_{z_0}}{c} \right) \int A \, d\varphi \right.$$
$$\left. - \frac{1}{2\omega c^2} \left(1 + \frac{p_{z_0}}{c} + \frac{p_{z_0}^2}{c^2} - \frac{\vec{p}_0^{\,2}}{2c^2} \right) \int A^2 \, d\varphi \right] . \quad (2.41)$$

To construct a Gaussian wave packet, a coordinate transformation in momentum space has to be carried out to eliminate the mixed term $p_{x_0} p_{z_0}$. The problem then reduces to three one-dimensional integrals which can be solved by means of Eq. (1.33). The quadratic form to be diagonalized is given by

$$qf \equiv \begin{pmatrix} p_{x_0} \\ p_{z_0} \end{pmatrix}^{\mathrm{T}} \begin{pmatrix} a & b \\ b & d \end{pmatrix} \begin{pmatrix} p_{x_0} \\ p_{z_0} \end{pmatrix} ,$$
$$a = -\frac{t}{2} + \frac{1}{4\omega c^4} \int A^2 \, d\varphi \, , \quad d = -\frac{t}{2} - \frac{1}{4\omega c^4} \int A^2 \, d\varphi \, , \quad (2.42)$$
$$b = \frac{1}{2\omega c^2} \int A \, d\varphi \, .$$

As seen in Sec. 2.1.3, such a quadratic form is diagonalized by the following rotation [see Eqs. (2.20) and (2.23)]:

$$\begin{pmatrix} p_{x_0} \\ p_{z_0} \end{pmatrix} = \begin{pmatrix} \cos\alpha & \sin\alpha \\ -\sin\alpha & \cos\alpha \end{pmatrix} \begin{pmatrix} \tilde{p}_{x_0} \\ \tilde{p}_{z_0} \end{pmatrix} , \quad \tan\alpha = -\frac{b}{a - \lambda_-} . \quad (2.43)$$

$\tilde{p}_{x_0}$ and $\tilde{p}_{z_0}$ are the momenta in the transformed coordinate system and $\lambda_\pm$ are the eigenvalues of the matrix in Eq. (2.42) given by

$$\lambda_\pm = \frac{a+d}{2} \pm \frac{a-d}{2}\sqrt{1+\frac{4b^2}{(a-d)^2}}\,. \tag{2.44}$$

With this coordinate transformation, the wave function is rewritten:

$$\begin{aligned}
\phi(\vec{x},t) &= (2\pi)^{-3/2}\exp i\left[-c^2t - \frac{1}{2\omega c^2}\int A^2\,d\varphi + f_x(\tilde{p}_{x_0}) + f_y(p_{y_0}) + f_z(\tilde{p}_{z_0})\right]\,,\\
f_y &= p_{y_0}y - \frac{1}{2}p_{y_0}^2\left(t - \frac{1}{2\omega c^4}\int A^2\,d\varphi\right)\,,\\
f_x &= \tilde{p}_{x_0}\left[\cos\alpha\left(x + \frac{1}{\omega c}\int A\,d\varphi\right) - \sin\alpha\left(z - \frac{1}{2\omega c^3}\int A^2\,d\varphi\right)\right] + \tilde{p}_{x_0}^2\lambda_+\,,\\
f_z &= \tilde{p}_{z_0}\left[\sin\alpha\left(x + \frac{1}{\omega c}\int A\,d\varphi\right) + \cos\alpha\left(z - \frac{1}{2\omega c^3}\int A^2\,d\varphi\right)\right] + \tilde{p}_{z_0}^2\lambda_-\,.
\end{aligned} \tag{2.45}$$

The terms for the eigenvalues and the rotation angle simplify considerably if the following condition is valid:

$$\left(\frac{2b}{a-d}\right)^2 = \left(\frac{\frac{1}{c^2}\int A\,d\varphi}{\frac{1}{2c^4}\int A^2\,d\varphi}\right)^2 \ll 1\,. \tag{2.46}$$

In the relativistic limit, where $A^2/c^4 \gg 1$, this approximation works very well. Furthermore, the vector potential is an oscillating function, because it describes a laser field. The denominator then increases steadily, whereas the numerator oscillates. This means that the validity of the condition in Eq. (2.46) becomes better as the particle propagates. With this condition, the eigenvectors reduce to

$$\lambda_\pm \approx a = -\frac{t}{2} \pm \frac{1}{4\omega c^4}\int A^2\,d\varphi\,, \tag{2.47}$$

and the rotation angle becomes

$$\alpha \approx \tan\alpha = \frac{b}{a-d} = c^2\,\frac{\int A\,d\varphi}{\int A^2\,d\varphi}\,. \tag{2.48}$$

Equations (1.33) and (2.45) yield the wave function of a Gaussian wave packet, where the maximum of the initial momentum $\vec{p}_m$ has been chosen to be zero which means

that the wave packet is initially at rest:

$$\begin{aligned}
\phi(\vec{x},t) &= \pi^{-3/2}\exp i\left[-c^2t-\frac{1}{2\omega c^2}\int A^2\,d\varphi\right]\\
&\quad\times\left[\prod_{m=x,y,z}\frac{1}{\sqrt[4]{\pi}\sqrt{\Delta p^{-1}-i\Delta p f_m''}}\exp-\frac{\frac{\Delta p}{2}f_m'^2}{\Delta p^{-1}-i\Delta p f_m''}\right],\\
f_x' &= \cos\alpha\left(x+\frac{1}{\omega c}\int A\,d\varphi\right)-\sin\alpha\left(z-\frac{1}{2\omega c^3}\int A^2\,d\varphi\right),\\
f_z' &= \sin\alpha\left(x+\frac{1}{\omega c}\int A\,d\varphi\right)+\cos\alpha\left(z-\frac{1}{2\omega c^3}\int A^2\,d\varphi\right),\\
f_x'' &= 2\lambda_+\approx -t+\frac{1}{2\omega c^4}\int A^2\,d\varphi\,,\quad f_y'=y\,,\\
f_z'' &= 2\lambda_-\approx -t-\frac{1}{2\omega c^4}\int A^2\,d\varphi\,,\quad f_y''=f_x''\,.
\end{aligned}\tag{2.49}$$

2.2.2 Charge density

According to Eq. (1.35), the charge density is given by

$$\rho(\vec{x},t)=\frac{i}{2c^2}\left[\phi^*\dot{\phi}-\phi\,\dot{\phi}^*\right]=-c^{-2}\mathrm{Im}(\phi^*\dot{\phi})=-|\phi|^2\mathrm{Im}\frac{\dot{\phi}}{\phi c^2}\,,\tag{2.50}$$

and it can be calculated for the above expression. The following is found:

$$\begin{aligned}
\rho(\vec{x},t) =&|\phi|^2\left[1+\frac{1}{2c^4}A^2\right.\\
&\left.+\sum_{m=x,y,z}\left(\frac{-\frac{1}{2c^2}\dot{f}_m''+\frac{\Delta p^2}{c^2}f_m'\dot{f}_m'f_m''+\frac{\Delta p^2}{2c^2}f_m'^2\dot{f}_m''\frac{\Delta p^{-2}-\Delta p^2 f_m''^2}{\Delta p^{-2}+\Delta p^2 f_m''^2}}{\Delta p^{-2}+\Delta p^2 f_m''^2}\right)\right],\\
|\phi|^2 =&\prod_{m=x,y,z}\frac{1}{\sqrt{\pi}\sqrt{\Delta p^{-2}+\Delta p^2 f_m''^2}}\exp-\frac{f_m'^2}{\Delta p^{-2}+\Delta p^2 f_m''^2}\,.
\end{aligned}\tag{2.51}$$

This expression can be simplified because most of the terms are very small and can be neglected with respect to others. To see this, the order of magnitude of the terms is considered. First, one can utilize the limited range of the Gaussian distribution in Eq. (2.51):

$$\frac{f_m'^2}{\Delta p^{-2}+\Delta p^2 f_m''^2}\equiv n_m\lesssim 5\,.\tag{2.52}$$

The numbers n_m can be estimated to be of the given order, since the Gaussian drops off very quickly, i.e., for higher values of n_m, the charge density approaches zero. For $n_m = 5$, the value for the charge density is already suppressed by a factor of $\exp(5)\approx 150$. The fraction in the numerator of Eq. (2.51) which depends on $\dot{f}_m''$ is a number q_m between one and minus one. The charge density can then be written as

follows:

$$\rho(\vec{x},t) = |\phi|^2 \left[1 + \frac{1}{2c^4}A^2 + \sum_{m=x,y,z}\left(-\frac{\frac{\Delta p^2}{2c^2}\dot{f}''_m}{1+\Delta p^4 f''^2_m} + \frac{\Delta p}{c}\sqrt{n_m}\frac{\dot{f}'_m}{c}\frac{\Delta p f''_m}{\sqrt{\Delta p^{-2}+\Delta p^2 f''^2_m}} + \frac{\Delta p^2}{2c^2}q_m n_m \dot{f}''_m\right)\right] \tag{2.53a}$$

$$\approx |\phi|^2 \left[1 + \frac{1}{2c^4}A^2 + \sum_{m=x,y,z}\frac{\Delta p}{c}\sqrt{n_m}\frac{\dot{f}'_m}{c}\frac{\Delta p f''_m}{\sqrt{\Delta p^{-2}+\Delta p^2 f''^2_m}}\right] \tag{2.53b}$$

The approximation applies because $\dot{f}''_m$ is of the same order as the term $[1 + A^2/(2c^4)]$ and due to the small factor of $\Delta p^2/c^2$ several terms can be neglected. To estimate the magnitude of the remaining terms, the following expressions are needed:

$$\dot{f}'_x = -f'_z\dot{\alpha} + \frac{1}{c}A\cos\alpha + \frac{1}{c^3}A^2\sin\alpha\,, \tag{2.54a}$$

$$\dot{f}'_z = f'_x\dot{\alpha} + \frac{1}{c}A\sin\alpha - \frac{1}{c^3}A^2\cos\alpha\,, \tag{2.54b}$$

$$\dot{f}'_y = 0\,, \tag{2.54c}$$

$$\dot{\alpha} = \frac{\frac{1}{c^2}A - \frac{1}{c^4}A^2\alpha}{\frac{1}{\omega c^4}\int A^2 d\varphi}\,. \tag{2.54d}$$

For the last of these equations, the approximate angle in Eq. (2.48) was used. By means of Eq. (2.52), the values of the following terms can be estimated:

$$f'_x \le \sqrt{n_x}\Delta p|f''_x| = \sqrt{n_x}\Delta p\left|-t + \frac{1}{\omega c^4}\int A^2 d\varphi\right|\,, \tag{2.55a}$$

$$f'_z \le \sqrt{n_z}\Delta p|f''_z| = \sqrt{n_z}\Delta p\left|t + \frac{1}{\omega c^4}\int A^2 d\varphi\right|\,. \tag{2.55b}$$

Since $\int A^2 d\varphi/(\omega c^4)$ grows faster than t in the relativistic case where $A^2/c^4 \gg 1$, the terms $f'_m\dot{\alpha}$ are shown to be smaller by a factor of $\Delta p/c$ compared to the other terms in Eqs. (2.54a) and (2.54b). With this result, the terms $\dot{f}'_m/c$ are seen to be of the order A^2/c^4. This means, the remaining terms in Eq. (2.53b) proportional to $\dot{f}'_m/c$ are reduced by a factor of $\Delta p/c$ with respect to the leading order term $A^2/(2c^4)$. Thus, these terms are the biggest corrections since the other terms which have been neglected have been suppressed by a factor of $(\Delta p/c)^2$.

In all, if correction terms which are suppressed to first order in $\Delta p/c$ with respect to $[1 + A^2/(2c^4)]$ are kept, the result reads:

$$\rho(\vec{x},t) = |\phi|^2\left[1 + \frac{1}{2c^4}A^2 + \sum_{m=x,z}\left(\frac{\frac{\Delta p^2}{c^2}f'_m\dot{f}'_m f''_m}{\Delta p^{-2}+\Delta p^2 f''^2_m}\right)\right]\,. \tag{2.56}$$

Note that this result is obtained without the condition (2.46) and it is valid as long as the condition $(\Delta p/c)^2 \ll 1$ applies.

If the lowest order corrections are neglected as well which can be a good approximation since $\Delta p/c$ is often a small number, one arrives at the rather simple form for the charge density:

$$\rho(\vec{x},t) = \left(1 + \frac{1}{2c^4}A^2\right)\prod_{m=x,y,z}\frac{1}{\sqrt{\pi}\sqrt{\Delta p^{-2}+\Delta p^2 f''^2_m}}\exp -\frac{f'^2_m}{\Delta p^{-2}+\Delta p^2 f''^2_m}\,. \tag{2.57}$$

Example

To visualize the result for the charge density (2.57), wave packets are plotted for different laser intensities and for different times. The electron is driven by the following laser pulse of 20 cycles with a $\cos^2$-like envelope:

$$A(\varphi) = A_0 \cos(\varphi - 20\pi) \cos^2[(\varphi - 20\pi)/40] \,, \quad 0 \leq \varphi \leq 40\pi \,, \tag{2.58}$$

The laser pulse is shown in Fig. 2.3. The initial width of the wave packet in momentum

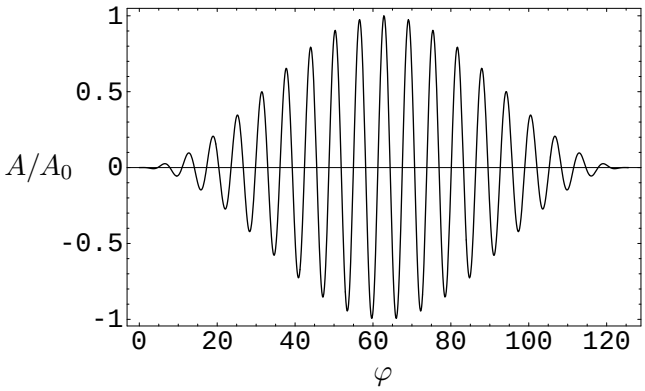

Figure 2.3: In the following, the electron dynamics in this laser pulse of 20 cycles with a $\cos^2$-like envelope is discussed.

space is chosen to be $\Delta p = 1$ a.u., and the laser wave length is 800 nm, again. The laser intensity is expressed by the maximum γ-factor which is reached when half of the laser pulse has passed the wave packet maximum, i.e. $\gamma_m = 1 + A_0^2/(2c^4)$. Charge densities are plotted in the x-z plane for the range between the maximal density and the density which is by a factor of e^4 smaller (with e being the Euler number).

Figure 2.4 shows the wave packets for different laser intensities as it is placed at the turning point $\varphi = 5.5\pi$. The wave packet changes from a symmetric to a bent shape as the laser intensity increases.

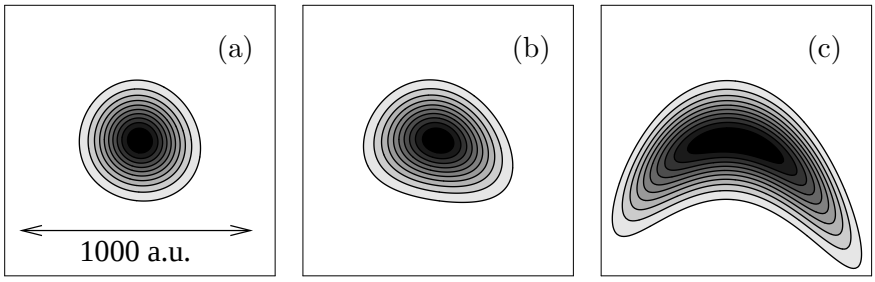

Figure 2.4: The charge densities for different energies [(a) $\gamma_m = 10$, (b) $\gamma_m = 50$, (c) $\gamma_m = 250$] are plotted for the early turning point $\varphi = 5.5\pi = 17.3$. It is seen that the wave packet changes its shape as the energy increases.

The plots at the instant when the maximum kinetic energy is reached are shown in Fig. 2.5. It is seen that with higher energies, the wave packet widths become smaller for one direction whereas they increase for the orthogonal direction. This behavior explains why in the relativistic recollision model which will be introduced in Chapter 4,

the yields of recollisions decrease for higher energies because the yields depend on the widths perpendicular to the direction of motion.

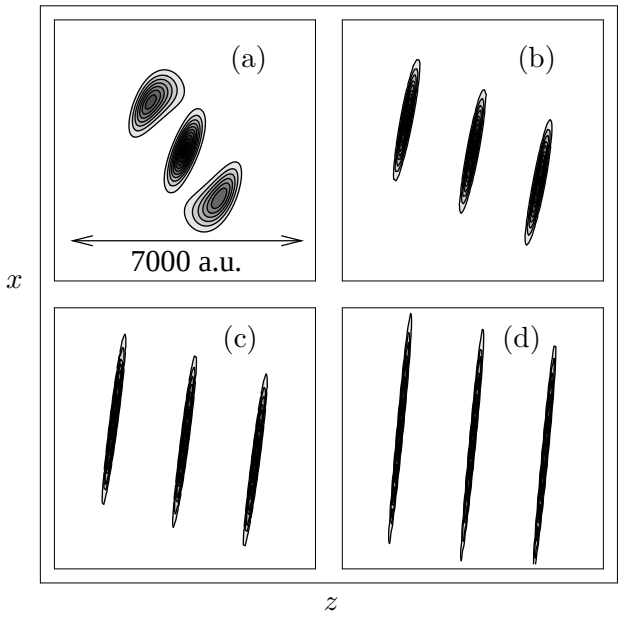

Figure 2.5: The wave packets are plotted at the instants of maximal energy ($\varphi = 20\pi = 62.8$) and both 30 a.u. earlier and later to indicate the motion [(a) $\gamma_m = 2$, (b) $\gamma_m = 10$, (c) $\gamma_m = 25$, (d) $\gamma_m = 50$]. This shows that the wave packets hardly change for high energies during this period of time.

Phase effects can nicely be seen when the wave packet has evolved to extensions comparable to the laser wave lengths. This is seen in Fig. 2.6, where the charge densities are plotted at an instant when the laser pulse has almost passed completely. For high energies, the charge distribution spreads quickly in the z direction and different parts see different laser phases such that the oscillations of the laser field can be seen. The amplitude of the curved charge density increases in the z direction since the passing laser pulse has a higher intensity there.

2.2.3 Time dilation and Lorentz contraction

Some expressions in Eq. (2.57) have simple interpretations, which become obvious if the classical physics of laser-driven particles is considered. According to the classical solution (A.9), the relativistic γ-factor of an electron is given by

$$\begin{aligned} \gamma &= \frac{\kappa}{2c} + \frac{c^2 + p_{x_0}^2 + p_{y_0}^2}{2\kappa c} - \frac{p_{x_0}}{\kappa c^2} A(\varphi) + \frac{1}{2\kappa c^3} A^2(\varphi)\,, \\ \kappa &\equiv \sqrt{c^2 + p_{x_0}^2 + p_{y_0}^2 + p_{z_0}^2} - p_{z_0}\,, \end{aligned} \tag{2.59}$$

which reduces to the simple form

$$\gamma = 1 + \frac{1}{2c^4} A^2(\varphi)\,, \tag{2.60}$$

if the initial velocity vanishes. Here, the wave packet consists of a Gaussian superposition which is centered about the solution with vanishing initial momentum. The

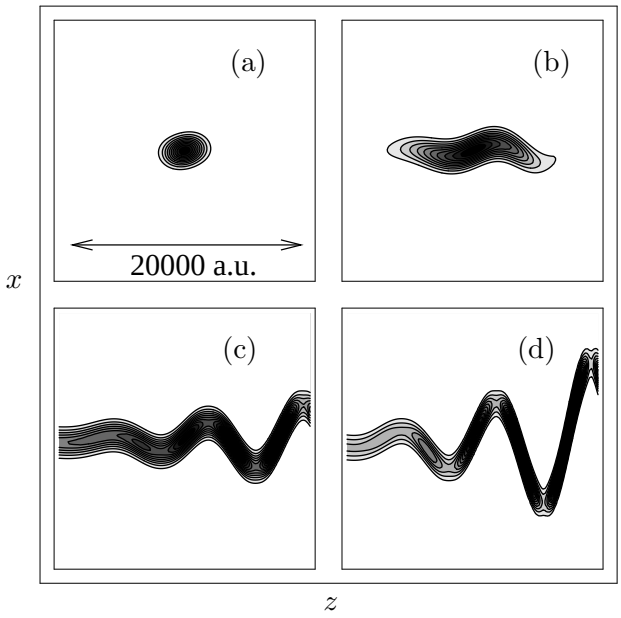

Figure 2.6: As shown here, the charge distributions have spread more extensively for higher energies [(a) $\gamma_m = 2$, (b) $\gamma_m = 10$, (c) $\gamma_m = 50$, (d) $\gamma_m = 250$] such that the phase dependence can be seen over several laser periods. The laser pulse has almost passed completely at the wave packet maximum ($\varphi = 36\pi = 113.1$).

expression in Eq. (2.60) is precisely the factor occurring in the probability density (2.57). The physical interpretation is that the probability density is increased by the γ-factor due to Lorentz contraction.

The electromagnetic laser fields do not exert a force on the particle in the y direction. However, the dynamics is influenced if the motion in the x-z plane is relativistic. The classical motion in the y direction is given by

$$y = \frac{p_{y_0} c}{\kappa\omega}\varphi\,. \tag{2.61}$$

The meaning of the dependence on the phase can be further analyzed. With the equation of motion in the z direction

$$z = \frac{c}{2\omega}\left(\frac{c^2 + p_{x_0}^2 + p_{y_0}^2}{\kappa^2} - 1\right)\varphi - \frac{p_{x_0}}{\kappa^2\omega}\int A(\varphi)d\varphi + \frac{1}{2\kappa^2\omega c}\int A^2(\varphi)d\varphi\,, \tag{2.62}$$

the following relation between the γ-factor and the phase is found:

$$\gamma = \frac{\kappa}{c}\frac{d}{d\varphi}\left(\varphi + \frac{\omega}{c}z(\varphi)\right) = \frac{\omega\kappa}{c}\frac{dt}{d\varphi}\,. \tag{2.63}$$

This equation is employed to yield the proper time τ of the laser driven particle:

$$\tau = \int \gamma^{-1} dt = \frac{c}{\kappa\omega}\varphi\,. \tag{2.64}$$

Thus, the proper time is found to be proportional to the phase. The equation of motion in the y direction (2.61) then reduces to the very intuitive form

$$y = p_{y_0}\tau\,, \tag{2.65}$$

which is equal to a free, nonrelativistic motion, where the time t is replaced by the proper time τ.

Such an effect is found for the wave packet dynamics, too. According to Eqs. (2.49) and (2.57), the time-dependent width in the y direction is given by

$$\Delta w_y = \sqrt{\Delta p^{-2} + \Delta p^2 \left(t - \frac{1}{2\omega c^4} \int A^2 \, d\varphi \right)^2} \,. \tag{2.66}$$

For vanishing initial momenta as for the maximum of the initial Gaussian superposition [see Eqs. (2.62) and (2.64)], this reduces to

$$\Delta w_y = \sqrt{\Delta p^{-2} + \Delta p^2 \tau^2} \,. \tag{2.67}$$

This is the nonrelativistic expression for a freely spreading particle [compare Eqs. (1.21b) and (2.17)], where again, the time t is replaced by the proper time τ. This means that wave packet spreading is slowed down in the y direction due to time dilation of the relativistically moving particle.

The same behavior is found in the x direction, whereas the spreading dynamics is different for the z direction. The reason is that the time dilation occurs next to other effects like the direct influence of the laser fields or Lorentz contraction.

Chapter 3

Electron dynamics in crossed laser beams

Crossed laser beams have been discussed in the context of various applications such as particle acceleration [82], high harmonic generation [83] or stochastic electron acceleration [84, 85]. Furthermore, standing wave configurations of linear [27, 28, 29] and circular [19] polarization have been proposed to overcome the problem of the Lorentz drift which suppresses recollisions in intense, propagating laser fields. These standing wave configurations are of interest here.

Experimentally, counterpropagating, strong laser fields have been created by means of a beam splitter and mirrors [86]. In this setup, an intensity of the order $10^{19}\,\mathrm{W/cm^2}$ was achieved which implies relativistic electron dynamics. Furthermore, a new laser system, the Astra Gemini project which is currently under construction, will provide two separate laser beams of intensities up to $10^{22}\,\mathrm{W/cm^2}$ (for details see [87]). Thus, crossed laser beams in the highly relativistic regime are expected to be available in the near future.

Whereas previous work on the electron dynamics in standing waves is based on numerical methods, it is examined analytically, in this chapter. This allows to gain more insight into the electron dynamics in crossed fields.

The two configurations of interest both have the feature that the Lorentz force due to the magnetic field vanishes on certain axes. However, the difference is that the magnetic field itself is zero only in the case of linear laser polarization. This gives rise to a different behavior of electrons moving in the vicinity of these axes.

In this chapter, the laser configurations are first introduced, before the classical, relativistic dynamics is established. A quantum mechanical analysis is then carried out for the nonrelativistic case. Finally, the results of the classical treatment are employed for a relativistic wave packet approach.

3.1 Laser configurations

First of all, the two laser configurations are introduced. They are constructed by the superposition of two counterpropagating plane waves which are either linearly or circularly polarized. The two configurations are discussed separately.

Linear polarization

The electromagnetic fields of two counterpropagating waves are superimposed as follows:

$$\vec{E}_l = \frac{1}{2}E_0[\cos(\omega t - kz) + \cos(\omega t + kz)]\hat{x} = E_0 \cos(\omega t)\cos(kz)\hat{x}\,, \tag{3.1a}$$

$$\vec{B}_l = \frac{1}{2}E_0[\cos(\omega t - kz) - \cos(\omega t + kz)]\hat{y} = E_0 \sin(\omega t)\sin(kz)\hat{y}\,, \tag{3.1b}$$

$$\vec{A}_l = -E_0\frac{c}{2\omega}[\sin(\omega t - kz) + \sin(\omega t + kz)]\hat{x} = -E_0\frac{c}{\omega}\sin(\omega t)\cos(kz)\hat{x}\,. \tag{3.1c}$$

Here, the light is polarized in the x direction and the propagation is in the $\pm z$ direction.

It is clear that the magnetic field vanishes for $kz = n\pi$ (with n being an integer) whereas the electric field has maximal amplitude. Thus, the dynamics of electrons moving in these planes will be dominated by the electric field. Figure 3.1 shows the field configuration for the vicinity of $z = 0$, i.e. for $(kz)^2 \ll 1$. The fields do not depend on x and y.

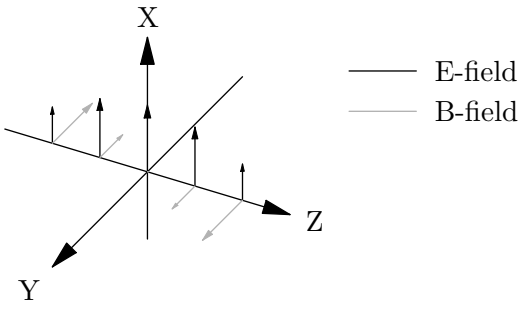

Figure 3.1: The field configuration for two counterpropagating laser fields with linear polarization in the x direction is depicted. The laser fields are plane waves propagating in the z direction. The fields are shown in the vicinity of $z = 0$, where the magnetic field is small.

Circular polarization

The other field configuration of interest is the superposition of the following two counterpropagating, circularly polarized waves:

$$\begin{aligned}\vec{E}_c &= \frac{1}{2}E_0\{[\cos(\omega t - kz)\hat{x} + \sin(\omega t - kz)\hat{y}] + [\cos(\omega t + kz)\hat{x} - \sin(\omega t + kz)\hat{y}]\} \\ &= E_0\cos(\omega t)[\cos(kz)\hat{x} - \sin(kz)\hat{y}]\,,\end{aligned} \tag{3.2a}$$

$$\begin{aligned}\vec{B}_c &= \frac{1}{2}E_0\,\{[\cos(\omega t - kz)\hat{y} - \sin(\omega t - kz)\hat{x}] + [-\cos(\omega t + kz)\hat{y} - \sin(\omega t + kz)\hat{x}]\} \\ &= -E_0\sin(\omega t)[\cos(kz)\hat{x} - \sin(kz)\hat{y}]\,,\end{aligned} \tag{3.2b}$$

$$\begin{aligned}\vec{A}_c &= -E_0\frac{c}{\omega}\{[\sin(\omega t - kz)\hat{x} - \cos(\omega t - kz)\hat{y}] + [\sin(\omega t + kz)\hat{x} + \cos(\omega t + kz)\hat{y}]\} \\ &= -E_0\frac{c}{\omega}\sin(\omega t)[\cos(kz)\hat{x} - \sin(kz)\hat{y}]\,.\end{aligned} \tag{3.2c}$$

In this configuration, the magnetic field is antiparallel to the electric field, i.e., if an electron moves in the E-field direction, the Lorentz force $\vec{F} = \dot{\vec{x}}/c \times \vec{B}$ vanishes despite

the fact that the magnetic field is nonzero. The field configuration is shown in Fig. 3.2. In contrast to the configuration of linear laser polarization, axes with vanishing Lorentz

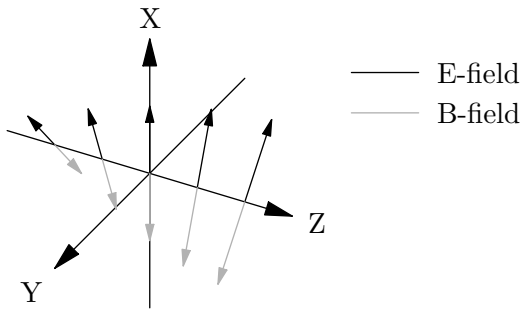

Figure 3.2: The field configuration for two counterpropagating laser fields with circular polarization are shown for the vicinity of $z = 0$. The plane laser waves propagate in the z direction. In this configuration, the magnetic field is antiparallel to the electric field.

force are given for any z position. This is a great advantage if the scheme is applied to an extended sample where many recollisions are driven in parallel [19].

3.2 Relativistic classical particle dynamics

Before discussing the quantum mechanical behavior, the classical dynamics of an electron is examined, which moves in the vicinity of an axis with vanishing Lorentz force. The classical electron dynamics is dominated by the simple one-dimensional oscillation which is found if the particle is placed exactly on the axis with vanishing initial momentum. With slightly different initial conditions, the motion deviates from the ideal oscillation. Different regimes of laser intensities are considered. Later on, the classical solutions are employed to describe the dynamics of wave packets by means of the Monte-Carlo approach discussed in Sec. 1.1.1.

3.2.1 Simplified equations of motion

A classical particle which is driven by the standing laser fields introduced in the previous section is described by three nonlinear coupled differential equations for which a general analytical solution is not available. However, if the particle dynamics deviates only slightly from the ideal one-dimensional motion along an axis, the equations can be simplified, decoupled and partly solved analytically.

Linear polarization

The relativistic classical equations of motion are given by

$$\frac{d}{dt}\left(\gamma\dot{\vec{x}}\right) = \vec{E} + \frac{\dot{\vec{x}}}{c} \times \vec{B} \quad \text{with} \quad \gamma = \left(1 - \frac{\dot{\vec{x}} \cdot \dot{\vec{x}}}{c^2}\right)^{-1/2} . \tag{3.3}$$

For the case of linear laser polarization [see Eqs. (3.1)], they read

$$\frac{d}{dt}\left(\gamma\dot{x}\right) = E_0\left(\cos(\omega t)\cos(kz) - \frac{\dot{z}}{c}\sin(\omega t)\sin(kz)\right), \tag{3.4a}$$

$$\frac{d}{dt}\left(\gamma\dot{y}\right) = 0\,, \tag{3.4b}$$

$$\frac{d}{dt}\left(\gamma\dot{z}\right) = E_0\frac{\dot{x}}{c}\sin(\omega t)\sin(kz)\,. \tag{3.4c}$$

To simplify these equations, several approximations can be applied. First, kz is assumed to be small. Consider the following example for visible laser light with the wave length $\lambda = 800$ nm. The absolute value of the wave vector evaluates to $k = 2\pi/\lambda \approx 4.2 \times 10^{-4}$ a.u. The particle is expected to move in the vicinity of the ideal plane $z = 0$, i.e., as long as the displacement is not greater than a few hundred atomic units, kz remains below a small number of the order 10^{-1}. The case of higher displacements means that the electron leaves the vicinity of the ideal axis. Thus, the trajectory cannot be considered to be stable anymore and its further dynamics is no longer of interest. However, the examples considered here are in the regime where kz remains small. Second, the motion in the y and the z direction is assumed to be nonrelativistic, i.e., $\dot{y}/c$ and $\dot{z}/c$ are small. This is reasonable, because the initial conditions are nonrelativistic and the acceleration by the electric field is in the x direction. If these assumptions are fulfilled, the small terms can be considered up to linear order and higher order terms are only small corrections. The results of the examples considered later on will comply with these assumptions, i.e., the following approximations are justified:

$$\sin(kz) \approx kz\,, \quad \cos(kz) \approx 1\,, \tag{3.5a}$$

$$\left(\frac{\dot{y}}{c}\right)^2 \approx \left(\frac{\dot{z}}{c}\right)^2 \approx \frac{\dot{y}}{c}\cdot\frac{\dot{z}}{c} \approx 0\,, \tag{3.5b}$$

$$\frac{\dot{y}}{c}\cdot kz \approx \frac{\dot{z}}{c}\cdot kz \approx 0\,. \tag{3.5c}$$

Now, the simplified set of equations adopts the following form:

$$\frac{d}{dt}\left(\gamma\dot{x}\right) = E_0\cos(\omega t)\,, \tag{3.6a}$$

$$\frac{d}{dt}\left(\gamma\dot{y}\right) = 0\,, \tag{3.6b}$$

$$\frac{d}{dt}\left(\gamma\dot{z}\right) = E_0\frac{\dot{x}}{c}\sin(\omega t)kz\,, \tag{3.6c}$$

$$\gamma = \left(1 - \frac{\dot{x}^2}{c^2}\right)^{-1/2}. \tag{3.6d}$$

From Eqs. (3.6a) and (3.6d) the γ-factor is found to be

$$\gamma = \sqrt{1 + \left(R\sin(\omega t) + \frac{p_{x_0}}{c}\right)^2} \approx \sqrt{1 + R^2\sin^2(\omega t)} + \frac{R\sin(\omega t)}{\sqrt{1 + R^2\sin^2(\omega t)}}\cdot\frac{p_{x_0}}{c}\,, \tag{3.7}$$

with the definition $R \equiv E_0/(\omega c)$ and the initial condition for the momentum $\gamma\dot{\vec{x}}(t=0) = \vec{p}_0 \equiv (p_{x_0}, p_{y_0}, p_{z_0})$. For nonrelativistic initial velocities considered here, i.e. for $p_{x_0}/c \ll 1$, the γ-factor can be expanded with respect to p_{x_0}/c and it is seen, that the term of first order in p_{x_0}/c is only a small correction to the leading term.

With the expression for the γ-factor, the motion in the x direction is found to be

$$\frac{\dot{x}}{c} = \frac{R\sin(\omega t) + \frac{p_{x_0}}{c}}{\sqrt{1 + \left(R\sin(\omega t) + \frac{p_{x_0}}{c}\right)^2}} \approx \frac{R\sin(\omega t)}{\sqrt{1 + R^2\sin^2(\omega t)}} + \frac{p_{x_0}/c}{\left(1 + R^2\sin^2(\omega t)\right)^{3/2}}\,, \tag{3.8a}$$

$$x \approx -\frac{c}{\omega}\arcsin\left[\frac{R}{\sqrt{1+R^2}}\cos(\omega t)\right] + p_{x_0}\int \frac{dt}{\left[1 + R^2\sin^2(\omega t)\right]^{3/2}} + x_0\,, \tag{3.8b}$$

where the initial position is defined by $\vec{x}(t=0) = (x_0, y_0, z_0)$. The approximations are again a first order expansion with respect to p_{x_0}/c.

Finally, the following equations of motion for the y and the z direction are found

$$\dot{y} = \frac{p_y}{\sqrt{1 + R^2\sin^2(\omega t)}}\,, \tag{3.9a}$$

$$\frac{d}{dt}(\gamma\dot{z}) = R^2\omega^2\frac{\sin^2(\omega t)}{\sqrt{1 + R^2\sin^2(\omega t)}}z\,, \tag{3.9b}$$

where the small terms p_{x_0}/c, p_{y_0}/c and kz are again considered to first order.

Figure 3.3 shows the motion of an electron for one laser period according to Eqs. (3.8) and (3.9). The diagrams depict the position depending on time for the moderately relativistic case of $R = 1.5$. It can be seen that the motion is dominated by an oscillatory motion in the electric field direction. The motion in the z direction is unstable, i.e., the distance from the plane $z = 0$ grows rapidly.

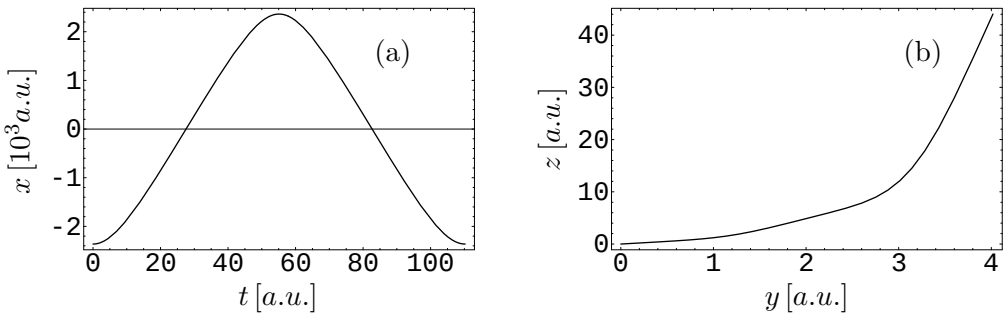

Figure 3.3: The motion of an electron in a linearly polarized standing laser field is shown for the moderately relativistic parameter of $R = 1.5$. The dynamics is plotted for one complete laser cycle with the initial momentum of the electron $p_{x_0} = 0$, $p_{y_0} = p_{z_0} = 0.05$ a.u. Part (a) shows the time-dependent motion in the polarization direction. In (b) the trajectory in the y-z plane is depicted. It is seen that the motion in the z direction is unstable.

Before further investigating Eqs. (3.9) for certain limits of R, the analog procedure is carried out for the case of circular laser polarization.

Circular polarization

The equations of motion (3.3) for circular laser polarization [see Eqs. (3.2)] adopt the following form:

$$\frac{d}{dt}(\gamma\dot{x}) = E_0\left[\cos(\omega t)\cos(kz) - \frac{\dot{z}}{c}\sin(\omega t)\sin(kz)\right], \tag{3.10a}$$

$$\frac{d}{dt}(\gamma\dot{y}) = -E_0\left[\cos(\omega t)\sin(kz) + \frac{\dot{z}}{c}\sin(\omega t)\cos(kz)\right], \tag{3.10b}$$

$$\frac{d}{dt}(\gamma\dot{z}) = E_0\left[\frac{\dot{x}}{c}\sin(\omega t)\sin(kz) + \frac{\dot{y}}{c}\sin(\omega t)\cos(kz)\right]. \tag{3.10c}$$

With the same approximations (3.5) as applied in the previous case, one finds the following simplified equations:

$$\frac{d}{dt}(\gamma\dot{x}) = E_0\cos(\omega t), \tag{3.11a}$$

$$\frac{d}{dt}(\gamma\dot{y}) = -E_0\left[kz\cos(\omega t) + \frac{\dot{z}}{c}\sin(\omega t)\right], \tag{3.11b}$$

$$\frac{d}{dt}(\gamma\dot{z}) = E_0\left[\frac{\dot{x}}{c}\sin(\omega t)kz + \frac{\dot{y}}{c}\sin(\omega t)\right], \tag{3.11c}$$

$$\gamma = \left(1 - \frac{\dot{x}^2}{c^2}\right)^{-1/2}. \tag{3.11d}$$

Comparing these equations with Eqs. (3.6), it is seen that the dynamics of the γ-factor and the motion in the x direction are identical to the case of linear laser polarization [see Eqs. (3.7) and (3.8)]. Now, Eq. (3.11b) can be integrated to yield

$$\dot{y} = \frac{p_y - R\omega\sin(\omega t)z}{\sqrt{1 + R^2\sin^2(\omega t)}}. \tag{3.12}$$

The dynamics in the z direction is then given by

$$\frac{d}{dt}(\gamma\dot{z}) \approx \frac{R\omega\sin(\omega t)p_y}{\sqrt{1 + R^2\sin^2(\omega t)}}, \tag{3.13a}$$

$$\dot{z} \approx \frac{p_z - p_y\left[\arcsin\left(\frac{R}{\sqrt{1+R^2}}\cos(\omega t)\right) - \arcsin\frac{R}{\sqrt{1+R^2}}\right]}{\sqrt{1 + R^2\sin^2(\omega t)}}. \tag{3.13b}$$

Here, quadratic terms of p_{x_0}/c, p_{y_0}/c and kz have again been dropped.

The motion of an electron according to Eqs. (3.8), (3.12) and (3.13b) is shown in Fig. (3.4) for the relativistic value $R = 25$. The diagram for the motion in the electric field direction reduces to an inharmonic triangular shape, because the velocity is limited by the speed of light. As compared to the case of linear polarization (see Fig. 3.3), there is no instability in the z direction.

3.2.2 Nonrelativistic limit

The equations of motion derived above can be further simplified if the nonrelativistic limit is considered. In this case, the velocity v of the particle is small compared to

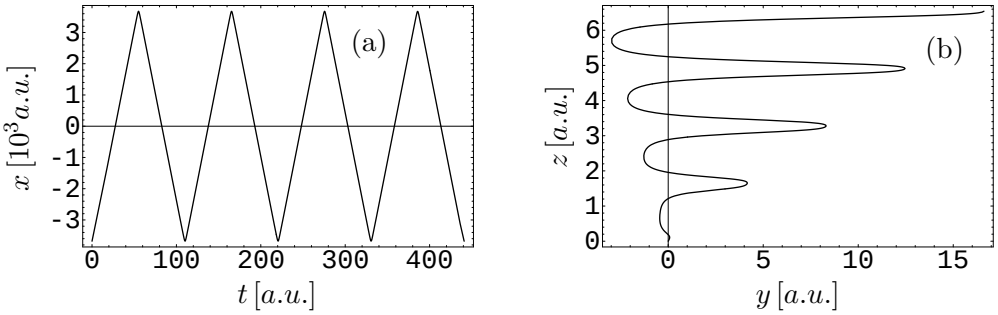

Figure 3.4: The motion of an electron in a circularly polarized standing laser field is depicted for four laser cycles. Part (a) shows the dynamics in the x directions whereas (b) shows the trajectory in the y-z plane, i.e. perpendicular to the electric field. With the parameter $R = 25$ the motion is relativistic. The initial momentum is chosen to be $p_{x_0} = 0$, $p_{y_0} = p_{z_0} = 0.05$ a.u.

the speed of light and quadratic terms of v/c can be neglected. The γ-factor then reduces to one and the equations of motion (3.3) simplify from the beginning. The nonrelativistic limit can as well be obtained from the fully relativistic equations of motion by considering the parameter R and the initial velocity over c to be small such that quadratic terms thereof can be neglected.

Linear polarization

With the γ-factor equal to unity, the equations of motion (3.6) are rewritten:

$$\ddot{x} = E_0 \cos(\omega t)\,, \tag{3.14a}$$

$$\ddot{y} = 0\,, \tag{3.14b}$$

$$\frac{d}{dt}\frac{\dot{z}}{c} = R\omega\frac{\dot{x}}{c}\sin(\omega t)kz \approx 0\,. \tag{3.14c}$$

The approximation in Eq. (3.14c) applies since besides kz both $\dot{x}/c$ and R are small numbers in the nonrelativistic case. These equations are solved immediately and yield the following result:

$$x = -\frac{Rc}{\omega}\cos(\omega t) + p_{x_0} t + x_0\,, \tag{3.15a}$$

$$y = p_{y_0} t + y_0\,, \tag{3.15b}$$

$$z = p_{z_0} t + z_0\,. \tag{3.15c}$$

The motion in the y and the z direction is equal to that of a free particle. In the polarization direction, one finds a harmonic oscillation caused by the electric field of the laser and an additional drift term $p_{x_0} t$.

Circular polarization

As in the relativistic case, the dynamics in the x direction is equal to the case of linear polarization. The motion in the other directions can be obtained with $\gamma = 1$ and by neglecting terms of the order R^2 in Eqs. (3.12) and (3.13a). The following equations

are found:

$$\dot{x} = Rc\sin(\omega t) + p_{x_0}\,, \tag{3.16a}$$
$$\dot{y} = p_{y_0} - R\omega\sin(\omega t)z\,, \tag{3.16b}$$
$$\dot{z} = p_{z_0} + R[1-\cos(\omega t)]p_{y_0}\,, \tag{3.16c}$$
$$x = -\frac{Rc}{\omega}\cos(\omega t) + p_{x_0}t + x_0\,, \tag{3.16d}$$
$$y = p_{y_0}t + y_0 + R\left(t - \frac{1}{\omega}\sin(\omega t)\right)p_{z_0} - R(p_{z_0}t + z_0)[1-\cos(\omega t)]\,, \tag{3.16e}$$
$$z = p_{z_0}t + z_0 + R\left(t - \frac{1}{\omega}\sin(\omega t)\right)p_{y_0}\,. \tag{3.16f}$$

The dynamics in the y and the z directions differ slightly by the terms proportional to R. This is due to the different magnetic fields of the two configurations.

3.2.3 Highly relativistic case

The fully relativistic equations of motion can also be simplified for the interesting case that the motion in the x direction becomes highly relativistic. In this limit, the approximation $R^2 \gg 1$ can be applied, i.e., terms of the order one are neglected with respect to those of the order R^2. With this approximation, the position can be determined analytically at several interesting instants of time, e.g., after a quarter of a period when the particle has reached its maximum speed or after a full period. According to Eq. (3.7) the maximum value of the γ-factor becomes $\gamma_m = R$.

Linear polarization

To integrate the equation of motion for the y direction (3.9a) two different periods of time are considered:

$$\dot{y} = \frac{p_y}{\sqrt{1+R^2\sin^2(\omega t)}} = \begin{cases} \dfrac{p_y}{\sqrt{1+(R\omega t)^2}}\,, & \sin^2(\omega t) \ll 1 \\ \dfrac{p_y}{R\sin(\omega t)}\,, & R^2\sin^2(\omega t) \gg 1\,. \end{cases} \tag{3.17}$$

These terms can be integrated to yield

$$y = \frac{p_y}{R\omega}\mathrm{arsinh}(R\omega t) + y_0\,,\ \text{for}\ \sin^2(\omega t) \ll 1\,, \tag{3.18a}$$
$$y = \frac{p_y}{R\omega}\log\left(\tan\frac{\omega t}{2}\right) + \tilde{y}_0\,,\ \text{for}\ R^2\sin^2(\omega t) \gg 1\,. \tag{3.18b}$$

Now, the integration constant $\tilde{y}_0$ needs to be matched such that the function is continuous. At the matching point $\tilde{t}$, which needs not to be specified here, both conditions $\sin^2(\omega\tilde{t}) \ll 1$ and $R^2\sin^2(\omega\tilde{t}) \gg 1$ have to be valid. These are used for the following approximations:

$$\mathrm{arsinh}(R\omega\tilde{t}) = \log\left(R\omega\tilde{t} + \sqrt{1+(R\omega\tilde{t})^2}\right) \approx \log(2R\omega\tilde{t})\,, \tag{3.19a}$$
$$\log\left(\tan\frac{\omega\tilde{t}}{2}\right) \approx \log\left(\frac{\omega\tilde{t}}{2}\right)\,. \tag{3.19b}$$

The condition that the function in Eqs. (3.18) is continuous gives

$$\tilde{y}_0 = \frac{p_y}{R\omega}\log(4R) + y_0\,. \tag{3.20}$$

The error of this result decreases as R increases, because the requirements $R^2\sin^2(\omega t) \gg 1$ and $\sin^2(\omega t) \ll 1$ can be better fulfilled simultaneously in the area where the two functions (3.18a) and (3.18b) have to match. A comparison of this result for $y(\omega t = \pi/2) = \tilde{y}_0$ with a numerical integration of Eq. (3.9a) for the moderate value of $R = 10$, gives a relative error of less than 0.2%.

Note, that the distance the particle travels in the y direction during the time given by $\omega t = \pi/2$ scales like $\log(4R)/R$, i.e., the greater the laser intensity becomes, the closer the electron stays to the initial position y_0. This can be understood as follows. According to Eq. (3.6b), the momentum in the y direction is constant: $\gamma\dot{y} = p_{y_0}$. This means, if the γ-factor becomes high due to the relativistic motion in the x direction, $\dot{y}$ becomes small.

Since the equation of motion (3.9a) is both symmetric with respect to $\omega t_0 = \pi/2$ and periodic in π, the y position for any multiple n of t_0 is given by

$$y\left(\omega t = n\frac{\pi}{2}\right) = n\frac{p_y}{R\omega}\log(4R) + y_0\,. \tag{3.21}$$

To investigate the dynamics in the z direction, the differential equation (3.9b) has to be analyzed. It can be rearranged to the form

$$\left[1 + R^2\sin^2(\omega t)\right]\frac{\ddot{z}}{\omega^2} = -R^2\sin(\omega t)\cos(\omega t)\frac{\dot{z}}{\omega} + R^2\sin^2(\omega t)z\,, \tag{3.22}$$

where the dependence of p_{x_0} has been neglected in the γ-factor (3.7), because in the relativistic regime, the term proportional to p_{x_0} is suppressed by the second order term $R^{-1}\cdot p_{x_0}/c$ with respect to the leading order term. The resulting equation is examined separately for two different time domains and reduces to the following simplified equations:

$$\left[1 + (R\omega t)^2\right]\frac{\ddot{z}}{\omega^2} = -R^2\omega t\frac{\dot{z}}{\omega} + (R\omega t)^2 z\,,\ \text{for}\ \sin^2(\omega t) \ll 1\,, \tag{3.23a}$$

$$\frac{\ddot{z}}{\omega^2} = -\cot(\omega t)\frac{\dot{z}}{\omega} + z\,,\ \text{for}\ R^2\sin^2(\omega t) \gg 1\,. \tag{3.23b}$$

The first equation can be solved perturbatively:

$$\left[R^{-2} + (\omega t)^2\right]\frac{\ddot{z}}{\omega^2} + \omega t\frac{\dot{z}}{\omega} - (\omega t)^2 z_0 = \lambda(\omega t)^2(z - z_0)\,, \tag{3.24a}$$

$$z(t) = f_0(t) + \lambda f_1(t) + \dots\,. \tag{3.24b}$$

The parameter λ is equal to unity and serves only to count the orders of the perturbation expansion. By inserting the ansatz (3.24b) into Eq. (3.24a), a differential equation is found for each order of λ which can be solved successively. With the right hand side of Eq. (3.24a) being a small perturbation, the series converges quickly. The dominating part of the solution is given by the zeroth order term $f_0(t)$, whereas the first order correction can be used to control the error.

The inhomogeneous linear differential equation of zeroth order in λ is solved by the ansatz

$$\frac{\dot{f}_0}{\omega} = \frac{p(t)}{\sqrt{1 + (R\omega t)^2}}\,. \tag{3.25}$$

This gives a condition for the function $p(t)$ introduced in the ansatz:

$$\frac{\dot{p}}{\omega} = \frac{(R\omega t)^2 z_0}{\sqrt{1+(R\omega t)^2}}\,. \tag{3.26}$$

With the integration of this expression one finds (to zeroth order of λ):

$$\dot{z} = \frac{p_{z_0}}{\sqrt{1+(R\omega t)^2}} + \frac{\omega}{2}\left(\omega t - \frac{\operatorname{arsinh}(R\omega t)}{R\sqrt{1+(R\omega t)^2}}\right) z_0\,, \tag{3.27a}$$

$$z = \frac{p_{z_0}}{R\omega}\operatorname{arsinh}(R\omega t) + z_0\left(1 + \frac{(\omega t)^2}{4} - \frac{\operatorname{arsinh}^2(R\omega t)}{4R^2}\right)\,. \tag{3.27b}$$

Note that Eq. (3.27b) yields the nonrelativistic solution (3.15c) if R becomes small such that $\operatorname{arsinh}(R\omega t) \approx R\omega t$ applies. This means that the lowest order of the expansion (3.24b) reduces to the exact solution as R decreases. In order to estimate how well the lowest order approximation works for high values of R, the correction term $f_1(t)$ of the order λ^1 is evaluated for the limit $R \gg 1$. Then, f_0 reduces to

$$f_0 \approx \left(1 + \frac{1}{4}(\omega t)^2\right) z_0\,. \tag{3.28}$$

The first order correction is found to be

$$\frac{\dot{f}_1}{\omega} = \frac{a(t)}{\sqrt{1+(R\omega t)^2}}\,, \quad \text{where} \quad \frac{\dot{a}(t)}{\omega} = \frac{R^2(\omega t)^4}{4\sqrt{1+(R\omega t)^2}} z_0\,. \tag{3.29}$$

With the estimate $(R\omega t)^4/\sqrt{1+(R\omega t)^2} \approx (R\omega t)^3$, one finds

$$f_1(t) = \frac{1}{64}(\omega t)^4 z_0\,. \tag{3.30}$$

For the times the differential equation (3.23a) is valid ($\sin^2(\omega t) \ll 1$), this correction is small compared to the lowest order term (3.28). In fact, this correction term can be neglected in accordance with the approximation applied to arrive at the equation of motion (3.23a), because the original differential equation (3.22) is approximated by negligence of terms of the order $(\omega t)^3$ or higher.

Now, the equation of motion has to be solved for the times when $R^2\sin^2(\omega t) \gg 1$ [see Eq. (3.23b)]. Linearity requires the solution to be of the form

$$z = h_1(\omega t)\frac{\tilde{p}_{z_0}}{\omega} + h_2(\omega t)\tilde{z}_0\,, \tag{3.31a}$$

$$\dot{z} = \dot{h_1}(\omega t)\frac{\tilde{p}_{z_0}}{\omega} + \dot{h_2}(\omega t)\tilde{z}_0 = h_1'(\omega t)\tilde{p}_{z_0} + h_2'(\omega t)\omega\tilde{z}_0\,, \tag{3.31b}$$

i.e., $z(t)$ can be written as a linear combination of two time-dependent functions $h_1(t)$ and $h_2(t)$, whereas the initial conditions at the initial time $\tilde{t}$ are given by $z(t=\tilde{t}) = \tilde{z}_0$ and $\dot{z}(t=\tilde{t}) = \tilde{p}_{z_0}$. The prime in Eq. (3.31b) denotes the derivative with respect to (ωt). Since the differential equation does not depend on R, the coefficients can be calculated numerically for some time t without specifying R. The constants $h_{1,2}$ and $h'_{1,2}$ are fixed by calculating the solutions for two linearly independent pairs of initial conditions. An interesting instant is reached when the particle reaches its maximum velocity, i.e. for $\omega t = \pi/2$. Eqs. (3.23a) and (3.23b) are coupled at time $\tilde{t}$, which

needs to be chosen suitably such that the validity of both limits $\sin^2(\omega t) \ll 1$ and $R^2 \sin^2(\omega t) \gg 1$ is ensured. With $\omega\tilde{t} = 0.1$ good agreement with the original differential equation (3.22) is expected for values $R > 50$, but as it will turn out, the results are valid for values much smaller. The coefficients are found to be

$$\begin{array}{ll} h_1\left(\omega t = \frac{\pi}{2}\right) = 0.44\,, & h_2\left(\omega t = \frac{\pi}{2}\right) = 1.79\,, \\ h_1'\left(\omega t = \frac{\pi}{2}\right) = 0.38\,, & h_2'\left(\omega t = \frac{\pi}{2}\right) = 1.32\,. \end{array} \tag{3.32}$$

The initial velocity $\tilde{p}_{z_0}$ and the initial position $\tilde{z}_0$ are determined by Eqs. (3.27) for the preceding time domain. The results for $z(\omega t = \pi/2)$ and $\dot{z}(\omega t = \pi/2)$ can be written in matrix form

$$\begin{pmatrix} z(\frac{\pi}{2}) \\ \dot{z}(\frac{\pi}{2})/\omega \end{pmatrix} = \mathbf{B}\begin{pmatrix} z(\tilde{t}) \\ \dot{z}(\tilde{t})/\omega \end{pmatrix} = \mathbf{B}\cdot\mathbf{A}\begin{pmatrix} z_0 \\ p_{z_0}/\omega \end{pmatrix}, \tag{3.33}$$

with the definitions

$$\mathbf{A} \equiv \begin{pmatrix} 1 - \frac{1}{4R^2}\log(\frac{R}{5})^2 & \frac{1}{R}\log(\frac{R}{5}) \\ 0.05 - \frac{5\log(\frac{R}{5})}{R^2} & \frac{10}{R} \end{pmatrix}, \qquad \mathbf{B} \equiv \begin{pmatrix} 1.79 & 0.44 \\ 1.32 & 0.38 \end{pmatrix}. \tag{3.34}$$

Matrix $\mathbf{A}$ follows from Eqs. (3.27), which can be simplified by means of the same approximations already applied to decompose the original differential equation [see Eqs. (3.22) and (3.23)], i.e. $\sin^2(\omega\tilde{t}) \approx (\omega\tilde{t})^2 \ll 1$ and $R^2\sin^2(\omega\tilde{t}) \approx R^2(\omega\tilde{t})^2 \gg 1$. $\mathbf{B}$ is determined by Eqs. (3.31) and (3.32).

In the same way, the position and the velocity can be calculated after half a period:

$$\begin{pmatrix} z(\pi) \\ \dot{z}(\pi)/\omega \end{pmatrix} = \mathbf{D}\cdot\mathbf{C}\begin{pmatrix} z(\frac{\pi}{2}) \\ \dot{z}(\frac{\pi}{2})/\omega \end{pmatrix} = \mathbf{D}\cdot\mathbf{C}\cdot\mathbf{B}\cdot\mathbf{A}\begin{pmatrix} z_0 \\ p_{z_0}/\omega \end{pmatrix}. \tag{3.35}$$

The matrix $\mathbf{C}$ is again calculated numerically by solving the differential equation (3.23b) in the interval $\pi/2 < \omega t < \pi - \omega\tilde{t}$. $\mathbf{D}$ can be constructed from Eq. (3.23a), because the differential equation (3.22) looks the same for the intervals $(\pi - \omega\tilde{t}) < \omega t < \pi$ and $0 < \omega t < \omega\tilde{t}$ (a time shift of half a period leaves the equation invariant), i.e.,

$$\begin{pmatrix} z(\pi) \\ \dot{z}(\pi)/\omega \end{pmatrix} = \mathbf{D}\begin{pmatrix} z(\pi-\omega\tilde{t}) \\ \dot{z}(\pi-\omega\tilde{t})/\omega \end{pmatrix} \Leftrightarrow \mathbf{D}^{-1}\begin{pmatrix} z(0) \\ \dot{z}(0)/\omega \end{pmatrix} = \begin{pmatrix} z(-\omega\tilde{t}) \\ \dot{z}(-\omega\tilde{t})/\omega \end{pmatrix}, \tag{3.36}$$

where $\mathbf{D}^{-1}$ follows immediately from Eqs. (3.27) with the time given by $t = -\tilde{t}$. Then, the following results are found:

$$\mathbf{C} = \begin{pmatrix} 3.81 & 4.41 \\ 13.20 & 17.89 \end{pmatrix}, \qquad \mathbf{D} = \begin{pmatrix} 1 & \frac{\log(R/5)}{10} \\ \frac{1}{20}R & \frac{10}{R} \end{pmatrix}. \tag{3.37}$$

To obtain $\mathbf{D}$, a term $\log(R/5)/200 = \log(2R\omega\tilde{t})\omega\tilde{t}/2$ has been considered to be small as compared to one. In principle, this term could become large, but for the corresponding high values of R the matching point $\tilde{t}$ can be chosen to be much smaller which increases the precision and changes the matrix entries.

The coefficients of the differential equation (3.22) are periodic in $\omega t = \pi$, i.e., z and $\dot{z}$ can be determined at any time $\omega t = n\cdot\pi/2$ (n being an integer) by subsequently multiplying the matrices $\mathbf{B}\cdot\mathbf{A}$ and $\mathbf{D}\cdot\mathbf{C}$.

The matrices which describe the particle state at $\omega t = \pi/2$ and $\omega t = \pi$ are given by

$$\mathbf{B}\cdot\mathbf{A} = \begin{pmatrix} 1.81 & (1.53 + 1.79\log R)/R \\ 1.33 & (1.68 + 1.31\log R)/R \end{pmatrix} \tag{3.38}$$

and

$$\mathbf{D}\cdot\mathbf{C}\cdot\mathbf{B}\cdot\mathbf{A} = \begin{pmatrix} 5.11 + 4.78\log R & 4.71(0.86+\log R)(1.28+\log R)/R \\ 4.84R & 5.11 + 4.78\log R \end{pmatrix}, \quad (3.39)$$

respectively.

There is an important difference between the dynamics in the y and the z direction. Whereas the motion in the y direction freezes as R becomes high [see Eq. (3.21)], the motion in the z direction is unstable. From Eqs. (3.38) and (3.39) the following limits for high values of R are read off:

$$z(\pi/2) = 1.81 z_0\,, \quad (3.40a)$$

$$z(\pi) \approx (5.11 + 4.78\log R) z_0\,. \quad (3.40b)$$

Thus, the distance to the plane $z = 0$ roughly doubles during a quarter of a period and depending on R it increases further for half a period.

For $R > 30$, the entries of the matrices (3.38) and (3.39) deviate from the exact results by less than about 1%. The error increases for smaller values, but for $R = 10$ it is still of the order of only 5%. The essential result is that in the strongly relativistic regime the motion in the z direction becomes unstable for times greater than half a laser period. This instability originates from the nonvanishing magnetic field in the vicinity of the plane $z = 0$. Obviously, the magnetic field in the y direction is directed such that, together with the motion in the x direction, the Lorentz force pushes the particle farther away from the plane $z = 0$.

Circular polarization

Now, the corresponding analysis will be carried out for circular laser polarization. The location and the velocity of the electron will be calculated for $\omega t = \pi/2$ such that a direct comparison with the case of linear polarization will be at hand. A further instant of interest is the time when the equations of motion adopt their original form again, which is after a full laser period. Knowing the state of the particle after a period, this allows for an analysis of the long-term behavior.

In the strongly relativistic case, i.e., for $R^2 \gg 1$ Eq. (3.13b) can be simplified by means of

$$\frac{R}{\sqrt{1+R^2}} \approx 1\,, \quad (3.41a)$$

$$\arcsin[\cos(\omega t)] = \begin{cases} \dfrac{\pi}{2} - \omega t\,, & 0 \le \omega t < \pi \\ \omega t - \dfrac{3\pi}{2}\,, & \pi \le \omega t < 2\pi\,. \end{cases} \quad (3.41b)$$

One then finds

$$\dot{z} = \frac{1}{\sqrt{1+R^2\sin^2(\omega t)}} \times \begin{cases} (p_{z_0} + p_{y_0}\,\omega t)\,, & 0 \le \omega t < \pi \\ (p_{z_0} + p_{y_0}(2\pi - \omega t))\,, & \pi \le \omega t < 2\pi\,. \end{cases} \quad (3.42)$$

Considering that $\int_0^\pi (\omega t - \pi/2)[1 + R^2\sin^2(\omega t)]^{-1/2} d(\omega t) = 0$, the integration of Eq. (3.42) over a whole period yields

$$z(2\pi) = \int_0^{2\pi} \frac{\left(p_{z_0} + \frac{\pi}{2} p_{y_0}\right)\, d(\omega t)}{\omega\sqrt{1+R^2\sin^2(\omega t)}} = 4\left(p_{z_0} + \frac{\pi}{2} p_{y_0}\right)\frac{\log(4R)}{R\omega} + z_0\,. \quad (3.43)$$

The integral in Eq. (3.43) has already been solved in the previous section [compare Eq. (3.17)].

If the integration is only over a quarter of a period, the following integral is split up into regions where either $\sin(\omega t) \approx (\omega t)$ or $R^2 \sin^2(\omega t) \gg 1$ can be exploited. ϵ is a matching point where both conditions are valid.

$$\begin{aligned}
&\int_0^{\pi/2} d(\omega t) \frac{\omega t}{\sqrt{1+R^2\sin^2(\omega t)}} \\
\approx &\int_0^{\epsilon} d(\omega t) \frac{\omega t}{\sqrt{1+(R\omega t)^2}} + \frac{1}{R}\int_0^{\pi/2} d(\omega t) \frac{\omega t}{\sin(\omega t)} - \frac{1}{R}\int_0^{\epsilon} d(\omega t) \frac{\omega t}{\sin(\omega t)} \qquad (3.44)\\
= &\frac{1}{R^2}\left(\sqrt{1+(R\epsilon)^2}-1\right) + \frac{1.832}{R} - \frac{\epsilon}{R} \approx \frac{1.832}{R} - \frac{1}{R^2}\,.
\end{aligned}$$

The first integral in the second line is carried out analytically, the second one can be evaluated numerically without spoiling the dependence on R and the third one simplifies because $\sin(\omega t) \approx (\omega t)$ for $t \leq \epsilon$. Finally, employing both conditions at the matching point $R^2 \sin^2(\epsilon) \approx (R\epsilon)^2 \gg 1$, the result becomes independent of ϵ.

In all, the z position after a quarter of a period is given by

$$z\left(\frac{\pi}{2}\right) = p_{z_0}\frac{\log(4R)}{R\omega} + \frac{p_{y_0}}{R\omega}\left(1.832 - \frac{1}{R}\right) + z_0\,. \qquad (3.45)$$

The position in the y direction is obtained by integrating Eq. (3.12). Therefor, the following integral needs to be analyzed:

$$\begin{aligned}
&-\int_0^{\omega t} z \frac{R\sin(\omega t)\, d(\omega t)}{\sqrt{1+R^2\sin^2(\omega t)}} \\
&\qquad = z(\omega t)\arcsin[\cos(\omega t)] - \frac{\pi}{2}z_0 - \int_0^{\omega t} z' \arcsin[\cos(\omega t)]\, d(\omega t)\,, \\
&\qquad\qquad \text{where} \qquad z' = \frac{p_{z_0} + p_{y_0}\left(\frac{\pi}{2} - \arcsin\cos(\omega t)\right)}{\omega\sqrt{1+R^2\sin^2(\omega t)}}\,. \qquad (3.46)
\end{aligned}$$

This is obtained by a partial integration and by employing Eq. (3.41a).

For a whole period, i.e., for $\omega t = 2\pi$ and by means of Eq. (3.41b) this reduces to

$$\frac{\pi}{2}\left(z(2\pi) - z_0\right) + \frac{2p_{y_0}}{\omega}\int_0^{\pi} \frac{\left(\frac{\pi}{2} - \omega t\right)^2}{\sqrt{1+R^2\sin^2(\omega t)}}\, d(\omega t)\,. \qquad (3.47)$$

With the same reasoning as applied to Eq. (3.44), the occurring integral is rearranged to

$$\begin{aligned}
&\int_0^{\pi} \frac{\frac{\pi^2}{4} - \omega t(\pi - \omega t)}{\sqrt{1+R^2\sin^2(\omega t)}}\, d(\omega t) \approx \int_0^{\pi} \frac{\frac{\pi^2}{4}}{\sqrt{1+R^2\sin^2(\omega t)}}\, d(\omega t) - 2\int_0^{\epsilon} \frac{\omega t(\pi - \omega t)}{\sqrt{1+(R\omega t)^2}}\, d(\omega t) \\
&\quad -\frac{2}{R}\left[\int_0^{\pi/2} \frac{\omega t(\pi - \omega t)}{\sin(\omega t)}\, d(\omega t) - \int_0^{\epsilon} \frac{\omega t(\pi - \omega t)}{\sin(\omega t)}\, d(\omega t)\right] \approx \frac{\pi^2}{2}\frac{\log 4R}{R} - \frac{8.414}{R} + \frac{2\pi}{R^2}\,. \qquad (3.48)
\end{aligned}$$

The first integral has the same form as the one in Eq. (3.43). A term $(2R^3)^{-1}\mathrm{arsinh}(R\epsilon)$ has been dropped here, because the dependence on R^{-3} makes it only a minor correction. Summarizing these results, the y position after a whole period is found to be

$$y(2\pi) = \frac{4\log 4R}{R\omega}\left[\left(1+\frac{\pi^2}{2}\right)p_{y_0}+\frac{\pi}{2}p_{z_0}\right]-\frac{p_{y_0}}{R\omega}\left(16.83-\frac{2\pi}{R}\right)+y_0\,. \tag{3.49}$$

Considering the y position after a quarter of a period, Eq. (3.46) becomes

$$-\frac{\pi}{2}z_0+\frac{p_{y_0}}{\omega}\int_0^{\pi/2}\frac{\left(\frac{\pi}{2}-\omega t\right)^2}{\sqrt{1+R^2\sin^2(\omega t)}}-\frac{p_{z_0}+\frac{\pi}{2}p_{y_0}}{\omega}\int_0^{\pi/2}\frac{\frac{\pi}{2}-\omega t}{\sqrt{1+R^2\sin^2(\omega t)}}\,d(\omega t)\,. \tag{3.50}$$

The integrals have just been considered [see Eqs. (3.44) and (3.47)]. The final result then reads

$$y(\pi/2) = \frac{\log 4R}{R\omega}\left(p_{y_0}-\frac{\pi}{2}p_{z_0}\right)-\frac{p_{y_0}}{R\omega}\left(7.085-\frac{\pi}{2R}\right)+\frac{p_{z_0}}{R\omega}\left(1.832-\frac{1}{R}\right)-\frac{\pi}{2}z_0+y_0\,. \tag{3.51}$$

Considering the limit of high values of R, this expression reduces to

$$y\left(\frac{\pi}{2}\right) = -\frac{\pi}{2}z_0+y_0\,. \tag{3.52}$$

Here, the initial z position appears with a factor similar to the case of linear polarization [compare Eq. (3.40)]. However, after a full period the particle returns to its initial position (y_0, z_0) according to Eqs. (3.43) and (3.49). This means that the configuration of circularly polarized light becomes superior to the other in the long-term behavior. This can be further investigated. The particle state after a full period is given by $\dot{y} = p_{y_0}$, $\dot{z} = p_{z_0}$ and by Eqs. (3.43) and (3.49). The equations of motion are periodic, i.e., these results can be used to obtain the particle state after any complete period by consecutively calculating the initial conditions of the next period. The following result is found for the state after n full periods:

$$\begin{aligned}
\dot{y}(\omega t = 2\pi n) &= p_{y_0}\,,\\
\dot{z}(\omega t = 2\pi n) &= p_{z_0}\,,\\
y(\omega t = 2\pi n) &= n[y(\omega t = 2\pi) - y_0] + y_0\,,\\
z(\omega t = 2\pi n) &= n[z(\omega t = 2\pi) - z_0] + z_0\,.
\end{aligned} \tag{3.53}$$

After any full period, the momentum takes its initial value whereas the distance to the origin increases linearly, i.e., there is no rapidly growing instability as in the case of linear polarization. The distance from the x axis even grows more slowly as the laser intensity increases which is seen from the $1/R$-dependence of $y(\omega t = 2\pi)$ and $z(\omega t = 2\pi)$ [see Eqs. (3.43) and (3.49)].

3.3 Quantum mechanical treatment

In the following, a quantum mechanical description of the electron dynamics is developed. As opposed to classical mechanics, the wave character of the particle is taken into account. With the quantum mechanical results at hand, it is seen how they are related to the classical description. As the particle dynamics becomes relativistic, the quantum mechanical treatment becomes rather complex. However, several relativistic effects are pointed out in the weakly relativistic limit.

3.3.1 Solution of the Schrödinger equation

The quantum mechanical dynamics of an electron in a laser field is determined by Schrödinger's equation:

$$i\frac{\partial}{\partial t}\psi = \hat{H}\psi = \frac{1}{2}\left[-i\vec{\nabla} - \frac{1}{c}\vec{A}\right]^2 \psi = \frac{1}{2}\left[-\vec{\nabla}^2 + \frac{2i}{c}\vec{A}\cdot\vec{\nabla} + \frac{1}{c^2}A^2\right]\psi\,. \tag{3.54}$$

The vector potential is assumed to be given in Coulomb gauge ($\vec{\nabla}\cdot\vec{A} = 0$). For the two laser configurations defined by the vector potentials (3.1c) and (3.2c), this equation can be solved for a spatially restricted area. It is assumed again, that the particle is found close to the plane $z = 0$, i.e., the calculation is carried out to linear order in kz. Once the solutions are known, wave packets describing localized particles can be constructed which conform to this assumption.

Linear polarization

The vector potential for the case of linear laser polarization [see Eq. (3.1c)] reads

$$\vec{A} = -E_0\frac{c}{\omega}\sin(\omega t)\,\hat{x}\,, \tag{3.55}$$

if terms of quadratic or higher order in kz are dropped. The following ansatz is then inserted into the Schrödinger equation (3.54):

$$\psi = \exp i[\vec{p}_0\cdot(\vec{x} - \vec{x}_0) + w(t)]\,, \tag{3.56}$$

which yields a condition for the time-dependent function $w(t)$:

$$-\dot{w}(t) = \frac{1}{2}\vec{p}_0^{\,2} + \frac{E_0}{\omega}p_{x_0}\sin(\omega t) + \frac{E_0^2}{2\omega^2}\sin^2(\omega t)\,. \tag{3.57}$$

This is easily integrated and the solution is found to be

$$\psi = \exp i\left[\vec{p}_0\cdot(\vec{x} - \vec{x}_0) - \frac{1}{2}\vec{p}_0^{\,2}t + \frac{E_0}{\omega^2}p_{x_0}\cos(\omega t) - \frac{E_0^2}{4\omega^2}\left(t - \frac{1}{2\omega}\sin(2\omega t)\right)\right]\,. \tag{3.58}$$

This solution can be written as a product of three factors, each depending only on one momentum variable p_{x_0}, p_{y_0} or p_{z_0}. Then, Eq. (1.34) with the maximum of the initial momentum given by $p_m = p_{x,y,z}$ is applied to each of the factors to yield the following result for the probability density:

$$\begin{aligned}|\psi(x,y,z,t)|^2 &= \pi^{-3/2}\left[\Delta p^{-2} + \Delta p^2 t^2\right]^{-3/2}\exp -\frac{f_x^2 + f_y^2 + f_z^2}{\Delta p^{-2} + \Delta p^2 t^2}\,,\\ f_x &\equiv x - x_0 + \frac{Rc}{\omega}\cos(\omega t) - p_{x_0}\cdot t\,, \quad f_y \equiv y - y_0 - p_{y_0}\cdot t\,, \quad f_z \equiv z - z_0 - p_{z_0}\cdot t\,.\end{aligned} \tag{3.59}$$

The dynamics of the maximum of this wave packet is found by equating the functions $f_{x,y,z}$ to zero. It is seen that the maximum describes the same trajectories as a classical particle [compare Eqs. (3.15)].

The wave packet remains spherically symmetric, with the spatial widths $\Delta x^2 = \Delta p^{-2} + \Delta p^2 t^2$. The spreading dynamics is identical to that of a free particle [compare Eq. (1.21b)], i.e., in the configuration of linear laser polarization, wave packet spreading is not affected by the laser fields.

Circular polarization

The simplification that only linear terms of (kz) are considered reduces the vector potential for circular laser polarization (3.2c) to the following form:

$$\vec{A} = -E_0 \frac{c}{\omega} \sin(\omega t)\big(\hat{x} - (kz)\hat{y}\big) \,. \tag{3.60}$$

As opposed to the case of linear laser polarization, the vector potential does not become independent of the z coordinate. The corresponding Hamiltonian reads

$$\hat{H} = \frac{1}{2}\left[-\nabla^2 - 2i\frac{E_0}{\omega}\sin(\omega t)\left(\frac{\partial}{\partial x} - (kz)\frac{\partial}{\partial y}\right) + \frac{E_0^2}{\omega^2}\sin^2(\omega t)\right] . \tag{3.61}$$

The solution to the Schrödinger equation is found in the same way as in the previous case. Due to the dependence on kz, the ansatz (3.56) is extended by an additional term $g(t) \cdot kz$ in the exponent:

$$\psi = \exp i\left[\vec{p}_0 \cdot (\vec{x} - \vec{x}_0) + w(t) + g(t) \cdot kz\right] . \tag{3.62}$$

By inserting this ansatz into the Schrödinger equation (3.54), two conditions for the unknown functions $w(t)$ and $g(t)$ are found, one for each order of kz:

$$g(t) = \frac{E_0}{\omega^2} p_{y_0}[1 - \cos(\omega t)] \,, \tag{3.63a}$$

$$\begin{aligned} -\dot{w}(t) &= \frac{1}{2}\left\{p_{x_0}^2 + p_{y_0}^2 + [p_{z_0} + k \cdot g(t)]^2\right\} + \frac{E_0}{\omega} p_{x_0}\sin(\omega t) + \frac{E_0^2}{2\omega^2}\sin^2(\omega t) \,, \\ &\approx \frac{1}{2}\vec{p}_0^{\,2} + R\, p_{y_0} p_{z_0}[1 - \cos(\omega t)] + \frac{E_0}{\omega} p_{x_0}\sin(\omega t) + \frac{E_0^2}{2\omega^2}\sin^2(\omega t) \,. \end{aligned} \tag{3.63b}$$

Here, the first equation contains all of the terms proportional to kz, the second one contains the remaining terms, which are independent of kz. In Eq. (3.63b) a term in $R^2 = (E/\omega c)^2$ has been neglected with respect to unity, because R is a small number in the nonrelativistic regime considered here. In all, the wave function ψ is given by

$$\begin{aligned} \psi = \exp i \Bigg[\vec{p}_0 \cdot (\vec{x} - \vec{x}_0) - \frac{1}{2}\vec{p}_0^{\,2} t + \frac{E_0}{\omega^2} p_{x_0}\cos(\omega t) - \frac{E_0^2}{4\omega^2}\left(t - \frac{1}{2\omega}\sin(2\omega t)\right) \\ - R\, p_{y_0} p_{z_0}\left(t - \frac{1}{\omega}\sin(\omega t)\right) + R\, p_{y_0}[1 - \cos(\omega t)] z \Bigg] . \end{aligned} \tag{3.64}$$

This solution of the Schrödinger equation contains a mixed term $p_{y_0} p_{z_0}$, i.e., it cannot simply be written as a product of three exponentials where each depends only on one momentum variable. In order to reduce the three-dimensional problem to three one-dimensional ones, a coordinate transformation is carried out, i.e., the quadratic form in the exponent of Eq. (3.64) is diagonalized. This is achieved by a rotation about the x axis by an angle of $\pi/4$. The new coordinates $\tilde{y}$ and $\tilde{z}$ are related to the old ones by the following time-independent transformation law:

$$\begin{aligned} \tilde{y} &= \frac{1}{\sqrt{2}}(y + z) \,, \qquad & y &= \frac{1}{\sqrt{2}}(\tilde{y} - \tilde{z}) \,, \\ \tilde{z} &= \frac{1}{\sqrt{2}}(z - y) \,, \qquad & z &= \frac{1}{\sqrt{2}}(\tilde{y} + \tilde{z}) \,. \end{aligned} \tag{3.65}$$

This transformation is applied to both the spatial and the momentum variables p_{y_0} and p_{z_0}. The wave function (3.64) can then be separated according to $\psi(p_{x_0}, \tilde{p}_{y_0}, \tilde{p}_{z_0}) = \exp(p_{x_0}) \cdot \exp(\tilde{p}_{y_0}) \cdot \exp(\tilde{p}_{z_0})$. Now, Eq. (1.34) can be applied to each factor. With the maximum of the initial momentum $p_m = p_{x,y,z}$, the probability density turns out to be

$$
\begin{aligned}
|\psi(x,y,z,t)|^2 &= \pi^{-3/2}(\Delta w_x \Delta w_+ \Delta w_-)^{-1} \exp\left[-\frac{f_x^2}{\Delta w_x^2} - \frac{f_y^2}{\Delta w_+^2} - \frac{f_z^2}{\Delta w_-^2}\right], \\
f_x &\equiv -(x - x_0) - \frac{Rc}{\omega}\cos(\omega t) + p_{x_0} \cdot t\,, \\
f_y &\equiv -(\tilde{y} - \tilde{y}_0) - \frac{1}{2}R[1 - \cos(\omega t)](\tilde{y} + \tilde{z}) + \tilde{p}_{y_0} \cdot t + R\,\tilde{p}_{y_0}\left(t - \frac{1}{\omega}\sin(\omega t)\right), \\
f_z &\equiv -(\tilde{z} - \tilde{z}_0) + \frac{1}{2}R[1 - \cos(\omega t)](\tilde{y} + \tilde{z}) + \tilde{p}_{z_0} \cdot t - R\,\tilde{p}_{z_0}\left(t - \frac{1}{\omega}\sin(\omega t)\right), \\
\Delta w_x &\equiv \sqrt{\Delta p^{-2} + \Delta p^2 t^2}\,, \quad \Delta w_\pm \equiv \sqrt{\Delta p^{-2} + \Delta p^2\left[t \pm R\left(t - \frac{1}{\omega}\sin(\omega t)\right)\right]^2}\,.
\end{aligned}
\tag{3.66}
$$

By equating the arguments of the exponential functions to zero, the motion of the maximum of this Gaussian is found. If the result is transformed back to the original coordinates by means of Eqs. (3.65), the classical equations of motion (3.16) are recovered.

The exponents in Eq. (3.66) contain mixed terms $\tilde{y}\tilde{z}$, i.e., the widths of the wave packet cannot simply be read off. Instead of carrying out a cumbersome coordinate transformation which diagonalizes the quadratic form in the exponent, the widths are examined only after full periods. At these times the mixed terms do not appear. Then, the following widths after n laser cycles are found:

$$
\Delta w_x = \sqrt{\Delta p^{-2} + \Delta p^2\left(\frac{\pi n}{\omega}\right)^2}, \quad \Delta w_{\tilde{y},\tilde{z}} = \sqrt{\Delta p^{-2} + \Delta p^2\left(\frac{\pi n}{\omega}(1 \pm R)\right)^2}. \tag{3.67}
$$

For full laser cycles, the wave packet widths are similar to those of the linear polarization configuration [compare Eq. (3.59)]. Differences are given by the factors $(1 \pm R)$ which only slightly deviate from unity in the nonrelativistic regime. The deviations originate from the nonvanishing magnetic field of this laser configuration.

3.3.2 Relativistic effects

In order to examine how relativity alters the quantum mechanical wave packet dynamics, the Schrödinger equation is extended by a correction term which is obtained from a nonrelativistic reduction of the Klein-Gordon equation (see for example [81]). Although the validity of this approach is restricted to the weakly relativistic regime this allows to extract some relativistic effects. This approach is only applied to the simpler case of linear laser polarization.

The Hamiltonian containing the lowest order relativistic correction is given by

$$
\hat{H} = \frac{1}{2}\left[-i\vec{\nabla} - \frac{1}{c}\vec{A}\right]^2 - \frac{1}{8c^2}\left[-i\vec{\nabla} - \frac{1}{c}\vec{A}\right]^4. \tag{3.68}
$$

The same ansatz (3.56) can be used to solve the Schrödinger equation. With the corre-

sponding vector potential (3.55), the second term then yields the following expression:

$$\left[-i\vec{\nabla}-\frac{1}{c}\vec{A}\right]^4 \rightarrow \left[\vec{p}_0^{\,2}+2p_{x_0}\frac{E_0}{\omega}\sin(\omega t)+\left(\frac{E_0}{\omega}\sin(\omega t)\right)^2\right]^2$$
$$\approx 2\left(3p_{x_0}^2+p_{y_0}^2+p_{z_0}^2\right)\left(\frac{E_0}{\omega}\sin(\omega t)\right)^2+4p_{x_0}\left(\frac{E_0}{\omega}\sin(\omega t)\right)^3+\left(\frac{E_0}{\omega}\sin(\omega t)\right)^4. \tag{3.69}$$

The approximation applies for the regime where the relativistic correction terms are small and the term $E_0/\omega = cR$ is distinctly greater than p_{x_0}, p_{y_0} and p_{z_0}. Then, those terms are neglected which do not contain the factor E_0/ω at least to quadratic order. The purpose of using this approximation is to avoid mixed terms like $p_{x_0}^2 p_{y_0}^2$, which would spoil an analytical wave packet analysis.

After an analogous calculation as in Sec. 3.3.1, the solution turns out to be

$$\psi = \exp i\left\{\vec{p}_0\cdot(\vec{x}-\vec{x}_0)-\frac{1}{2}\vec{p}_0^{\,2}t+\frac{E_0}{\omega^2}p_{x_0}\cos(\omega t)\right.$$
$$-\frac{E_0^2}{4\omega^2}\left(t-\frac{1}{2\omega}\sin(2\omega t)\right)-\frac{E_0^4}{\omega^4}\left(\frac{3}{16}t-\frac{1}{8\omega}\sin(2\omega t)+\frac{1}{64\omega}\sin(4\omega t)\right)$$
$$+\frac{1}{8c^2}\left[\left(3p_{x_0}^2+p_{y_0}^2+p_{z_0}^2\right)\frac{E_0^2}{\omega^2}\left(t-\frac{1}{2\omega}\sin(2\omega t)\right)\right.$$
$$\left.\left.-\frac{E_0^3}{\omega^4}p_{x_0}\left(3\cos(\omega t)-\frac{1}{3}\cos(3\omega t)\right)\right]\right\}. \tag{3.70}$$

Now, Eq. (1.34) is applied again (with $p_m = p_{x,y,z}$) to yield the probability density of a localized wave packet:

$$|\psi(x,y,z,t)|^2 = \pi^{-3/2}(\Delta w_x\Delta w_y\Delta w_z)^{-1}\exp\left[-\frac{f_x^2}{\Delta w_x^2}-\frac{f_y^2}{\Delta w_y^2}-\frac{f_z^2}{\Delta w_z^2}\right],$$
$$f_x \equiv -(x-x_0)+p_{x_0}(t-3\chi),$$
$$-\frac{E_0}{\omega^2}\cos(\omega t)+\frac{E_0}{8\omega^2}R^2\left(3\cos(\omega t)-\frac{1}{3}\cos(3\omega t)\right), \tag{3.71}$$
$$f_y \equiv -(y-y_0)+p_{y_0}(t-\chi), \quad f_z \equiv -(z-z_0)+p_{z_0}(t-\chi),$$
$$\Delta w_x \equiv \sqrt{\Delta p^{-2}+\Delta p^2(t-3\chi)^2}, \quad \Delta w_y = \Delta w_z \equiv \sqrt{\Delta p^{-2}+\Delta p^2(t-\chi)^2},$$
$$\chi \equiv \frac{1}{4}R^2\left(t-\frac{1}{2\omega}\sin(2\omega t)\right).$$

Several relativistic effects appear. First of all, the oscillatory motion in the x direction becomes inharmonic [note the additional term $\cos(3\omega t)$] as opposed to the nonrelativistic case. The reason is that—given a certain external force—the acceleration of the electron decreases as the electron approaches the speed of light, due to increasing inertia.

Furthermore, time dilation becomes noticeable, i.e., the wave packet spreads at a lower rate as the velocity of the electron becomes higher (see also Sec. 2.2.3 and [88]). In the y and the z direction wave packet spreading is reduced since the time variable t is replaced by $(t-\chi)$ [compare the nonrelativistic solution (3.59)]. This term has

a simple interpretation. The weakly relativistic limit of the γ-factor (3.7), i.e., its expansion to the order R^2 is given by $\gamma \approx (1 + R^2 \sin^2(\omega t)/2)$. The time t is related to the particle's proper time τ by $dt = \gamma\, d\tau$. Integration shows that $(t - \chi)$ is nothing but the proper time τ. In the x direction, wave packet spreading is even suppressed further [t is replaced by $(t - 3\chi)$].

Here, it is seen that time dilation inhibits wave packet spreading also in the z direction whereas no instability occurs. However, the term of the vector potential which is linear in kz vanishes for the case of linear laser polarization [see Eq. (3.55)], i.e., there is no magnetic field according to $\vec{B} = \vec{\nabla} \times \vec{A}$. In order to see instabilities caused by the magnetic field, the vector potential would have to be considered at least to the order $(kz)^2$. Therefore, the classical approach, where the magnetic field is included explicitly in the equations of motion up to the first order of kz yields more information about the dynamics in the z direction than considering the vector potential to the same order as done in the quantum mechanical approach.

The instability which has been found in the classical, relativistic case will be included in the next section where the wave packet is modeled by an ensemble of classical particles.

3.4 Relativistic wave packet approach

For a fully relativistic quantum mechanical description of wave packets one has to deal with relativistic wave equations. However, an analytical solution for crossed laser fields is not available. Therefore, the problem is treated with the classical approach of phase-space averaging. As described in Sec. 1.1, the basic idea is to calculate the initial momentum which is needed for a classical particle to propagate from some initial to some final point. Since both the initial position and the initial momentum are subject to some probability distribution, the probability can be calculated for the particle to be found at any point of interest.

3.4.1 Linear polarization

In the case of linear polarization, the classical equations of motion decouple and one arrives at one-dimensional problems. Therefore, the general formula for the probability density (1.3) is first applied to a general one-dimensional equation of motion with linear dependence on the initial momentum p_0 and position x_0:

$$x(t) = a(t) \cdot p_0 + b(t) \cdot x_0 + d(t)\,. \tag{3.72}$$

The coefficients a, b and d will be specified later on when the result are applied. From this equation, one immediately arrives at the expressions needed to calculate the probability density $\rho(x,t)$ according to Eq. (1.3):

$$g(x, x_0, t) = p_0 = \frac{x - b(t)x_0 - d(t)}{a(t)}\,, \tag{3.73a}$$

$$\frac{\partial g}{\partial x} = a(t)^{-1}\,, \tag{3.73b}$$

$$\rho(x,t) = \int \tilde{\rho}(g(x, x_0, t))\frac{\partial g}{\partial x}\rho_0(x_0)dx_0\,. \tag{3.73c}$$

Here, ρ_0 and $\tilde{\rho}$ are the initial distributions in coordinate and momentum space, respectively, which are chosen to be the one-dimensional analogs of the Gaussians in Eqs. (1.10). The resulting Gaussian integral in Eq. (3.73c) can then be carried out to yield the following expression for the probability density:

$$\begin{aligned}\rho(\vec{x},t) &= \int_{-\infty}^{\infty} \frac{\exp -\frac{(x-b(t)x_0-d(t))^2}{\Delta p^2 a(t)^2}}{\sqrt{\pi}\Delta p\, a(t)} \cdot \frac{\exp -\frac{x_0^2}{\Delta w^2}}{\sqrt{\pi}\Delta w}\, dx_0 \\ &= \frac{1}{\sqrt{\pi}\sqrt{\Delta w^2 b(t)^2 + \Delta p^2 a(t)^2}} \exp -\frac{[x-d(t)]^2}{\Delta w^2 b(t)^2 + \Delta p^2 a(t)^2}\,.\end{aligned} \tag{3.74}$$

The initial widths in coordinate space Δw and momentum space Δp can be adapted to mimic some localized initial state.

For the case of linear polarization, there are three one-dimensional, linear classical equations of motion [see Eqs. (3.8b), (3.9a) and (3.22)] which determine the corresponding coefficients $a(t)$, $b(t)$, $d(t)$. An analytical solution for the highly relativistic regime can be given for the time after a quarter of a period. From Eqs. (3.8b), (3.33), (3.38) and (3.21), the following electron position is found:

$$x = \frac{p_{x_0}}{\omega\sqrt{1+R^2}}\mathrm{EllipticE}\left(\frac{R^2}{1+R^2}\right) + x_0 \approx \frac{p_{x_0}}{R\omega} + x_0\,, \tag{3.75a}$$

$$y = \frac{p_{y_0}}{R\omega}\log(4R) + y_0\,, \tag{3.75b}$$

$$z = \frac{p_{z_0}}{R\omega}(1.53 + 1.79\log R) + 1.81 z_0\,. \tag{3.75c}$$

EllipticE denotes the complete elliptic function of the second kind [89]. The approximation applies in the relativistic regime where $R^2 \gg 1$. With these results, the following probability density is found:

$$\begin{aligned}\rho(\vec{x}, t = \pi/(2\omega)) &= \pi^{-3/2}(\Delta w_x \Delta w_y \Delta w_z)^{-1} \exp\left[-\frac{x^2}{\Delta w_x^2} - \frac{y^2}{\Delta w_y^2} - \frac{z^2}{\Delta w_z^2}\right]\,, \\ \Delta w_x &\equiv \sqrt{\Delta w^2 + \Delta p^2 \frac{1}{(R\omega)^2}}\,, \\ \Delta w_y &\equiv \sqrt{\Delta w^2 + \Delta p^2 \left(\frac{\log(4R)}{R\omega}\right)^2}\,, \\ \Delta w_z &\equiv \sqrt{3.28\Delta w^2 + \Delta p^2 \left(\frac{1.53 + 1.79\log R}{R\omega}\right)^2}\,.\end{aligned} \tag{3.76}$$

Figure 3.5 depicts the evolution of the wave packet in the y-z plane which is perpendicular to its direction of motion. The wave packets are plotted for a full period based on Eqs. (3.9a), (3.22) and (3.74). Two different parameters R have been chosen to compare the nonrelativistic to the relativistic wave packet dynamics. It is seen that wave packet spreading is inhibited in the relativistic case. However, for long times the instability becomes dominant stretching the wave packet in the z direction.

3.4.2 Circular polarization

The solutions of the classical equations of motion in the y and the z direction (3.12) and (3.13b) depend linearly on the initial momenta and positions. The dynamics in

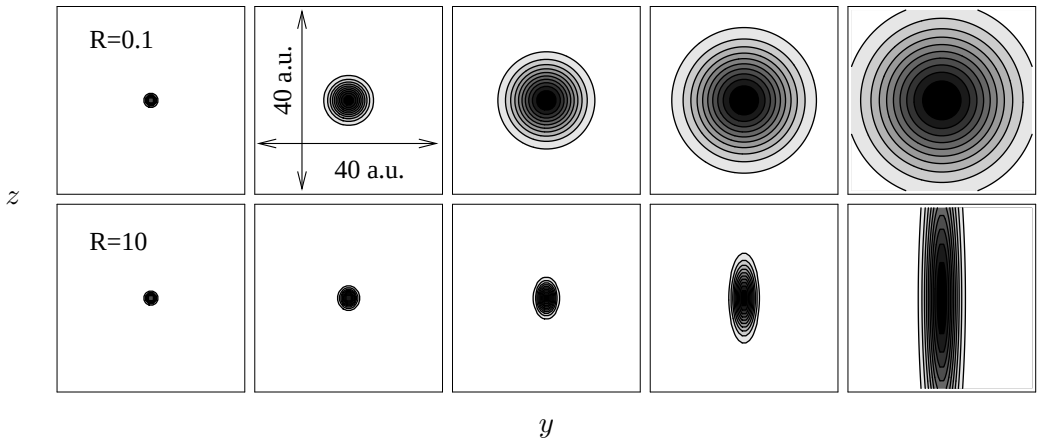

Figure 3.5: The nonrelativistic wave packet evolution (top row, $R = 0.1$) is compared to the relativistic case (bottom row, $R = 10$) for linearly polarized crossed laser fields. The probability densities in the y-z plane, i.e., perpendicular to the driving electric field, are shown for the times $\omega t = \{0, \pi/4, \pi/2, 3\pi/4, \pi\}$ (from the left to the right) with the initial widths $\Delta p = 0.5$ a.u. As long as the wave packet is small, spreading is suppressed in the relativistic case, but after some time the instability in the z direction becomes dominant.

the x direction is identical to the case of linear polarization, i.e., these results can be transferred immediately. The motion in the y and the z direction does not decouple. Therefore, one has to deal with a two-dimensional problem. The equations of motion have the following structure:

$$\begin{aligned} y(t) &= g_1(t) \cdot p_{y_0} + g_3(t) \cdot p_{z_0} + g_5(t) \cdot z_0 + y_0 \,, \\ z(t) &= g_2(t) \cdot p_{z_0} + g_4(t) \cdot p_{y_0} + z_0 \,. \end{aligned} \tag{3.77}$$

These equations need to be inverted, such that the momentum is found which is needed for a classical particle to travel from the initial position (y_0, z_0) to some other point (y, z) at time t:

$$\begin{aligned} p_{y_0}(t) &= \frac{g_2(t)(y - y_0 - g_5 z_0) - g_3(t)(z - z_0)}{g_1 g_2 - g_3 g_4} \,, \\ p_{z_0}(t) &= \frac{g_1(t)(z - z_0) - g_4(t)(y - \tilde{y} - g_5 z_0)}{g_1 g_2 - g_3 g_4} \,. \end{aligned} \tag{3.78}$$

The function needed to determine the probability density ρ according to Eq. (1.34) is $\vec{g} = (p_{y_0}, p_{z_0})$ and one arrives at the following expression:

$$\rho(y, z, t) = \iint \tilde{\rho}(g(y, y_0, z, z_0, t)) \left| \frac{\partial \vec{g}}{\partial (y, z)} \right| \rho_0(y_0, z_0)\, dy_0 dz_0 \,. \tag{3.79}$$

The initial probability distributions are two-dimensional Gaussians, analogous to Eqs. (1.10). Note that the Jacobi determinant in this expression does not depend on the initial position (y_0, z_0). This means that the double integral is a two-dimensional Gaussian integral which can be solved by means of the formula

$$\iint dx\, dy\, \exp - \left(ax^2 + by^2 - dxy + fx + gy\right) = h(a, b, d) \exp \frac{bf^2 + dfg + ag^2}{4ab - d^2} \,. \tag{3.80}$$

The calculation and the results simplify considerably if only the instants after n complete laser cycles are considered, because with this restriction the coefficient g_5 vanishes and g_3 and g_4 become equal. Both is seen if the equation of motion in the y direction (3.12) is partially integrated:

$$y(t) = \left(\int_0^t \dot{z}(t')dt' + z_0\right) \arcsin\left[\frac{R}{\sqrt{1+R^2}}\cos(\omega t)\right] - z_0 \arcsin\left[\frac{R}{\sqrt{1+R^2}}\right] - \int_0^t dt' \dot{z}(t') \arcsin\left[\frac{R}{\sqrt{1+R^2}}\cos(\omega t')\right] + \int_0^t dt' \frac{p_y}{\sqrt{1+R^2\sin^2(\omega t')}}\,. \quad (3.81)$$

For full periods, the terms depending on z_0 cancel. The equality of g_3 and g_4 is seen by formally integrating Eq. (3.13b) and by comparing the terms proportional to p_{y_0} to the terms of Eq. (3.81) which are proportional to p_{z_0}. Furthermore, the initial spatial width is chosen to be $\Delta w = 1/\Delta p$, which corresponds to the minimal uncertainty allowed by Heisenberg's relation. After some algebra, the probability density can then be written in the following way:

$$\rho(y, z, \omega t = 2\pi n) \propto \exp - \frac{\Delta p^{-2}(y^2+z^2) + \Delta p^2[(g_3 z - g_2 y)^2 + (g_3 y - g_1 z)^2]}{\left[\Delta p^{-2} + \Delta p^2(g_3^2 - g_1 g_2)\right]^2 + (g_1+g_2)^2}\,. \quad (3.82)$$

The factor which renders this proportionality an equality can be found by normalizing the probability density. This is accomplished by calculating the widths of the wave packet. These are found by diagonalizing the quadratic form in Eq. (3.82). The probability density can be rewritten with coordinates (Y, Z) which reduce the two-dimensional Gaussian distribution to a product of two one-dimensional ones with the widths $\Delta w_\pm$:

$$\begin{aligned} \rho(Y,Z) &= \frac{1}{\pi \Delta w_+ \Delta w_-} \exp\left[-\frac{Y^2}{\Delta w_+^2} - \frac{Z^2}{\Delta w_-^2}\right], \\ \Delta w_\pm^2 &\equiv \frac{\left[\Delta p^{-2} + \Delta p^2(g_3^2 - g_1 g_2)\right]^2 + (g_1+g_2)^2}{\Delta p^{-2} + \Delta p^2\left[g_3^2 + \frac{1}{2}(g_1^2+g_2^2) \pm \frac{1}{2}\sqrt{(g_1^2-g_2^2)^2 + 4g_3^2(g_1+g_2)^2}\right]}\,. \end{aligned} \quad (3.83)$$

The normalization factor in front of the exponential is independent of the coordinate system and therefore it normalizes the distribution (3.82) as well.

There is an important result which can be deduced from these complicated looking terms $\Delta w_\pm$. In the relativistic limit of the classical equations of motion (3.43), (3.49) and (3.53), one finds that all of the coefficients g_1, g_2, g_3 are proportional to R^{-1}:

$$g_1 = \frac{n}{R\omega}\left[4\left(1+\frac{\pi^2}{2}\right)\log 4R - 16.83 + \frac{2\pi}{R}\right], \quad (3.84a)$$

$$g_2 = \frac{4n\log 4R}{R\omega}\,, \quad (3.84b)$$

$$g_3 = \frac{2\pi n \log 4R}{R\omega}\,. \quad (3.84c)$$

This means that the greater R is chosen, the smaller the widths will be after n periods. This behavior has an intuitive explanation. As the particle approaches the speed of light, time dilation inhibits wave packet spreading. The theoretical limit for the minimal widths is given by the initial widths of $\Delta w_\pm = 1/\Delta p$. As opposed to the case of linear laser polarization, the dynamics is not unstable in the z direction.

A comparison of the relativistic and the nonrelativistic regime is shown in Fig. 3.6. The probability densities are plotted according to Eqs. (3.12), (3.13b) and (3.82). It is seen, that wave packet spreading is reduced in the relativistic case.

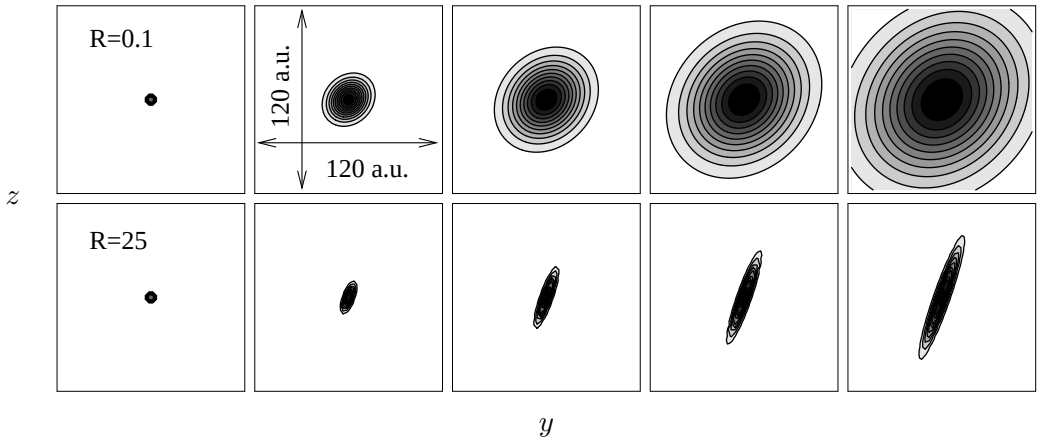

Figure 3.6: The wave packets in the y-z plane, i.e., perpendicular to the electric field, are depicted for counterpropagating circularly polarized laser fields at the initial time and at four consecutive full periods. The initial widths are $\Delta p = 0.2$ a.u. In the highly relativistic regime (bottom row, $R = 25$), wave packet spreading is strongly suppressed compared to the nonrelativistic case (top row, $R = 0.1$).

As already mentioned, the dynamics in the x direction is identical to the case of linear laser polarization. In the previous section, the probability density has been determined after a quarter of a laser period. Since the integral in Eq. (3.8b) is symmetric with respect to $t = \pi/(2\omega)$ and periodic in π/ω, this result is immediately generalized to the times $t = m\pi/(2\omega)$ where m is an integer. With Eq. (3.74) the probability distribution for the x direction in the relativistic limit is given by

$$\begin{aligned} \rho(x, t = m\pi/(2\omega)) &= \frac{1}{\sqrt{\pi}\Delta w_x} \exp - \frac{\left\{x + \frac{c}{\omega} \arcsin\left[\cos\left(\frac{m\pi}{2\omega}\right)\right]\right\}^2}{\Delta w_x^2}, \\ \Delta w_x &\equiv \sqrt{\Delta w^2 + \Delta p^2 \left(\frac{m}{R\omega}\right)^2}. \end{aligned} \tag{3.85}$$

Nonrelativistic limit

It is interesting to compare the nonrelativistic limit of the probability distribution (3.82) with the corresponding quantum mechanical solution. According to Eqs. (3.16e) and (3.16f) the coefficients are given by $g_1 = g_2 = 2n\pi/\omega$ and $g_3 = Rg_1$ after n periods. Rewriting the probability distribution with the coordinates $\tilde{y}, \tilde{z}$ according to Eqs. (3.65) and considering that $R^2 \ll 1$ in the nonrelativistic limit, Eq. (3.82) can be arranged such that it reduces to a special case of Eq. (3.66):

$$\rho(y, z) \propto \exp - \left[\frac{\tilde{y}^2}{\Delta\tilde{p}^{-2} + \Delta\tilde{p}^2 \left(\frac{\pi n}{\omega}\right)^2 (1+R)^2} + \frac{\tilde{z}^2}{\Delta\tilde{p}^{-2} + \Delta\tilde{p}^2 \left(\frac{\pi n}{\omega}\right)^2 (1-R)^2} \right]. \tag{3.86}$$

This means that in the nonrelativistic limit, the result of this classical wave packet approach is in agreement with the result found by means of quantum mechanics.

3.5 Conclusions

Summarizing, the dynamics of a laser-driven electron has been analyzed for two different standing wave configurations with either linear or circular laser polarization. In both cases, the electron oscillates close to an ideal axis where the Lorentz force vanishes.

For the case where the electron can be described nonrelativistically, i.e., the velocity is small compared to the speed of light and terms of higher order than $1/c$ are negligible, the systems have been described classically and quantum mechanically. It has been shown that the maximum of a Gaussian wave packet moves like a classical particle. For both configurations, wave packet spreading has been found to be similar to that of a free particle.

To examine how relativity alters the wave packet dynamics, the case of linear laser polarization has been analyzed for the weakly relativistic limit. The Hamiltonian has been extended by a relativistic correction term which follows from the Klein-Gordon equation. Besides the fact that the oscillation becomes inharmonic, it has been shown that wave packet spreading is somewhat reduced on account of time dilation.

The strongly relativistic electron dynamics has been described analytically by passing over to the classical method established in Sec. 1.1 where wave packets are described by an ensemble of classical trajectories. This Monte-Carlo approach requires the knowledge of the classical particle dynamics. Considering a classical electron after a quarter of a period, i.e., at the time when it reaches its maximum velocity for the first time, both configurations yield similar results. However, if the time is chosen to be longer, the configuration with linear laser polarization becomes highly unstable in the laser propagation direction, i.e., the distance from the ideal axis increases quickly. This behavior transfers to the wave packet dynamics in the Monte-Carlo approach. After a quarter of a laser period when the electron has reached its maximum energy, both configurations work equally well, whereas higher laser intensities reduce wave packet spreading. However, for longer periods of time, the case of circular polarization turns out to be much more effective. The reduction of wave packet spreading increases with the strength of the driving laser fields. The configuration of linear laser polarization shows a different behavior. For strong fields, the instability in the laser propagation direction dominates over the positive effect of time dilation on spreading, i.e., the wave packet is stretched. This effect increases with stronger laser fields.

In all, it has been found that the dynamics of electrons oscillating close to an axis of vanishing Lorentz force, have similar properties in both configurations if the dynamics is nonrelativistic. For short times like a quarter of a laser period, this even holds for the highly relativistic case. Differences occur in the relativistic long-term behavior. Opposite to the case of circular polarization the configuration with linear polarization shows an instability in the direction of laser propagation.

Chapter 4

Relativistic recollisions

In the nonrelativistic regime, recollisions in bound systems are achieved by means of simple propagating laser fields. First, electrons tunnel out of the Coulomb barrier, then they are accelerated and finally, they are driven back to the core to recollide. The recollision energy depends on the laser phase at which the electron leaves the core (see, e.g., one of the reviews [1, 2, 3, 4, 5, 6]).

As shown in Sec. 2, the electron drifts in the laser propagation direction if the motion becomes relativistic. Recollisions are therefore inhibited for intense laser fields and consequently, the maximum collision energy is limited in this simple scheme. As described in the introduction, there are several proposals to circumvent this problem, e.g., via standing laser fields [27, 28, 29, 19] or by employing positronium as the initial system [25, 26].

A further problem is the immediate ionization for weakly bound electrons by strong laser fields (*over the barrier ionization* (OBI), see e.g. [5]). For the case OBI occurs, the electron energy is higher than the barrier formed by the laser field and the Coulomb potential. With the immediate ionization, recollisions generally do not occur with maximal energy. The situation is different in the tunneling regime because the most likely instant of ionization is the moment when the laser electric field is maximal. By considering tightly bound electrons, the ionization process can be turned to the tunneling regime for high laser intensities as well, but in this case, tunneled wave packets spread very quickly which reduces the probability of recollisions.

In this chapter, a scheme is introduced which allows for relativistic recollisions with two consecutive, counterpropagating laser pulses. The first pulse separates an electron from the core, and the second one drives it back. The vector potential can be chosen in a way that recollisions occur with the maximum kinetic energy which a laser driven electron is able to reach in a propagating laser field.

But first, it is shown for different schemes, by means of a classical picture, what the highest achievable energies are for given laser intensities.

4.1 Collision energies in laser-driven recollisions

In the following, the recollision energies in standing wave configurations and for laser-driven positronium are discussed by means of a classical picture. The analysis holds for the limit the binding potential can be neglected with respect to the strong laser fields corresponding to the case of immediate ionization (OBI). Furthermore, the energy of an electron colliding with a nucleus in a propagating laser field is determined. This

case applies to the recollision model which will be introduced in Sec. 4.2.

4.1.1 Recollisions in standing laser fields

As discussed in Chapter 3, standing waves can be employed for relativistic recollisions. If the electron is placed on an axis of vanishing Lorentz force, the classical motion is one-dimensional. For a general time-dependence of the laser fields, the equation of motion for an electron moving on this axis is given by

$$\frac{d}{dt}(\gamma\dot{x}) = E(t) = -\frac{1}{c}\dot{A}(t)\,, \quad \gamma = \frac{\dot{x}}{\sqrt{1-\frac{\dot{x}^2}{c^2}}}\,. \tag{4.1}$$

This equation can be solved and one finds

$$\gamma = \sqrt{1+\frac{1}{c^4}A^2}\,, \tag{4.2a}$$

$$\dot{x} = -c\frac{\frac{1}{c^2}A}{\sqrt{1+\frac{1}{c^4}A^2}}\,, \tag{4.2b}$$

$$x = -c\int_0^t \frac{-\frac{1}{c^2}A(t')}{\sqrt{1+\frac{1}{c^4}A^2(t')}}dt'\,. \tag{4.2c}$$

The initial conditions are chosen such that the electron is initially found at rest at the origin. The highest kinetic energy is obtained when the vector potential reaches its maximum. Now, this energy should be reached at the instant of recollision, i.e., at the moment when the electron returns to its initial position $x = 0$. In the highly relativistic regime, it is easy to see how this can be accomplished. For $A^2/c^4 \gg 1$, the electron moves approximately with the speed of light $\dot{x} = \pm c$ and the shape of the pulse is not important anymore. Then, recollisions occur when the time duration with positive vector potential becomes equal to the period with negative potential. To obtain recollisions with maximal energy, the vector potential needs to be at its maximum. In Fig. 4.1, an example is given where this conditions is fulfilled. If the motion is not highly relativistic, the solutions look slightly different because the velocity of the electron cannot be approximated by the speed of light. In this case, the problem has to be analyzed numerically.

For light nuclei, the total collision energy is somewhat different from the electron energy, because the nucleus is accelerated as well. The energies and momenta of the nucleus (E_M and P_M) and the electron (E_e and P_e) are given by

$$\begin{aligned} E_e &= c^2\sqrt{1+\tfrac{1}{c^4}A^2}\,, & P_e &= \dot{x}\gamma = -c\tfrac{1}{c^2}A\,, \\ E_M &= Mc^2\sqrt{1+\tfrac{1}{M^2c^4}A^2}\,, & P_M &= Mc\tfrac{1}{Mc^2}A = -P_e\,, \end{aligned} \tag{4.3}$$

where M is the nuclear mass in atomic units. Since $P_M = P_e$, it is clear that the center of momentum remains at the origin. The total recollision energy E is then found to be

$$E = E_e + E_M = \left(\sqrt{1+\tfrac{1}{c^4}A^2} + M\sqrt{1+\tfrac{1}{M^2c^4}A^2}\right)c^2 \approx E_e + \left(M + \tfrac{1}{2Mc^4}A^2\right)c^2\,, \tag{4.4}$$

where the approximation holds for $[A^2/(M^2c^4)]^2 \ll 1$ which is the case for any laser intensity of interest here (note that the mass of the core is at least as high as the proton mass $M_P \approx 1800$).

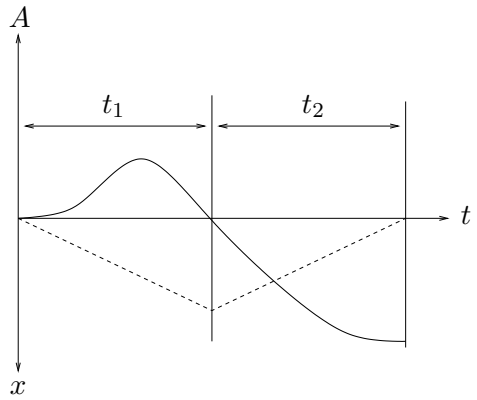

Figure 4.1: In the highly relativistic regime, recollisions with maximal kinetic energy of the electron can be achieved with the vector potential depicted here. The times t_1 and t_2 are equal and the vector potential reaches its maximum at the moment of recollision. The dashed line shows the electron trajectory, which is a motion close to the speed of light.

4.1.2 Recollision energy of laser-driven positronium

The advantage of employing positronium for recollisions is that the electron and the positron have equal masses. Thus, the Lorentz drift in the propagation direction is equal and relativistic recollisions can occur. However, in the highly relativistic regime, the motion of the particles is strongly directed in the laser propagation direction. This means that a lot of the collision energy is lost to kinetic energy in order to conserve the total momentum. The recollision energy in the frame where the pair collides head-on is therefore much smaller.

According to Eqs. (A.8) and (A.9), the dynamics of the particles is given by the following equations:

$$\gamma = 1 + \frac{1}{2c^4} A^2 \,, \tag{4.5a}$$

$$\dot{x} = \mp c \cdot \frac{\frac{1}{c^2} A(\varphi)}{1 + \frac{1}{2c^4} A^2(\varphi)} \,, \tag{4.5b}$$

$$\dot{z} = -c \cdot \frac{\frac{1}{2c^4} A^2(\varphi)}{1 + \frac{1}{2c^4} A^2(\varphi)} \,, \tag{4.5c}$$

$$x = \mp \frac{c}{\omega} \int \frac{1}{c^2} A d\varphi \,, \tag{4.5d}$$

$$z = \frac{c}{\omega} \int \frac{1}{2c^4} A^2 d\varphi \,. \tag{4.5e}$$

The motions of the electron and the positron differ only by the signs in Eqs. (4.5b) and (4.5d) for the motion in the polarization direction (the minus sign holds for the electron). Recollisions occur if the integral in this equation vanishes. Maximal recollision energies can be obtained with different amplitudes of the positive and negative parts of the vector potential. An example is given in Fig. 4.2.

The collision energy in the center of momentum frame is found via the following argument. The collision has to be observed in a co-moving frame which moves in the z direction. In this frame, the electron momentum in the z direction vanishes, whereas

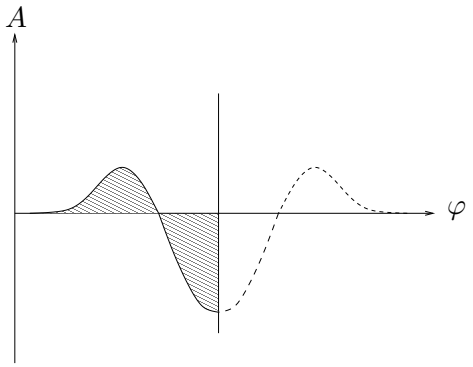

Figure 4.2: Recollisions with the highest energy are achieved if the vector potential has a maximum when the surfaces of positive and negative potential are equal.

the momentum in the x direction P_x is not changed by a Lorentz transformation. The total electron energy E' in the center of momentum frame is then given by

$$E'^2 = c^4 + c^2 P_x^2 \,, \tag{4.6a}$$

$$P_x = \gamma \dot{x} = -\frac{1}{c} A \,, \tag{4.6b}$$

and the corresponding γ-factor is

$$\gamma' = \sqrt{1 + \frac{1}{c^4} A^2} \,. \tag{4.7}$$

This is equal to the electron energy in a standing laser field [compare Eq. (4.2a)]. Note that the positron holds the same energy and thus the total recollision energy is given by

$$E' = 2\gamma' c^2 = 2c^2 \sqrt{1 + \frac{1}{c^4} A^2} \,. \tag{4.8}$$

4.1.3 Electron core collisions in propagating laser fields

The equations of motion for an electron which is driven by a propagating laser field are equal to those discussed in the previous section on laser-driven positronium [see Eqs. (4.5)]. The dependence of the electron energy in a laser field is quadratic in the vector potential:

$$\gamma = 1 + \frac{1}{2c^4} A^2 \,. \tag{4.9}$$

For high laser intensities $A^2/c^2 \gg 1$, the electron energy is much higher than in the previously discussed cases where the dependence becomes linear for high energies:

$$\gamma = \sqrt{1 + \frac{1}{c^4} A^2} \approx \frac{1}{c^2} A \,. \tag{4.10}$$

In the next section, a scheme will be introduced which allows for recollisions in propagating laser fields with energies given by Eq. (4.9). The idea is to compensate the drift in the laser propagation direction by a second, counterpropagating laser pulse which drives the electron back to the core. In this scheme with two consecutive laser pulses, the relativistic electron recollides with the core. Since the core is not fixed at the origin,

the collision energy slightly changes for light nuclei in the strongly relativistic regime. The particles have the following energies and momenta

$$\begin{array}{lll} E_e = c^2\left(1+\frac{1}{2c^4}A^2\right), & P_{x_e} = -c\frac{1}{c^2}A, & P_{z_e} = -c\frac{1}{2c^2}A^2, \\ E_M = Mc^2\left(1+\frac{1}{2M^2c^4}A^2\right), & P_{z_M} = -P_{x_e}, & P_{z_M} = -Mc\frac{1}{2M^2c^2}A^2, \end{array} \tag{4.11}$$

where the index e holds for the electron and M for the nucleus. The total energy E' in the center of momentum frame is easily derived by exploiting the invariance of the scalar quantity $E^2 - \vec{P}\cdot\vec{P}c^2 = E'^2 - \vec{P}'\cdot\vec{P}'c^2 = E'^2$, where E and $\vec{P}$ denote the total energy and the total momentum in the rest frame. The total momentum in the transformed frame $\vec{P}'$ vanishes and one arrives at the following expression for the total energy:

$$E' = (M+1)c^2\sqrt{1+\tfrac{1}{Mc^4}A^2} \approx E_e + \left(M+\tfrac{1}{2Mc^4}A^2\right)c^2. \tag{4.12}$$

The approximation holds for $[A^2/(Mc^4)]^2 \ll 1$ which is the case if the electron energy remains small compared to the rest energy of the nucleus.

As opposed to the other case [see Eq. (4.4) and (4.8)], the collision energy scales quadratic with the vector potential. For strong laser fields $A/c^2 \gg 1$, this can be an enormous gain of collision energy.

4.2 Relativistic recollisions with two consecutive laser pulses

In this section, a double-pulse recollision scheme is introduced which enables relativistic recollisions with the highest electron energy accessible in a propagating plane laser wave (see the previous section). The first laser pulse separates an electron from the core where the laser intensity is assumed to be so high that the ionization occurs immediately. Then, a second, counterpropagating pulse drives it back for recollision (see Fig. 4.3). The core moves similarly, but due to its high mass its excursion is very small. Experimentally, the two laser pulses can be created by separating a single pulse with a beam splitter and deflecting the pulses appropriately as demonstrated in [86] for intensities of the order $10^{19}\,\mathrm{W/cm^2}$. Laser pulses with the experimentally available intensity of $10^{22}\mathrm{W/cm^2}$ [32] would enable recollisions approaching the GeV-regime. Laser intensities of that order will also be provided at the Astra Gemini laser system [87] for two separate laser beams.

4.2.1 Classical trajectories

In this scheme, the two laser-pulses act one after the other, i.e., the analytical solutions of charged particles driven by a propagating, plane laser wave can be employed. The equations of motion for laser fields which are linearly polarized in the x direction and propagating in the z direction are derived in Sec. A.1. The motion for a counterpropagating laser wave is easily obtained by rotating the coordinate system by an angle of π about the x axis, i.e., one has to replace all variables y and z by $-y$ and $-z$, respectively. Note that the initial momenta are redefined, too ($p_{y_0} \to -p_{y_0}$, $p_{z_0} \to -p_{z_0}$). For

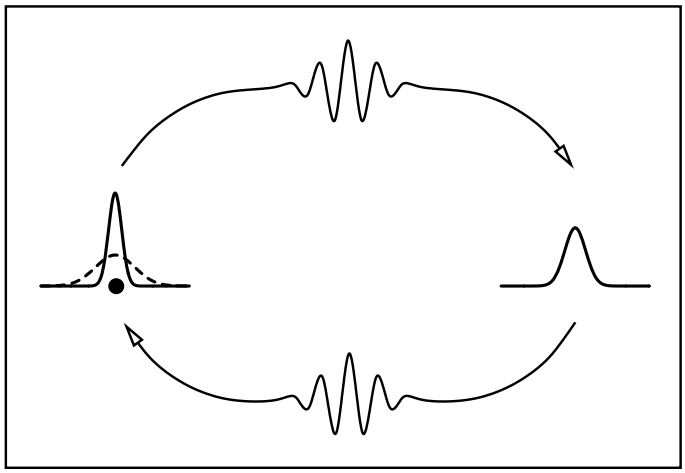

Figure 4.3: The first of two counterpropagating laser pulses ionizes an atom and the second one drives the electron wave packet back to the nucleus. With different pulse intensities, recollisions can be achieved when the kinetic energy reaches its maximum. This may be realized by means of a single pulse and a beam splitter, where the separated pulses are deflected and focused to different intensities. The laser pulses should be short to keep wave packet spreading of the electron small.

the laser propagation in the $\pm z$ direction, the equations of motion then read

$$x = \frac{p_{x_0} c}{\kappa\omega}\varphi - \frac{1}{\kappa\omega}\int A(\varphi)d\varphi\,, \tag{4.13a}$$

$$y = \frac{p_{y_0} c}{\kappa\omega}\varphi\,, \tag{4.13b}$$

$$\pm z = \frac{c}{2\omega}\left(\frac{c^2 + p_{x_0}^2 + p_{y_0}^2}{\kappa^2} - 1\right)\varphi - \frac{p_{x_0}}{\kappa^2\omega}\int A(\varphi)d\varphi + \frac{1}{2\kappa^2\omega c}\int A^2(\varphi)d\varphi\,, \tag{4.13c}$$

$$\kappa \equiv \sqrt{c^2 + p_{x_0}^2 + p_{y_0}^2 + p_{z_0}^2} \mp p_{z_0}\,, \qquad \varphi \equiv \omega t \mp \frac{\omega}{c} z\,. \tag{4.13d}$$

The initial momentum of the electron, which is placed at the origin at time $t = 0$, is given by $(p_{x_0}, p_{y_0}, p_{z_0})$, assuming the vector potential is zero at the beginning.

As discussed in Sec. 1.1.1 (*Linearization*), the equations of motion can be linearized with respect to the initial momenta over the speed of light, because the initial momenta originate from small quantum mechanical uncertainties of the initial state. If the phase in the drift terms (those terms which do not contain the vector potential) is expressed according to the definition in Eq. (4.13d), the equations of motion reduce to

$$x = p_{x_0}\left(t - \frac{1}{2\omega c^4}\int A^2(\varphi)d\varphi\right) - \frac{1}{\omega c}\left(1 \pm \frac{p_{z_0}}{c}\right)\int A(\varphi)d\varphi + x_0\,, \tag{4.14a}$$

$$y = p_{y_0}\left(t - \frac{1}{2\omega c^4}\int A^2(\varphi)d\varphi\right) + y_0\,, \tag{4.14b}$$

$$z = p_{z_0} t \mp \frac{p_{x_0}}{\omega c^2}\int A(\varphi)d\varphi + \frac{1}{2\omega c^3}\left(\pm 1 + \frac{p_{z_0}}{c}\right)\int A^2(\varphi)d\varphi + z_0\,. \tag{4.14c}$$

An initial position (x_0, y_0, z_0) different from zero has been inserted at this point by means of the following simple argument: The coordinates are shifted by the initial

position, i.e., $\vec{x}$ is replaced by $\vec{x} - \vec{x}_0$, and then the vector potential $A(\varphi(z - z_0))$ is replaced by $A(\varphi((z - z_0) + z_0)) = A(\varphi(z))$ to account for the change of the laser phase due to the shifted initial position. In other words, the coordinates of the electron are changed, whereas the laser wave remains at its former position.

Now, the classical dynamics can be determined for an electron which is driven by the two consecutive, counterpropagating laser pulses denoted by the vector potentials $A_{1,2}$. In between the laser pulses, the electron propagates freely according to the equation

$$\vec{x} = \vec{p}_0 t + \vec{x}_0 \,. \tag{4.15}$$

This expression is nonrelativistic since the particle moves with its initial velocity again after the first pulse has passed completely. This is seen if Eqs. (4.14) are differentiated with respect to time with $A(0) = \dot{A}(0) = 0$. In order to find the equations of motion during the second pulse, the initial conditions need to be adapted such that the location after the first pulse matches the initial position of the free propagation etc.

If the three parts—separation, free propagation and recollision—are combined, the following equations of motion for the returning electron are found:

$$x = p_{x_0} g_1 + p_{z_0} g_3 + \Delta x + x_0 \,, \tag{4.16a}$$
$$y = p_{y_0} g_5 + y_0 \,, \tag{4.16b}$$
$$z = p_{z_0} g_2 + p_{x_0} g_4 + \Delta z + z_0 \,. \tag{4.16c}$$

The abbreviations used are defined as follows:

$$\Delta x \equiv -\frac{1}{\omega c} \left(\int_{-\infty}^{\infty} A_1(\varphi_1) d\varphi_1 + \int A_2(\varphi) d\varphi \right) , \tag{4.17a}$$
$$\Delta z \equiv \frac{1}{2\omega c^3} \left(\int_{-\infty}^{\infty} A_1^2(\varphi_1) d\varphi_1 - \int A_2^2(\varphi) d\varphi \right) , \tag{4.17b}$$
$$g_1 = g_5 \equiv t - \frac{1}{2\omega c^4} \int A_2^2(\varphi) d\varphi + t_1 - \frac{1}{2\omega c^4} \int_{-\infty}^{\infty} A_1^2(\varphi_1) d\varphi_1 + t_C \,, \tag{4.17c}$$
$$g_2 \equiv t + \frac{1}{2\omega c^4} \int A_2^2(\varphi) d\varphi + t_1 + \frac{1}{2\omega c^4} \int_{-\infty}^{\infty} A_1^2(\varphi_1) d\varphi_1 + t_C \,, \tag{4.17d}$$
$$g_3 = g_4 \equiv \frac{1}{\omega c^2} \left(\int A_2(\varphi) d\varphi - \int_{-\infty}^{\infty} A_1(\varphi_1) d\varphi_1 \right) . \tag{4.17e}$$

Here, t_1 is the time after the first laser pulse, t is the time since the beginning of the second pulse and t_C denotes the propagation time in between the pulses.

4.2.2 Wave packet dynamics

The dynamics of the laser-driven electron is described by the analytical approach of phase-space averaging. As discussed in Sec. 1.1.1, the equations of motion need to be solved for the initial momentum to determine the probability for an electron to move from some initial point (x_0, y_0, z_0) to some other point (x, y, z) at time t. The initial momentum distribution $\tilde{\rho}$ is again chosen to be the Gaussian in Eq. (1.10b). The required function $\vec{g} \equiv (p_{x_0}, p_{y_0}, p_{z_0})$ follows from Eq. (4.16):

$$p_{x_0} = g_1^{-1} \left(x - x_0 - \Delta x - g_3 p_{z_0} \right) \approx g_1^{-1} \left(x - x_0 - \Delta x \right) , \tag{4.18a}$$
$$p_{y_0} = g_5^{-1} \left(y - y_0 \right) , \tag{4.18b}$$
$$p_{z_0} = g_2^{-1} \left(z - z_0 - \Delta z - g_4 p_{x_0} \right) \approx g_2^{-1} \left(z - z_0 - \Delta z \right) . \tag{4.18c}$$

The approximations apply if the initial width Δp is small compared to c: For initial momenta much greater than Δp the Gaussian distribution drops off quickly, i.e., $p_{x_0} \sim p_{z_0} \sim \Delta p$ and thus, the terms $g_3 p_{z_0}$ are by a factor of $\Delta p/c$ smaller than the terms of Δx (see Eq. [4.17a)]. In the relativistic regime, where the terms of Δz are greater than those of Δx, the same argument yields $g_4 p_{x_0} \ll \Delta z$. With the vector potential which will be chosen later on [see Eqs. (4.21)], the coefficients g_3 and g_4 vanish for the instant of recollision and thus, the approximations become equalities for the time of interest.

The Jacobian which is needed in Eq. (1.3) to calculate the probability distribution ρ is found to be

$$\left|\frac{\partial(p_{x_0}, p_{y_0}, p_{z_0})}{\partial(x, y, z)}\right| = \left|\frac{\partial p_{x_0}}{\partial x} \cdot \frac{\partial p_{y_0}}{\partial y} \cdot \frac{\partial p_{z_0}}{\partial z}\right| = \left|\frac{1 + \frac{1}{2c^4} A_2^2 - \frac{g_2'}{g_2}(z - z_0 - \Delta z)}{g_1 g_2 g_5}\right| \approx \frac{1 + \frac{1}{2c^4} A_2^2}{g_1 g_2 g_5} \,. \quad (4.19)$$

For the approximation here, $(z - z_0 - \Delta z) \sim \Delta p g_2$ was employed which follows from ρ as Eq. (4.18c) is inserted into the Gaussian initial momentum distribution[1] $\tilde{\rho}$. The neglected term is then found to be suppressed by a small factor of $\Delta p/c$.

With the Gaussian distribution (1.10a) for the initial position, the formula for the probability density (1.3) then yields the following result:

$$\rho(\vec{x}, t) = \frac{1 + \frac{1}{2c^4} A_2^2}{\sqrt{\pi}^3} \frac{\exp\left[-\frac{(x-\Delta x)^2}{\Delta w^2 + \Delta p^2 g_1^2} - \frac{y^2}{\Delta w^2 + \Delta p^2 g_5^2} - \frac{(z-\Delta z)^2}{\Delta w^2 + \Delta p^2 g_2^2}\right]}{\sqrt{\Delta w^2 + \Delta p^2 g_1^2}\sqrt{\Delta w^2 + \Delta p^2 g_5^2}\sqrt{\Delta w^2 + \Delta p^2 g_2^2}} \,. \quad (4.20)$$

In the following, the vector potentials of the laser pulses are specified:

$$A_1(\varphi) \propto \begin{cases} \cos\varphi \cdot \cos^2(\varphi/l) & |\varphi/l| \le \pi/2 \\ 0 & |\varphi/l| > \pi/2 \end{cases} , \quad (4.21a)$$

$$A_2(\varphi) = \sqrt{2}\, A_1(\varphi) \,, \text{ where } l = 4, 6, 8, \ldots \,. \quad (4.21b)$$

These are sinusoidal pulses with a $\cos^2$-like amplitude, where the parameter l is related to the pulse length. The number of laser cycles is given by $l/2$. Since the laser pulses should drive the electron back to the origin, both Δx and Δz [see Eqs. (4.17a) and (4.17b)] have to vanish at the same time. The maximum of the wave packet (4.20) is then found at the origin. Furthermore, the recollision should occur when the electron reaches its maximum kinetic energy. These conditions are fulfilled by the vector potentials chosen here: The second pulse has twice the intensity of the first one such that together with their symmetric shapes, the electron returns to its initial position in the z direction ($\Delta z = 0$) when half of the second pulse has passed. This is the instant when the vector potential and therefore the electron energy (4.9) reaches its maximum. The return of the electron in the x direction ($\Delta x = 0$) at the same time is ensured by the vanishing integrals $\int_{-\infty}^{0} A_{1,2} d\varphi = \int_{0}^{\infty} A_{1,2} d\varphi = 0$. Of course, to apply these pulse shapes which are centered about $\varphi = 0$, they need to be shifted in a way, that the pulses arrive at the electron position at the desired instant of time.

If the laser pulses have a form where Δx does not vanish exactly, it is still possible to achieve recollisions by choosing a somewhat different laser propagation direction in the x-z plane for the second laser pulse. One just has to make sure, that the two-dimensional trajectory of the laser-driven electron runs through the origin again.

[1] The same argument has been discussed in more detail in Sec. 2.2.2.

4.2.3 Reaction rates

To calculate the reaction probability N, the reaction rate $\dot{N} = \sigma \cdot j$ needs to be integrated over time, where j is the corresponding current density and σ denotes the total reaction cross section of some recollision reaction. In Sec. 1.1.1, it has been shown that the current density can be approximated by $j = v(\varphi) \cdot \rho$ [see Eq. (1.7)], where the velocity v follows from the classical expression $\gamma = (1 - v^2/c^2)^{-1/2}$. The dependence on the initial velocity has been shown to be negligible in the relativistic regime with the condition that the dependence of the initial momenta on the γ-factor is small [see Eq. (1.6)]. The validity of this condition can be checked here. According to Eq. (A.9), the γ-factor for an electron driven by a propagating field is given by

$$\begin{aligned}\gamma &= \frac{\kappa}{2c} + \frac{c^2 + p_{x_0}^2 + p_{y_0}^2}{2\kappa c} - \frac{p_{x_0}}{\kappa c^2} A(\varphi) + \frac{1}{2\kappa c^3} A^2(\varphi) \\ &\approx 1 + \frac{1}{2c^4} A_2(\varphi)^2 - \frac{p_{x_0}}{c} \frac{1}{c^2} A(\varphi) + \frac{p_{z_0}}{c} \frac{1}{2c^4} A(\varphi)^2 \,, \\ \kappa &\equiv \sqrt{c^2 + p_{x_0}^2 + p_{y_0}^2 + p_{z_0}^2} - p_{z_0} \,,\end{aligned} \tag{4.22}$$

where the approximation applies since the quadratic dependences of the initial momenta over the speed of light are negligible. It is seen that the terms depending on the initial momenta are small with respect to the leading term A^2/c^4. Thus the relative variation of the γ-factor with respect to the initial momentum is small, as required:

$$\frac{\vec{\nabla}_{\vec{p}_0} \gamma}{\gamma} = \frac{1}{c} \begin{pmatrix} \frac{2}{\frac{1}{c^2} A(\varphi)} \\ 0 \\ 1 \end{pmatrix} \frac{\frac{1}{2c^4} A(\varphi)^2}{1 + \frac{1}{2c^4} A(\varphi)^2} = \frac{1}{c} \begin{pmatrix} \frac{2}{\frac{1}{c^2} A(\varphi)} \\ 0 \\ 1 \end{pmatrix} (1 - \gamma^{-1}) \,. \tag{4.23}$$

The reaction rate for an electron driven by a strong propagating laser field can then be approximated by

$$\dot{N} = \sigma \frac{c}{\sqrt{1 - \left[1 + \frac{1}{2c^4} A_2^2\right]^{-2}}} \rho \,. \tag{4.24}$$

During the time of recollision, the time-dependent terms $g_{1,2,5}$ in Eq. (4.20) which determine the wave packet widths can be considered to be constant. This is reasonable because the spreading time of the whole process, i.e., from ionization to recollision is much longer than the time needed for the wave packet to pass the nucleus. Therefore, the relative variation of the terms $g_{1,2,5}$ is small. Furthermore, $\Delta x(t)$ and $\Delta z(t)$ can be expanded linearly with respect to time which means that during the recollision, the wave packet is considered to move along a straight line. In all, the reaction rate at the origin during the time of recollision is found to be

$$\begin{aligned}\dot{N}(t) = \sigma &\frac{\frac{1}{c} A_2(t_0) \sqrt{1 + \frac{1}{4c^4} A_2(t_0)^2}}{\sqrt{\pi}^3 \sqrt{\Delta w^2 + \Delta p^2 g_1(t_0)^2} \sqrt{\Delta w^2 + \Delta p^2 g_5(t_0)^2} \sqrt{\Delta w^2 + \Delta p^2 g_2(t_0)^2}} \\ &\times \exp\left[- \frac{\left[\frac{1}{c} A_2(t_0)(t - t_0)\right]^2}{\Delta w^2 + \Delta p^2 g_1(t_0)^2} - \frac{\left[\frac{1}{2c^3} A_2(t_0)^2 (t - t_0)\right]^2}{\Delta w^2 + \Delta p^2 g_2(t_0)^2} \right] \,,\end{aligned} \tag{4.25}$$

where t_0 denotes the time when the maximum recollides. The time dependence of the vector potential vanishes to linear order because the wave packet recollides when the vector potential has a maximum.

With this expression for the current density, the total reaction probability N is found by carrying out a simple Gaussian integral which yields

$$N = \frac{\sigma}{\pi}\sqrt{1+\frac{1}{4c^4}A_2^2}\left[\Delta w^2+\Delta p^2\left(\frac{3\pi l}{2\omega}+t_C\right)^2\right]^{-1} \times\left[\Delta w^2+\Delta p^2\left(\frac{3\pi l}{2\omega}\left(\frac{1}{2c^4}A_2^2\right)+t_C\right)^2 +\frac{1}{4c^4}A_2^2\left(\Delta w^2+\Delta p^2\left(\frac{3\pi l}{2\omega}+t_C\right)^2\right)\right]^{-1/2}. \quad (4.26)$$

For calculating the reaction probability, it has been assumed that the nucleus is a point-like object which is found at the origin during the recollision process. However, these simplifications are justified as will be discussed in the following.

The laser fields act on the nucleus as well, but it returns to the origin at the same time as the electron. In principle, the motion is similar to the electron trajectory with the difference that the mass is much higher. The γ-factor for a laser driven nucleus is given by [compare Eq. (4.9)]

$$\gamma_N = 1+\frac{1}{2Mc^4}A^2\,, \quad (4.27)$$

where M is the nuclear mass in atomic units. Since even a proton, which is the lightest nucleus, is by a factor of $M \approx 1800$ heavier than an electron, the γ-factor remains of the order of one for the laser intensities of interest here (i.e. for electron energies of $\gamma = 1+A^2/(2c^4) < 2000$). Especially the motion of heavy nuclei as considered later on remain nonrelativistic. For example, the velocity of a cesium nucleus ($M = 133\times 1800$) at the moment of recollision is found to be only 0.035 a.u. if the electron has a maximum energy of $\gamma_m = 2000$. If necessary, e.g., for very light nuclei and extremely high laser intensities, the nuclear motion can be taken into account by considering the electron current density at the location of the nucleus instead of considering it at the origin.

The extension of any nucleus is small on an atomic scale. The radius of a nucleus is roughly given by $2\times 10^{-5}M^{1/3}$ a.u. If the reaction rate is calculated for an extended object such as an electron bound to the nucleus, one needs to average over its probability density $\tilde{\rho}$ to get the reaction rate:

$$\dot{N} = \sigma\int j(\vec{x})\tilde{\rho}(\vec{x})d^3x\,. \quad (4.28)$$

This reduces to the previously used expression $\dot{N} = \sigma\cdot j$ for point-like projectiles.

Deviations due to thermal initial velocities or the interaction of electrons in a thin gas are negligible. These effects will be discussed in Sec. 6.1.3 for the recollision model with magnetic refocusing, where the whole recollision process is much longer than here.

4.2.4 Results and discussion

For the following discussion, short laser pulses of two cycles ($l = 4$) are chosen to minimize the time for wave packet spreading which reduces the reaction probability [see the dependence on l in Eq. (4.26)]. Few cycle pulses are experimentally available, where powers up to the petawatt regime seem to be feasible today [51].

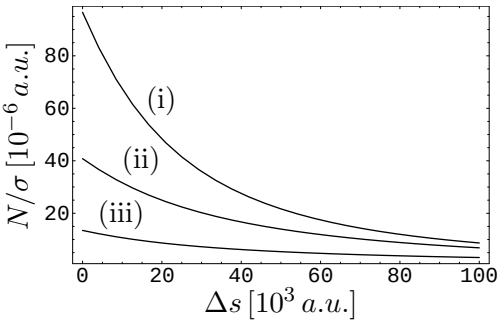

Figure 4.4: The reaction probability over the cross section N/σ is plotted versus the distance Δs between the initial z position of the electron and the plane where the time interval between the laser pulses is zero. The curves (i), (ii) and (iii) correspond to the recollision energies with the relativistic γ-factors of $\gamma_m = 20$, $\gamma_m = 200$ and $\gamma_m = 2000$, respectively. The laser wavelength is taken to be $\lambda = 800$ nm and the initial widths in momentum space are $\Delta p = 0.1$ a.u.

Now, the initial electron wave packets should originate from a bound atomic system. To mimic this situation, the initial wave packet widths in momentum and coordinate space are chosen to be those of a spherically symmetric atomic s-orbital with the principle quantum number n. The mean square distance is given by $\overline{r^2} = n^2(5n^2+1)/(2Z^2)$, where Z is the nuclear charge number (e.g. see [90]). With $\overline{r^2} = 3\Delta w^2$ for a spherical wave packet, one finds

$$\Delta w = n/Z \cdot \sqrt{(5n^2+1)/6}\,. \tag{4.29}$$

Similar relations $\overline{p^2} = Z^2/n^2$ and $\overline{p^2} = 3\Delta p^2$ hold for the mean square of the momentum. This yields

$$\Delta p = Z/(n\sqrt{3}) \tag{4.30}$$

for the width in momentum space.

Due to the finite velocity of light, the time interval between the laser pulses t_C depends on z_0 which is the initial position of the atom in the laser propagation direction. As the initial z position of the electron decreases, the first laser pulse arrives earlier whereas the second one is retarded. The time difference is $t_C = 2\Delta s/c$, where Δs is the distance from the plane with $t_C = 0$. The highest recollision probability is achieved for $t_C = 0$, because in this case, the spreading time is shortest and therefore the wave packet widths are smallest. For overlapping laser fields (i.e. $t_C < 0$), the electrons miss the nucleus as seen by means of a classical, numerical analysis.

Figure 4.4 shows how the reaction probability decreases as Δs increases. The behavior is depicted for different laser intensities, i.e. for different electron energies which are denoted by the relativistic γ-factor γ_m at the instant of recollision. For small values Δs, the reaction probability decreases with high energies. As Δs increases, the free wave packet evolution between the two laser pulses becomes the dominant factor for the wave packet widths, i.e., the reaction rates for different energies have the same asymptotical behavior.

To calculate the number of reactions R which is expected in a gas sample with the particle density n, the dependence of the single particle reaction probability N on the initial z position of the electron needs to be taken into account. The total yield in a

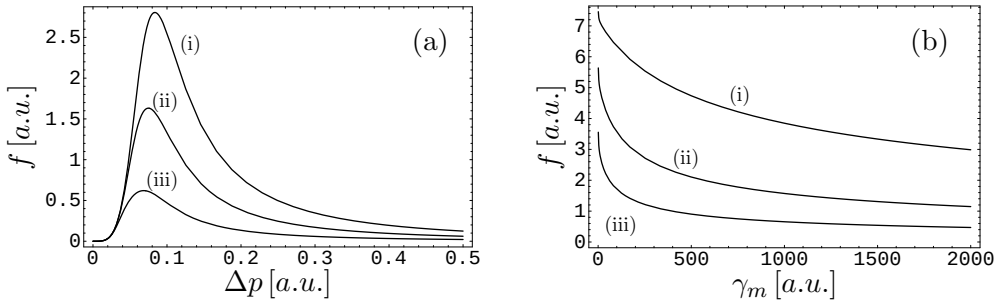

Figure 4.5: The function f in Eq. (4.31) which is proportional to the expected number of reactions is plotted for different parameters. In (a) the dependence on the initial momentum width Δp is depicted. The electron energy is given by (i) $\gamma_m = 20$, (ii) $\gamma_m = 200$ and (iii) $\gamma_m = 2000$, and the laser wave length is $\lambda = 800$ nm. In (b) it is shown how the yield depends on the electron energy, i.e., the function f is plotted versus the γ-factor. Furthermore, the dependence on the laser wave length is illustrated. The curves (i), (ii) and (iii) correspond to the wavelengths $\lambda = 200$ nm, $\lambda = 400$ nm and $\lambda = 800$ nm, respectively. It is seen that the yield decreases with higher energies and longer wave lengths. The initial momentum width is taken to be $\Delta p = 0.1$ a.u.

gas sample is given by

$$R = n \cdot S \int_0^{\Delta s_m} N(z) dz \equiv n \cdot S \cdot \sigma \cdot f \,, \tag{4.31}$$

where S denotes the surface area of the sample in the x-y plane and Δs_m is its width in the z direction. In the following, Δs_m will be taken to be $\Delta s_m = 60000$ a.u., which corresponds to roughly 3 μm. n, S and σ will be kept general.

The yield depends on the initial widths in momentum space Δp. For small values, spreading is slow, but the initial spatial widths are large. On the other hand, small initial spatial widths imply quick spreading. As shown in Fig. 4.5(a), there is an optimum value in between these two limits which maximizes the yield.

The dependence of the yield on the electron energy is shown in Fig. 4.5(b). It is seen that the yield decreases with increasing recollision energy. Higher yields can be achieved by shorter laser wave lengths, because this implies shorter laser pulses which reduces the spreading time of the electron wave packets.

Now, numbers can be specified to estimate the luminosity, or the reaction rates for some reaction. The luminosity is defined by $\mathcal{L} = \dot{R}/\sigma$, i.e., by the ratio of the reaction rate and the cross section. The averaged value for the reaction rate is given by $\dot{R} = R \cdot \nu$, where ν is the repetition rate of the laser system. With Eq. (4.31), the luminosity is found to be

$$\mathcal{L} = n \cdot S \cdot f \cdot \nu \,. \tag{4.32}$$

For $n = 10^{15}$ cm^{-3}, $S = (10\ \mu\text{m})^2$, $f = 1.3$ and $\nu = 100$ Hz, the luminosity becomes $\mathcal{L} = 7.1 \cdot 10^{20}\text{cm}^{-1}\text{s}^{-1}$. The value for f is found for the parameters $\lambda = 800$ nm, $\gamma_m = 200$ and $\Delta p = 0.1$ a.u. (see Fig. 4.5), where the value for the momentum width corresponds to an s-orbital with principal quantum number $n = 6$ as for the valence electron of a cesium atom. The repetition rate of $\nu = 100$ Hz is easily achieved for nonrelativistic laser systems. For high intensities, repetition rates are smaller, but rates of the order $\nu = 100$ Hz are likely to be available in the nearer future. Consider the process of bremsstrahlung. The differential cross section with respect to the photon

energy which is found, e.g., in [91], can be integrated to yield the cross section for the case that at least half of the electron kinetic energy is carried away by a photon. The total cross section for this reaction is found to be $\sigma = 1.9 \times 10^{-23}\text{cm}^2$ for cesium atoms. This gives a reaction rate of $\dot{R} = 0.013\ \text{s}^{-1}$, i.e., a photon of at least 50 MeV is expected every 75 seconds.

However, for other reactions such as the creation of particle-antiparticle pairs, the reaction rates are very small. For example, consider the creation of electron-positron pairs by electron-nucleus collisions with the electron energy of 100 MeV. In this case, the cross section is found to be $\sigma = 6.3 \times 10^{-25}\text{cm}^2$ [92] which yields a rate of one event in 37 minutes for the same luminosity as considered above.

The luminosity is small if the reaction probability is averaged over the time between two laser shots, because of the small repetition rate of 100 Hz. If the average is only taken over the time duration of the process, i.e., from ionization to recollision, the luminosity reaches $\mathcal{L} = 10^{32}\ \text{cm}^{-1}\text{s}^{-1}$ which is a typical value for a conventional particle accelerator.

The luminosities could be increased with higher particle densities n, but then the returning electrons would not only react with the original ion, but also with others of the sample. The reaction probability for an electron to react with a particle in a gas sample is given by the gas density n multiplied by the volume which is spanned by the cross section σ and the distance s the electron travels in the sample. This needs to be multiplied by the number of electrons in the gas volume $n \cdot S \cdot d$, where d is the extension of the gas sample in the z direction. The expected number of reactions is then given by

$$\tilde{R} = \sigma \cdot n^2 \cdot S \cdot d \cdot s\,. \tag{4.33}$$

The number of these random reactions can be minimized if the sample width is given by $d = \Delta s_m$, i.e. by the range of the initial z position which is relevant for recollisions (see Fig. 4.4). The traveling distance in the sample s is also limited by Δs_m. In the relativistic regime, s can be approximated by the distance Δz an electron is carried away by the laser field in the z direction. For electron energies corresponding to $\gamma_m > 22$ and $\lambda = 800$ nm, values of $\Delta z > \Delta s_m \approx 60000$ a.u. are found, i.e., in this case s is given by Δs_m. With Eq. (4.31), the ratio of recollision reactions and random events is then given by $R/\tilde{R} = f/(n \cdot \Delta s_m^2)$. It is seen that this ratio scales like $1/n$, i.e., for high gas densities, random collisions become dominant over recollisions. For the examples given in the last paragraph, this ratio is given by $R/\tilde{R} = 6.3$, i.e., 71% of the expected events originate from electron collisions with the original ion.

Chapter 5

Refocused wave packets

Spreading is a general problem occuring in recollision schemes. The more electron wave packets spread, the more the probability of recollisions reduces. This has also be seen in the relativistic recollision scheme introduced in Sec. 4.2 where wave packet spreading inhibits effective recollisions. Therefore, it is of interest to consider ways of manipulating the spreading dynamics of the electron. In this chapter, two methods are discussed which allow for refocusing a spreading electron wave packet to its original width. The spreading dynamics can be reversed by means of a magnetic field pulse or via a harmonic potential which is turned on for a certain time. These ideas are introduced in the following two sections before they will be applied in relativistic recollision schemes.

5.1 Magnetic refocusing

The basic idea of magnetic refocusing is to reverse the electron momentum, independent of the initial conditions. The wave packet which is considered as an ensemble of particles will then be restored because all electron trajectories revisit their points of origin at the same time. Such a momentum reversal can be achieved by a time-dependent magnetic field. Figure 5.1(a) shows a trajectory where the electron momentum is reversed. The magnetic field which guides the electron along this trajectory is seen in Fig. 5.1(b). Of course, refocusing can only be achieved in the plane perpendicular to the magnetic field, because the Lorentz force vanishes in the field direction. Momentum reversal can therefore be achieved in two dimensions, whereas the third one is not affected by the magnetic field. In the absence of any electric field, the curvature of the electron trajectory is proportional to the magnetic field $B(t)$, i.e., the time-dependence of the field represents the curvature of the trajectory. However, time-varying magnetic fields induce disturbing electric fields. This can be accounted for but since the momentum reversal is required to be independent of the direction of the electron momentum, cylindrical symmetry of the induced electric field is required. For example, this can be achieved if the magnetic field is created by a cylindrical solenoid. The cylindrical symmetry also implies that the electron needs to be placed on the symmetry axis in order to achieve refocusing. In the following, an example is given which can be treated analytically. Momentum reversal can be achieved for two identical rectangular magnetic field pulses with proper timing. The electron can be guided along the trajectory shown in Fig. 5.2. The field configuration has to be rotationally symmetric such that the momentum reversal works for every direction of the initial momentum. The homogeneous magnetic field is turned on when the electron reaches point T and the electron

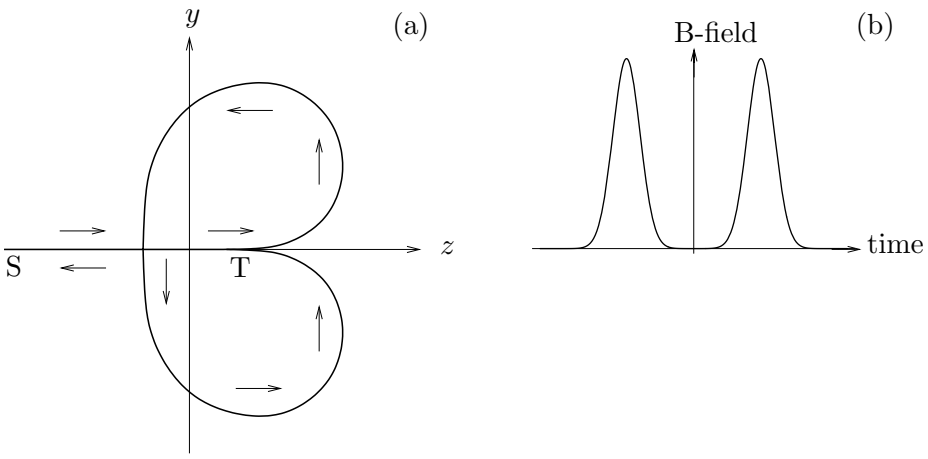

Figure 5.1: Image (a) shows a schematic drawing of a classical electron trajectory in a time-dependent magnetic field perpendicular to the y-z plane. The particle with velocity v starts at point S and travels to T where the magnetic field is turned on. The magnetic field pulse is chosen in a way that the momentum of the electron has reversed when it arrives at T for the second time. Then, the electron will return to its initial position S. If this is applied to an ensemble of particles representing an electron wave packet, the original distribution can consequently be restored in the planes perpendicular to the magnetic field. Such electron trajectories which imply a momentum reversal can be achieved by two magnetic field pulses with proper widths and time delay as depicted schematically in (b).

moves on a circular path. Additionally, the induced electric field changes the momentum of the electron and an edge occurs in the trajectory. The induced electric field is rotationally symmetric and the electron experiences a kick to the left. The magnitude of the electric field is calculated from the following Maxwell equation:

$$\oint \vec{E} d\vec{s} = -\frac{1}{c}\dot{\vec{B}} \cdot \vec{F} \quad \Rightarrow \quad E = \frac{r}{2c}\dot{B}\,, \tag{5.1}$$

where the line-integral is evaluated along the circular edge of the area denoted by $\vec{F}$. The equation on the right side is a relation for the absolute values of the fields. The momentum kick Δv is given by

$$\Delta v = \int E dt = \frac{r}{2c}B = \frac{v_0 t_1}{2c}B\,. \tag{5.2}$$

Here, t_1 denotes the time interval which the electron needs to move from S to T with velocity v_0. In the following, it will be shown, that the relation between the magnetic field and the time interval needs to be $B/c = 2/t_1$. With this condition, one finds $\Delta v = v_0$. Thus, the direction of motion changes by 45 degrees and the velocity increases from v_0 to $\sqrt{2}v_0$. The radius of the circular trajectory in the magnetic field is then found to be

$$r' = \frac{\sqrt{2}v_0 c}{B} = \frac{\sqrt{2}}{2}v_0 t_1 = \frac{\sqrt{2}}{2}r\,. \tag{5.3}$$

From these results, it is seen, that the center of the circle is at the point M and the electron motion is given as shown in Fig. 5.2.

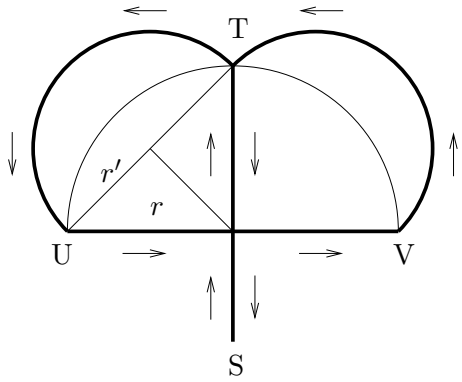

Figure 5.2: The electron moves upwards when the magnetic field is turned on and the motion describes a circle until the magnetic field is turned off again. The kinks in the trajectories are due to the induced electric fields. After two magnetic pulses with the correct timing the electron has reversed its momentum.

When the magnetic field is turned off again as the electron arrives at the point U, the induced electric field pushes the electron upwards. Since the kick has the same strength as the first one, the electron is slowed down in a way that it moves with its initial velocity v_0 to the right.

The pulse length of the magnetic field is given by the time the electron needs to travel from T to U which is found to be $T = \pi t_1/2$.

The same procedure with a second magnetic pulse is repeated as the electron reaches V. Finally, when the electron returns to S, it has reversed its momentum. Note that the momentum reversal works for arbitrary initial velocities concerning both the direction and the absolute value.

The whole process is summarized in Fig. 5.3.

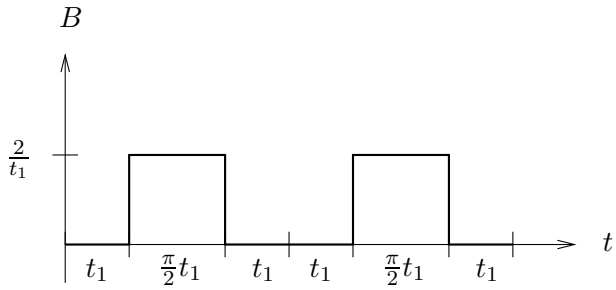

Figure 5.3: Two rectangular magnetic pulses with proper timing and amplitude can be applied for a momentum reversal. These pulses give rise to the trajectory shown in Fig. 5.2.

Other pulse shapes such as two Gaussian pulses [as depicted in Fig. 5.1(b)] are possible for implementing magnetic refocusing, but the correct timing and the required pulse widths have to be determined numerically.

5.2 Refocusing by a harmonic potential

Wave packets can also be refocused by means of a harmonic potential which is turned on for a certain time. This can be understood with the classical picture where the wave packet is modeled with an ensemble of classical trajectories and it can as well be verified quantum mechanically.

5.2.1 Classical analysis

In the following, the one-dimensional case is considered which can be applied to all three dimensions separately. If a harmonic potential with the frequency Ω is turned on for the time t_C after the classical particle has propagated freely for some time t_1, the particle moves freely again with some other velocity. It moves either towards or away from its initial position. Now, it is assumed that the particle will return to its initial position x_0 at some time t after the harmonic potential has been turned off again. If the parameters t_1, Ω and t_C are chosen properly, the instant when the particle revisits its initial position can become independent of the initial conditions x_0 and p_0. This can be expected, since there are three parameters and only two independent initial conditions. Note that the equations of motion after the harmonic field pulse can be written as a linear superposition $x(t) = f_1(t)x_0 + f_2(t)p_0$ of two functions $f_1(t)$ and $f_2(t)$ because both the free propagations and the dynamics in the potential follow from linear equations of motion ($\ddot{x} = 0$ and $\ddot{x} = -\Omega^2 x$).

The solutions are given by the following equations

$$x(t) = p_2 t + x_2\,, \tag{5.4a}$$

$$x_2 = x_1 \cos\Omega t_C + \frac{p_1}{\Omega}\sin\Omega t_C\,, \quad p_2 = -x_1\Omega\sin\Omega t_C + p_1\cos\Omega t_C\,, \tag{5.4b}$$

$$x_1 = p_1 t_1 + x_0\,, \quad p_1 = p_0\,. \tag{5.4c}$$

The first and the third line describe the free propagations, whereas the second line is the solution of the harmonic oscillator. These equations are coupled by the initial conditions. One finds the following:

$$x(t) = [(1-\Omega t\Omega t_1)\sin(\Omega t_C) + (\Omega t + \Omega t_1)\cos(\Omega t_C)]\frac{p_0}{\Omega} + [\cos(\Omega t_C) - \Omega t\sin(\Omega t_C)]x_0\,. \tag{5.5}$$

The condition that the particle revisits its initial position $x = x_0$ independent of its initial conditions yields two equations. The term proportional to p_0 has to vanish and the one proportional to x_0 has to be equal to one. This reduces to these conditions:

$$\cos(\Omega t_C) - \Omega t\sin(\Omega t_C) = 1\,, \tag{5.6a}$$

$$\Omega t + \Omega t_1 + [(\Omega t)^2 + 1]\sin(\Omega t_C) = 0\,. \tag{5.6b}$$

These equations have a variety of solutions. Here, with $\Omega t_C = 3\pi/2$ and $\Omega t_1 = 1$, the simplest one will be discussed. In this case, the particle revisits its initial position at the instant when $\Omega t = 1$. In the classical picture, any (one-dimensional) distribution of an ensemble of classical particles will be restored at this moment since each ensemble member revisits its origin, independent of its initial conditions. This mechanism can be applied in three orthogonal directions to yield three-dimensional refocusing.

5.2.2 Quantum mechanical analysis

The result of the last section is employed to verify that refocusing with a harmonic potential is also found in quantum mechanics. The idea is to calculate the propagator for the whole process and to show that the initial probability density distribution is reproduced.

The propagator for a free particle D_F and the one for the harmonic oscillator D_H are given by (see e.g. [93]):

$$D_F(x',t;x,0) = \frac{1}{\sqrt{2\pi i t}} \exp i\frac{(x'-x)^2}{2t}\,, \tag{5.7a}$$

$$D_H(x',t;x,0) = \sqrt{\frac{\Omega}{2\pi i}}\sin^{-1/2}(\Omega t)\exp i\Omega\frac{(x'^2+x^2)\cos(\Omega t)-2x'x}{2\sin(\Omega t)}\,. \tag{5.7b}$$

These functions propagate the amplitude of a wave function from some point x at time $t=0$ to some other point x' at time t. For the special case with $\Omega t_C = 3\pi/2$ and $\Omega t_1 = \Omega t = 1$, where refocusing is expected, these propagators reduce to

$$D_F(x',\Omega^{-1};x,0) = \sqrt{\frac{\Omega}{2\pi i}}\exp i\frac{\Omega}{2}(x'-x)^2\,, \tag{5.8a}$$

$$D_H(x',3\pi(2\Omega)^{-1};x,0) = \sqrt{\frac{\Omega}{2\pi i}}\exp i\Omega\, x'x\,. \tag{5.8b}$$

The propagator D for the whole process is found by coupling the propagators in Eqs. (5.8):

$$\begin{aligned} D(x,x_0) &= \int_{-\infty}^{\infty} D_F(x,x_2)\int_{-\infty}^{\infty} D_H(x_2,x_1)D_F(x_1,x_0)dx_1dx_2 \\ &= \left(\frac{\Omega}{2\pi i}\right)^{3/2}\iint \exp i\frac{\Omega}{2}[(x-x_2)^2+2x_2x_1+(x_1-x_0)^2]dx_1dx_2\,. \end{aligned} \tag{5.9}$$

By means of the Fourier representation of the δ-function, the following propagator is found:

$$D(x,x_0) = i\exp\left(i\frac{\Omega}{2}x^2\right)\delta(x-x_0)\,. \tag{5.10}$$

If this result is applied to some arbitrary wave function $\psi(x)$, it is found that the propagator only changes the phase of the wave function:

$$\psi(x) \to \int D(x,x_0)\psi(x_0) = i\exp\left(i\frac{\Omega}{2}x^2\right)\psi(x)\,. \tag{5.11}$$

The initial probability distribution $|\psi(x)|^2$ is therefore recovered after the process. This means that quantum mechanics yields the result in terms of magnetic refocusing which has been expected on account of the classical analysis.

5.2.3 Harmonic potentials in laser beams

For implementing the idea of refocusing with harmonic potentials, strong harmonic fields are needed which can be turned on and off very quickly. An idea to realize strong harmonic potentials is to utilize the ponderomotive potential of an intense laser beam. As will be shown below, an electron has some potential energy if it is placed inside of a

laser beam, where the energy is related to the amplitude of the vector potential. With the corresponding beam profile, various ponderomotive potentials can be realized. For example, it has been demonstrated that electrons can be confined in the ponderomotive potential of an intense laser beam [94]. The classical motion of the electron in the laser beam can be considered as the superposition of a quick oscillation following the time-dependent laser electric field and a slower motion which corresponds to the motion in the ponderomotive potential. Thus, with a certain spatial laser profile, the motion of an electron in an effective harmonic potential can be realized. The period of time the harmonic potential is turned on is determined by the length of the laser pulse. The physics of effective motions in oscillating fields is well-known from high-frequency traps, where charged particles are confined in an effective potential (see, for instance, [95]).

Classical description

The equations of motion for a classical electron in a laser field are easily obtained from the Hamiltonian equations:

$$\dot{x}_i = \frac{\partial H}{\partial p_i}\,, \quad \dot{p}_i = -\frac{\partial H}{\partial x_i}\,, \quad H = \frac{1}{2}\left(\vec{p} - \frac{1}{c}\vec{A}\right)^2\,, \tag{5.12a}$$

$$\Rightarrow \ddot{x}_i = -\frac{1}{c}\dot{A}_i + \frac{1}{c}\dot{x}_k\left(\frac{\partial A_k}{\partial x_i} - \frac{\partial A_i}{\partial x_k}\right)\,. \tag{5.12b}$$

Here, the Einstein sum convention is applied[1], where the indices denote the components of the vector potential $\vec{A}$, the momentum $\vec{p}$ and the position $\vec{x}$, respectively. In the nonrelativistic regime, the motion is dominated by the electric field, i.e. by the term $-\dot{A}_i/c$. The electron position is therefore written as the sum $x_i = x_i^E + x_i^P$, where x_i^E and x_i^P denote the motion due to the electric field and due to the ponderomotive potential, respectively. The amplitude of x_i^E is assumed to be small, whereas there is no restriction on x_i^P. Thus, the spatial dependence of the electric field is expanded about x_i^P to linear order:

$$\dot{A}_i(x_k) = \dot{A}_i(x_k^P) + \frac{\partial \dot{A}_i}{\partial x_{k'}}(x_k^P)x_{k'}^E\,. \tag{5.13}$$

Since the Lorentz force depends on the velocity, the terms due to the magnetic field $(\partial A_i/\partial x_j)$ are suppressed by a small factor of $\dot{x}_i/c$. Then, it is sufficient to approximate the spatial dependence of the magnetic terms on $x_i = x_i^E + x_i^P$ by $x_i \approx x_i^P$ because together with the small term $\dot{x}_i/c$ the error is of quadratic order.

The time-dependence of the vector potential in a laser field is chosen to be an oscillation with an optical frequency ω:

$$A_i(x_k, t) = A_i^0(x_k)\cos(\omega t)\,. \tag{5.14}$$

Such a sinusoidal time-dependence is exact for standing laser waves [compare e.g. Eq. (3.1c)].

[1] If an index occurs twice in a product, it is summed over. For example, $x_i p_i + x_i p_j$ is an abbreviation for $(\sum_i x_i p_i) + x_i p_j$.

The oscillating motion x_i^E is then given by

$$\ddot{x}_i^E = -\frac{1}{c}\dot{A}_i(x_k^P) = \frac{\omega}{c}A_i^0(x_k^P)\sin(\omega t)\,, \tag{5.15a}$$

$$\dot{x}_i^E = -\frac{1}{c}A_i^0(x_k^P)\cos(\omega t)\,, \tag{5.15b}$$

$$x_i^E = -\frac{1}{\omega c}A_i^0(x_k^P)\sin(\omega t)\,. \tag{5.15c}$$

General initial conditions are included in the motion x_i^P due to the ponderomotive potential. This result is inserted into the equation of motion (5.12b) to yield

$$\begin{aligned}\ddot{x}_i^P = &-\frac{1}{c^2}A_k(x_i^P)\frac{\partial A_i^0}{\partial x_k}(x_i^P)\sin^2(\omega t)\\ &+\frac{1}{c}\left(\dot{x}_k^P - \frac{1}{c}A_k^0(x_i^P)\cos(\omega t)\right)\left(\frac{\partial A_k^0}{\partial x_i}(x_i^P) - \frac{\partial A_i^0}{\partial x_k}(x_i^P)\right)\cos(\omega t)\,.\end{aligned} \tag{5.16}$$

The quickly varying functions $\cos(\omega t)$ and $\sin(\omega t)$ can be averaged over several periods, whereas factors depending on x_i^P are considered to be constant during the time of averaging. With

$$\overline{\sin(\omega t)} = \overline{\cos(\omega t)} = 0\,, \tag{5.17a}$$

$$\overline{\sin^2(\omega t)} = \overline{\cos^2(\omega t)} = \frac{1}{2}\,, \tag{5.17b}$$

the following effective motion is then found:

$$\ddot{x}_i^P = -\frac{1}{2c^2}A_k^0(x_i^P)\frac{\partial A_k^0}{\partial x_i}(x_i^P)\,, \tag{5.18}$$

which in vector notation reads

$$\ddot{\vec{x}}^P = -\vec{\nabla}\Phi_p\,, \quad \vec{\nabla}\Phi_p \equiv \frac{1}{4c^2}\vec{A}^0(\vec{x}^P)\cdot\vec{A}^0(\vec{x}^P)\,, \tag{5.19}$$

where Φ_p is the ponderomotive potential. This equation describes the classical motion of a particle in a potential.

Quantum mechanical description

The same effective potential can be derived by means of the Schrödinger equation [96] which reads

$$\begin{aligned}i\dot{\psi} &= \frac{1}{2}\left(-i\vec{\nabla} - \frac{1}{c}\vec{A}\right)^2\psi\\ &= -\frac{1}{2}\Delta\psi - \frac{i}{c}\vec{A}^0\cdot\vec{\nabla}\cos(\omega t)\psi + \frac{1}{2c^2}\vec{A}^0\cdot\vec{A}^0\cos^2(\omega t)\psi\,.\end{aligned} \tag{5.20}$$

The same time-dependence as previously [see Eq. (5.14)] has been inserted, here. With the averaging procedure as in Eqs. (5.17) and assuming that the wave function ψ varies slowly, the Schrödinger equation for a particle in a potential is found:

$$i\dot{\psi} = -\frac{1}{2}\Delta\psi + \frac{1}{4c^2}\vec{A}^0\cdot\vec{A}^0\psi = -\frac{1}{2}\Delta\psi + \Phi_p\psi\,. \tag{5.21}$$

Effective harmonic potentials in laser fields

The previous results can now be applied to construct a ponderomotive potential in which the electron wave packet can be refocused. An effective harmonic potential can be achieved by means of a laser which is run in the TEM01 mode[2]. Such a laser pulse has the following beam profile perpendicular to the propagation direction [98]:

$$\vec{E}_x = E^0(t)\hat{e}_x \frac{x}{w_x} \exp - \left(\frac{x^2}{w_x^2} + \frac{y^2}{w_y^2} \right) . \tag{5.22}$$

The parameters $w_{x,y}$ determine the widths of the laser focus. As opposed to the usual case where the beam profile is Gaussian, the electric field is proportional to x. Close to the center of the beam, i.e. for $x^2/w_x^2 \ll 1$ and $y^2/w_y^2 \ll 1$, the electric field strength depends linearly on x. The corresponding vector potential is then given by

$$\vec{A}_x \approx A^0(t)\hat{e}_x \frac{x}{w_x} , \tag{5.23}$$

which according to Eq. (5.19) yields an effective harmonic potential for the x direction. This can be extended to three dimensions if three, mutually perpendicular laser beams with the same mode $\vec{A}_x$, $\vec{A}_y$ and $\vec{A}_z$ are superimposed. The ponderomotive potential then has the desired form:

$$\Phi_p = \frac{1}{4c^2} \left(\vec{A}_x + \vec{A}_y + \vec{A}_z \right)^2 = \frac{1}{4c^2} \left[\left(A_x^0 \frac{x}{w_x} \right)^2 + \left(A_y^0 \frac{y}{w_y} \right)^2 + \left(A_z^0 \frac{z}{w_z} \right)^2 \right] . \tag{5.24}$$

With this potential, electron wave packets can be refocused in three dimensions.

[2]This way of creating a potential has been discussed in [97] for trapping electron bunches.

Chapter 6

Refocused relativistic recollisions

A relativistic recollision scheme with two consecutive laser pulses has been introduced in Sec. 4.2. The luminosity has turned out to be rather low for currently available laser systems which makes, for instance, the creation of electron-positron pairs rare events. One reason for the low luminosity is the limited repetition rate of strong laser systems. Additionally, there is the more fundamental problem of wave packet spreading which is responsible for the low reaction rates. In the previous chapter, two different methods have been introduced which can be employed to reverse the spreading dynamics of wave packets. In the following, these ideas of magnetic refocusing and refocusing by means of a harmonic potential are incorporated into the relativistic recollision scheme with two consecutive laser pulses.

6.1 Recollisions with magnetic refocusing

The magnetic field pulse which reverses the spreading dynamics is applied between the two laser pulses. This means that the wave packet refocuses in two dimensions when it is driven back to the core. Since refocusing only works in the plane perpendicular to the magnetic field direction there is one direction left in which refocusing does not occur. For that reason, the orientation of the magnetic field has to be chosen in a way that the reaction probability is maximized. This is the case if the orientation of the nonrefocused direction of the wave packet coincides with the direction of motion.

Although the core is much heavier than the electron, it is still moved by the lasers, but it returns to its original place at the same instant as the electron.

As in the double-pulse scheme of Sec. 4.2, the system can be tuned in a way that the recollision occurs when the kinetic energy of the electron has reached its maximum. Furthermore, the recollision takes place as the wave packet is refocused to its initial width.

6.1.1 Classical trajectories

The wave packet is again described by means of the classical Monte-Carlo approach of phase-space averaging. Therefore, the classical equations of motion need to be known. The dynamics of the electron in the two laser pulses has been discussed in Sec. 4.2. The solutions which are linearized in the initial momenta are given by the following

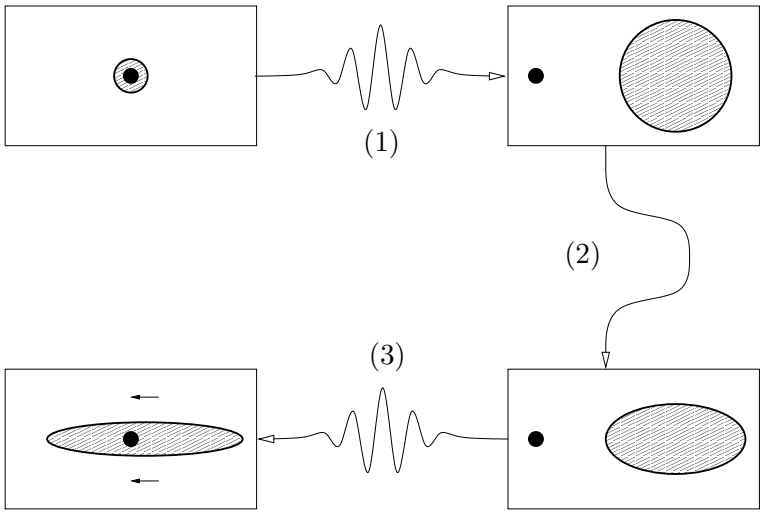

Figure 6.1: The first intense laser pulse ionizes an atom (1). As the electron is separated from the core, its probability density distribution spreads. A magnetic field pulse is employed (2) to reverse spreading in two dimensions. Finally, the electron is driven back to the core by means of another intense laser pulse (3). The system can be tuned in a way that the electron recollides with maximal kinetic energy and the direction in which the electron wave packet is not refocused is parallel to its velocity vector.

equations [see Eqs. (4.14)]:

$$x = p_{x_0}\left(t - \frac{1}{2\omega c^4}\int A^2(\varphi)d\varphi\right) - \frac{1}{\omega c}\left(1 \pm \frac{p_{z_0}}{c}\right)\int A(\varphi)d\varphi + x_0\,, \tag{6.1a}$$

$$y = p_{y_0}\left(t - \frac{1}{2\omega c^4}\int A^2(\varphi)d\varphi\right) + y_0\,, \tag{6.1b}$$

$$z = p_{z_0}t \mp \frac{p_{x_0}}{\omega c^2}\int A(\varphi)d\varphi + \frac{1}{2\omega c^3}\left(\pm 1 + \frac{p_{z_0}}{c}\right)\int A^2(\varphi)d\varphi + z_0\,, \tag{6.1c}$$

$$\varphi \equiv \omega t \mp \frac{\omega}{c}z\,. \tag{6.1d}$$

The laser propagation is again in the z direction for the first laser pulse and in the $-z$ direction for the second.

The effect of the magnetic field pulse is to reverse the initial momentum of the electron in two dimensions, whereas the dynamics in the third dimension is a free propagation. If the magnetic field points in the z direction, the classical particle state after the magnetic pulse is given by the following equations in matrix notation:

$$\begin{pmatrix} x \\ \dot{x} \\ y \\ \dot{y} \\ z \\ \dot{z} \end{pmatrix} = \begin{pmatrix} 1 & 0 & & & & \\ 0 & -1 & & & & \\ & & 1 & 0 & & \\ & & 0 & -1 & & \\ & & & & 1 & t_C \\ & & & & 0 & 1 \end{pmatrix} \cdot \begin{pmatrix} x_0 \\ p_{x_0} \\ y_0 \\ p_{y_0} \\ z_0 \\ p_{z_0} \end{pmatrix} \equiv \tilde{M} \cdot \begin{pmatrix} x_0 \\ p_{x_0} \\ y_0 \\ p_{y_0} \\ z_0 \\ p_{z_0} \end{pmatrix}. \tag{6.2}$$

To align the broadening direction with the velocity vector at the instant of recollision, the magnetic field needs to be tilted by an angle δ about the y axis. The matrix $\tilde{M}$ is

transformed via the rotation matrix T:

$$M \equiv T \cdot \tilde{M} \cdot T^{-1}\,, \quad T = \begin{pmatrix} \cos\delta & 0 & & \sin\delta & 0 \\ 0 & \cos\delta & & 0 & \sin\delta \\ & & 1 \;\; 0 & & \\ & & 0 \;\; 1 & & \\ -\sin\delta & 0 & & \cos\delta & 0 \\ 0 & -\sin\delta & & 0 & \cos\delta \end{pmatrix}. \tag{6.3}$$

Eq. (6.2) then transforms to

$$\begin{pmatrix} x \\ \dot{x} \\ y \\ \dot{y} \\ z \\ \dot{z} \end{pmatrix} = \begin{pmatrix} 1 & t_C \sin^2\delta & & & 0 & t_C \sin\delta\cos\delta \\ 0 & -\cos 2\delta & & & 0 & \sin 2\delta \\ & & 1 & 0 & & \\ & & 0 & -1 & & \\ 0 & t_C \sin\delta\cos\delta & & & 1 & t_C \cos^2\delta \\ 0 & \sin 2\delta & & & 0 & \cos 2\delta \end{pmatrix} \cdot \begin{pmatrix} x_0 \\ p_{x_0} \\ y_0 \\ p_{y_0} \\ z_0 \\ p_{z_0} \end{pmatrix} = M \cdot \begin{pmatrix} x_0 \\ p_{x_0} \\ y_0 \\ p_{y_0} \\ z_0 \\ p_{z_0} \end{pmatrix}. \tag{6.4}$$

Now, the dynamics of the electron in the two laser pulses and the magnetic field [see Eqs. (6.1) and (6.4)] need to be connected by the corresponding initial conditions in order to yield the trajectory of the returning electron. The following equations of motion are found:

$$x = p_{x_0} g_1 + p_{z_0} g_3 + \Delta x + x_0\,, \tag{6.5a}$$

$$y = p_{y_0} g_5 + y_0\,, \tag{6.5b}$$

$$z = p_{z_0} g_2 + p_{x_0} g_4 + \Delta z + z_0\,, \tag{6.5c}$$

with the abbreviations

$$\Delta x \equiv -\frac{1}{\omega c} \int A_2(\varphi) d\varphi\,, \tag{6.6a}$$

$$\Delta z \equiv \frac{1}{2\omega c^3} \left(\int_{-\infty}^{\infty} A_1^2(\varphi_1) d\varphi_1 - \int A_2^2(\varphi) d\varphi \right), \tag{6.6b}$$

$$g_1 \equiv -\cos 2\delta \left(t - \frac{1}{2\omega c^4} \int A_2^2(\varphi) d\varphi \right) + \frac{1}{\omega c^2} \sin 2\delta \int A_2(\varphi) d\varphi + \left(t_1 - \frac{1}{2\omega c^4} \int_{-\infty}^{\infty} A_1^2(\varphi_1) d\varphi_1 + t_C \sin^2\delta \right), \tag{6.6c}$$

$$g_2 \equiv \cos 2\delta \left(t + \frac{1}{2\omega c^4} \int A_2^2(\varphi) d\varphi \right) + \frac{1}{\omega c^2} \sin 2\delta \int A_2(\varphi) d\varphi + \left(t_1 + \frac{1}{2\omega c^4} \int_{-\infty}^{\infty} A_1^2(\varphi_1) d\varphi_1 + t_C \sin^2\delta \right), \tag{6.6d}$$

$$g_3 \equiv \sin 2\delta \left(t - \frac{1}{2\omega c^4} \int A_2^2(\varphi) d\varphi \right) + \frac{1}{\omega c^2} \cos 2\delta \int A_2(\varphi) d\varphi + t_C \sin\delta\cos\delta\,, \tag{6.6e}$$

$$g_4 \equiv \sin 2\delta \left(t + \frac{1}{2\omega c^4} \int A_2^2(\varphi) d\varphi \right) - \frac{1}{\omega c^2} \cos 2\delta \int A_2(\varphi) d\varphi + t_C \sin\delta\cos\delta\,, \tag{6.6f}$$

$$g_5 \equiv \left(t_1 - \frac{1}{2\omega c^4} \int_{-\infty}^{\infty} A_1^2(\varphi_1) d\varphi_1 \right) - \left(t - \frac{1}{2\omega c^4} \int A_2^2(\varphi) d\varphi \right). \tag{6.6g}$$

The wave packet maximum is described by the trajectory with vanishing initial momentum $\vec{p}_0 = 0$ because this will be—according to the initial momentum distribution

chosen later on—the most likely initial state. Recollisions therefore occur if Δx and Δz vanish at the same time as seen from Eqs. (6.5). These recollision conditions are identical to the ones in the model without refocusing. Therefore, the same vector potentials chosen previously can be applied which ensure recollisions with maximal kinetic energy [see Eq. (4.21)]:

$$A_1(\varphi) \propto \begin{cases} \cos\varphi \cdot \cos^2(\varphi/l) & |\varphi/l| \leq \pi/2 \\ 0 & |\varphi/l| > \pi/2 \end{cases}, \tag{6.7a}$$

$$A_2(\varphi) = \sqrt{2}\, A_1(\varphi)\,, \text{ where } l = 4, 6, 8, \ldots\,. \tag{6.7b}$$

Now, the classical dynamics is known and it can be employed to construct a wave packet as shown in the next section.

6.1.2 Wave packet dynamics

The equations of motion have to be solved for the initial momenta to yield the function $\vec{g} = (p_{x_0}, p_{y_0}, p_{z_0})$ and the corresponding Jacobian needed in the formula for the probability density (1.3). One arrives at

$$p_{x_0} = \frac{g_2(x - x_0 - \Delta x) - g_3(z - z_0 - \Delta z)}{g_1 g_2 - g_3 g_4}\,, \tag{6.8a}$$

$$p_{y_0} = \frac{y - y_0}{g_5}\,, \tag{6.8b}$$

$$p_{z_0} = \frac{g_1(z - z_0 - \Delta z) - g_4(x - x_0 - \Delta x)}{g_1 g_2 - g_3 g_4}\,, \tag{6.8c}$$

and

$$\left|\frac{\partial \vec{g}}{\partial \vec{x}}\right| = \frac{1 + \frac{1}{2c^4}A_2^2}{(g_1 g_2 - g_3 g_4) g_5} + \frac{(g_3 g_4' - g_1 g_2')(z - z_0 - \Delta z) + (g_4 g_2' - g_2 g_4')(x - x_0 - \Delta x)}{(g_1 g_2 - g_3 g_4)^2 g_5}\,. \tag{6.9}$$

The initial position and momentum distributions ρ_0 and $\tilde{\rho}$ are again chosen to be the Gaussians (1.10), where the initial widths are related according to Heisenberg's relation by the minimal uncertainty of $\Delta w \cdot \Delta p = 1$. Now, all ingredients are available to calculate the probability density (1.3):

$$\rho(\vec{x}, t) = \iiint \rho'(\vec{x}, \vec{x}_0, t)\rho_0(\vec{x}_0)\, d^3x_0 = \iiint \tilde{\rho}(\vec{g}(\vec{x}, \vec{x}_0, t))\left|\frac{\partial \vec{g}(\vec{x}, \vec{x}_0, t)}{\partial \vec{x}}\right| \rho_0(\vec{x}_0)\, d^3x_0\,. \tag{6.10}$$

Refocusing directions

Before carrying out the integrals, some useful and instructive information will be extracted from ρ' which is the probability distribution if the initial probability density of the wave packet is point-like, i.e., the particle is initially found at the point $\vec{x}_0$. If magnetic refocusing works for laser-driven particles, the distribution ρ' is expected to become narrow again in two directions. In order to find out if and in which directions the probability density refocuses, it is analyzed in the vicinity of the wave packet maximum.

The motion of the maximum is described by the classical, implicit equations (6.5) with zero initial momentum which according to $\tilde{\rho}$ is the most likely initial condition:

$$x_m = -\frac{1}{\omega c}\int_0^{\omega(t+z_m/c)} A_2(\varphi)d\varphi + x_0\,, \tag{6.11a}$$

$$y_m = y_0\,, \tag{6.11b}$$

$$z_m = \frac{1}{2\omega c^3}\left(\int_{-\infty}^{\infty} A_1^2(\varphi_1)d\varphi_1 - \int_0^{\omega(t+z_m/c)} A_2^2(\varphi)d\varphi\right) + z_0\,. \tag{6.11c}$$

The solution of these equations does not need to be known explicitly in order to find the expression for the wave packet in the vicinity of its maximum.

The first step, is to expand the integral expressions in Eqs. (6.8) linearly about z_m according to

$$\int A_2(\varphi)d\varphi \approx \int_0^{\omega(t+z_m/c)} A_2(\varphi)d\varphi + A_2(t+z_m/c)\frac{\omega}{c}(z-z_m)\,. \tag{6.12}$$

With a typical sin-like shape of the vector potential, the linear approximation works well as long as $(z-z_m)\omega/c$ is small compared to one. In the vicinity of interest for refocused wave packets, this condition is fulfilled since $\omega/c \approx 4\times10^{-4}$ for the laser wave length of 800 nm. Neglecting terms higher than linear order in $(z-z_m)\omega/c$ and $(x-x_m)\omega/c$, Eqs. (6.8) reduce to:

$$p_{x_0} = \frac{g_2(z_m)\left[(x-x_m)+\frac{1}{c^2}A_2(z-z_m)\right] - g_3(z_m)\left[1+\frac{1}{2c^4}A_2^2\right](z-z_m)}{g_1g_2-g_3g_4}\,, \tag{6.13a}$$

$$p_{y_0} = \frac{y-y_0}{g_5}\,, \tag{6.13b}$$

$$p_{z_0} = \frac{g_1(z_m)\left[1+\frac{1}{2c^4}A_2^2\right](z-z_m) - g_4(z_m)\left[(x-x_m)+\frac{1}{c^2}A_2(z-z_m)\right]}{g_1g_2-g_3g_4}\,. \tag{6.13c}$$

The probability density ρ' then reads

$$\begin{aligned}\rho'(\vec{x},t) \propto{}& \exp-\frac{(y-y_m)^2}{\Delta p^2 g_5^2}\\ &\times\exp-\frac{a(z_m)(x-x_m)^2+2b(z_m)(x-x_m)(z-z_m)+d(z_m)(z-z_m)^2}{\Delta p^2(g_1g_2-g_3g_4)^2}\,,\\ a ={}& g_2^2+g_4^2\,,\\ b ={}& (g_2^2+g_4^2)\frac{1}{c^2}A_2-(g_2g_3+g_1g_4)\left(1+\frac{1}{2c^4}A_2^2\right)\,,\\ d ={}& \left[g_2\frac{1}{c^2}A_2-g_3\left(1+\frac{1}{2c^4}A_2^2\right)\right]^2+\left[-g_4\frac{1}{c^2}A_2+g_1\left(1+\frac{1}{2c^4}A_2^2\right)\right]^2\,.\end{aligned} \tag{6.14}$$

The width in the y direction is read off to be $\Delta p g_5$. With the recollision condition $\Delta z = 0$ [see Eq. (6.6b)] which holds for the maximum, g_5 is found to be zero for $t = t_1$, i.e., when the time duration of the electron in the second laser pulse equals the duration in the first one. The probability density is then strongly focused in the vicinity of the plane $y = 0$. Note that for outer parts of the distribution ($z \neq z_m$), the recollision condition is not fulfilled exactly and thus refocusing is not perfect (this effect is nicely seen in Fig. 6.4(c) for the second refocusing direction).

To analyze the wave packet in the x and the z direction, the density can be rewritten with the coordinates of a rotated system $(\tilde{x}, \tilde{z})$ such that the following quadratic form in Eq. (6.14) is diagonal:

$$a(z_m)(x-x_m)^2 + 2b(z_m)(x-x_m)(z-z_m) + d(z_m)(z-z_m)^2 = \begin{pmatrix} x-x_m \\ z-z_m \end{pmatrix}^T \begin{pmatrix} a & b \\ b & d \end{pmatrix} \begin{pmatrix} x-x_m \\ z-z_m \end{pmatrix} . \quad (6.15)$$

With the eigenvalues $\lambda_\pm$ of the matrix in Eq. (6.15)

$$\lambda_\pm = \frac{a+d}{2} \pm \sqrt{\left(\frac{a+d}{2}\right)^2 - (g_1 g_2 - g_3 g_4)^2 \left(1 + \frac{1}{2c^4} A_2^2\right)^2} , \quad (6.16)$$

the probability density reduces to the form:

$$\rho'(x,z) \propto \exp - \left[\frac{\tilde{x}^2}{w_1^2} + \frac{\tilde{z}^2}{w_2^2}\right] , \quad w_{1,2} \equiv \sqrt{\frac{\Delta p^2 (g_1 g_2 - g_3 g_4)^2}{\lambda_\pm}} . \quad (6.17)$$

Additionally to the y direction, the distribution is expected to refocus for one further direction. Thus, one of the values $\Delta w_{1,2}$ should tend to zero whereas the other one remains finite. With some algebra and by means of the recollision condition $\Delta z = 0$ for the maximum, the following expression is found:

$$g_1 g_2 - g_3 g_4 = (t - t_1)(t + t_1 + \Delta t \cos^2 2\delta) . \quad (6.18)$$

As $t - t_1$ becomes small, this yields the following limits:

$$\Delta w_1 = 0 , \quad \Delta w_2 = \frac{\Delta p \sqrt{a+d}}{1 + \frac{1}{2c^4} A_2^2} . \quad (6.19)$$

This means, refocusing occurs in the $\tilde{x}$ direction with the smallest width reached at the same time $t - t_1$ as for the y direction.

Although the analysis here is for Gaussian wave packets, it can be argued that refocusing occurs as well for other wave packets with different momentum compositions. The minimum widths in the refocusing directions Δw_1 and Δw_y do not depend on Δp, i.e., if the spectrum of initial momenta is broadened by increasing Δp, the minimum widths remain zero. The initial momentum distribution does therefore not affect refocusing. However, since the width Δw_2 is proportional to Δp, the initial momentum distribution determines how the wave packet is distributed along the broadening direction, which has a certain influence on the reaction rate of recollisions. As will be seen in the next section, averaging over the initial position to get the final form for the probability density ρ corresponds to a superposition of slightly shifted probability densities, which does not spoil refocusing either. Refocusing is therefore independent of the initial electron state.

Magnetic field direction

With the eigenvector corresponding to λ_-, which is found to be $(-b, a - \lambda_-)$, the angle α between the z and the $\tilde{z}$ direction is given by [compare the diagonalization of the quadratic form (2.20)]:

$$\tan \alpha = -\frac{b}{a - \lambda_-} . \quad (6.20)$$

At the instant when the wave packet is refocused, λ_- approaches zero, and with some algebra the result for the angle α reduces to

$$\tan\alpha = -\frac{1}{c^2}A_2 + \frac{t_C + 2\left(t - \frac{1}{2\omega c^4}\int A_2^2(\varphi)d\varphi\right)}{t_C + 2\left(t + \frac{1}{2\omega c^4}\int A_2^2(\varphi)d\varphi\right)}\left(1 + \frac{1}{2c^4}A_2^2\right)\tan\delta\,. \tag{6.21}$$

Note that the magnetic field direction (determined by δ) only coincides with the broadening direction (given by α) in the nonrelativistic limit of weak fields $A_2/c^2 \ll 1$ where even magnetic field effects are negligible.

Now, the goal is to chose the angle δ in a way that the directions of minimal widths are orthogonal to the velocity of the particle in order to maximize the current as the maximum of the particle recollides. This calculation is accurate only for the maximum of the wave packet. However, the influence of outer parts on the total reaction rate of recollisions will be shown to be negligible (see Fig. 6.9).

The velocity is derived from the classical equations of motion (6.5) where the trajectory of the wave packet maximum has no initial momentum. Differentiating with respect to time yields the following result:

$$\dot{x} = -c\cdot\frac{\frac{1}{c^2}A_2(\varphi)}{1+\frac{1}{2c^4}A_2^2(\varphi)}\,, \tag{6.22a}$$

$$\dot{z} = -c\cdot\frac{\frac{1}{2c^4}A_2^2(\varphi)}{1+\frac{1}{2c^4}A_2^2(\varphi)}\,. \tag{6.22b}$$

With the condition that the wave packet has the desired orientation

$$\tan\alpha = \dot{x}/\dot{z} = \frac{2c^2}{A_2}\,, \tag{6.23}$$

the optimum angle δ_m for the magnetic field direction is found to be:

$$\tan\delta_m = \frac{2c^2}{A_2}\cdot\frac{t_C + 2\left(t + \frac{1}{2\omega c^4}\int A_2^2(\varphi)d\varphi\right)}{t_C + 2\left(t - \frac{1}{2\omega c^4}\int A_2^2(\varphi)d\varphi\right)}\,. \tag{6.24}$$

Laser timing

There is another important point which needs to be addressed. The instant of maximal refocusing $t = t_1$ needs to coincide with the moment of recollision which is not trivial since the two laser pulses have different intensities. This condition can be fulfilled by the correct timing of the two laser pulses. The times t and t_1 which elapse while the lasers act follow from the phase (6.1d), where the motion of the maximum in the z direction is given by $z = \Delta z$ [see Eq. (6.5c)]:

$$\omega t_1 = \varphi_1 + \frac{1}{2c^4}\int A_1^2(\varphi')d\varphi'\,, \quad \omega t = \varphi + \frac{1}{2c^4}\int A_2^2(\varphi')d\varphi'\,. \tag{6.25}$$

Together with the recollision condition $\Delta z = 0$ the time difference reduces to

$$\omega(t_1 - t) = \varphi_1 - \varphi\,. \tag{6.26}$$

For the pulse shape chosen [see Eq. (6.7)] and considering that the recollision is supposed to occur when half of the laser pulse has passed, the difference between the periods of time in the laser fields is found to be

$$\Delta t = t_1 - t = \frac{\pi l}{2\omega}\,. \tag{6.27}$$

The time difference between recollision and maximal refocusing can be compensated with a delay of Δt between the magnetic field pulse and the second laser pulse, i.e., in the theoretical description, the vector potential A_2 simply remains equal to zero until the second pulse arrives at $t = \Delta t$.

Probability density

The expression for the probability density (6.10) contains a three-dimensional integral which averages the density ρ' over the initial probability distribution ρ_0. However, with a suitable approximation, the problem can be reduced to two one-dimensional integrals. First, the integration with respect to y_0 is a Gaussian integral which can be carried out immediately. The idea to simplify the remaining double integral is to omit the integration corresponding to the broadening direction because for this case, the width of the initial probability density is small compared to the width of the wave packet. In other words, the initial probability distribution can be approximated by a δ-function and the integration becomes trivial. This leaves another one-dimensional integration.

To incorporate this idea, one needs to analyze how the probability density ρ' depends on the initial position. A variation of the initial position involves a shift of the maximum whose position is given by the implicit Eqs. (6.11). For the time when the maximum is close to the origin, i.e., at the time of recollision, they can be solved approximately. The integral expressions are expanded about $z = 0$ (see Eq. (6.12) with $z_m = 0$). With the recollision conditions $\Delta x = \Delta z = 0$, the following result is obtained:

$$x_m = x_0 - \frac{\frac{1}{c^2}A_2}{1 + \frac{1}{2c^4}A_2^2} z_0 \,, \tag{6.28a}$$

$$z_m = \frac{z_0}{1 + \frac{1}{2c^4}A_2^2} \,. \tag{6.28b}$$

These equations show how a shift of the initial position changes the location of the maximum of the probability density when it recollides. To shift the wave packet along the broadening direction characterized by the angle α, the initial position has to be changed according to

$$\tan\alpha = \frac{x_m}{z_m} = -\frac{1}{c^2}A_2 + \left(1 + \frac{1}{2c^4}A_2^2\right)\frac{x_0}{z_0} \,, \quad \frac{x_0}{z_0} \equiv \tan\eta \,, \tag{6.29}$$

where the corresponding angle η is different from α for non-negligible values of the vector potential. The integration over the initial position should be carried out perpendicular to the direction defined by η, i.e., in the direction which corresponds to the refocusing direction. To carry out the one-dimensional integral, the initial position is replaced by

$$x_0 = s_0 \sin\beta \,, \quad z_0 = s_0 \cos\beta \,, \tag{6.30}$$

where s_0 is the new integration parameter and β denotes the angle between the integration direction and the z axis which is given by $\beta = \eta + \pi/2$. With Eq. (6.21), the following relation is found for the angles of the magnetic field direction δ and the integration direction β:

$$\cot\beta = -\frac{t_C + 2\left(t - \frac{1}{2\omega c^4}\int A_2^2(\varphi)d\varphi\right)}{t_C + 2\left(t + \frac{1}{2\omega c^4}\int A_2^2(\varphi)d\varphi\right)} \tan\delta \,. \tag{6.31}$$

This equation is closely related to Eq. (6.21) which describes the connection of the broadening direction (given by α) and the magnetic field direction (given by δ). If the density distribution is considered at rest, it is not distorted by the laser field (by retardation effects) and the broadening and the integration direction should be perpendicular. In theory, the particle can be stopped if the vector potential drops off to zero right after the maximum has reached the point of recollision. As expected with this argument, Eq. (6.31) is reproduced if in Eq. (6.21) the vector potential drops off to zero and α is replaced by $\beta+\pi/2$. With this argument it is easy to show that averaging along the broadening direction can be neglected, simply by analyzing the probability density with $A_2 = 0$. ρ' then reduces to a simple two-dimensional Gaussian distribution with the widths $\Delta w_1 = 0$ and $\Delta w_2 = \Delta p\sqrt{a+d}$ [see Eqs. (6.19)]. The smallest value $\Delta w_2 = 2t_1\Delta p$ is found for $t_c = 0$ and $\gamma_m \to 1$ which for the pulse shape given by Eq. (6.7a) equals $\Delta w_2 = 2\pi l\Delta p/\omega$. For a typical value $\Delta p = 0.5$ a.u. and for a short laser pulse with $l = 6$, one finds $\Delta w_2 \approx 330$ which is much greater than the widths $\Delta x_0 = \Delta z_0 = 1/\Delta p = 2$ of the corresponding initial position distribution. With higher laser intensities the width Δw_2 increases quickly, showing that the approximation of a point-like initial probability distribution in the broadening direction becomes even better. Of course, Δw_2 can be shown to be large for $A_2 \neq 0$ as well, i.e., without the above argument by plugging in the parameters needed. Due to Lorentz contraction Δw_2 is smaller by a factor of γ, but the effect of different initial conditions on the position of the maximum is reduced likewise [see Eqs. (6.28)].

Finally, with Eq. (6.30), the expression for the probability distribution (6.10) simplifies to the following form which contains two one-dimensional integrals:

$$\rho(x,y,z) \approx \iint \rho'(x,y,z,s_0\sin\beta,y_0,s_0\cos\beta)\left(\frac{\Delta p^2}{\pi}\right)^{3/2}\exp -\Delta p^2(y_0^2+s_0^2)\,dy_0 ds_0\,. \tag{6.32}$$

After some algebra the result is found to be:

$$\rho(x,y,z) = \frac{\exp -\frac{y^2}{\Delta w_y^2} - \frac{\Delta p^{-4}f_5^2+f_1^2+f_3^2}{\Delta w_{xz}^2}}{\sqrt{\pi}^3\Delta w_y\Delta w_{xz}\Delta p}\left[1+\frac{1}{2c^4}A_2^2 - \frac{\Delta p^{-2}f_5(f_2g_2'-f_4g_4')}{\Delta w_{xz}^2}\right.$$
$$\left. + \frac{\Delta p^2[(g_3g_4'-g_1g_2')(z-\Delta z)+(g_4g_2'-g_2g_4')(x-\Delta x)](g_1g_2-g_3g_4)}{\Delta w_{xz}^2}\right], \tag{6.33}$$

with the definitions

$$f_1 \equiv g_2(x-\Delta x) - g_3(z-\Delta z)\,, \tag{6.34a}$$
$$f_2 \equiv g_2\sin\beta - g_3\cos\beta\,, \tag{6.34b}$$
$$f_3 \equiv -g_4(x-\Delta x) + g_1(z-\Delta z)\,, \tag{6.34c}$$
$$f_4 \equiv -g_4\sin\beta + g_1\cos\beta\,, \tag{6.34d}$$
$$f_5 \equiv -(x-\Delta x)\cos\beta + (z-\Delta z)\sin\beta\,, \tag{6.34e}$$
$$\Delta w_y \equiv \sqrt{\Delta p^{-2}+\Delta p^2 g_5^2}\,, \tag{6.34f}$$
$$\Delta w_{xz} \equiv \sqrt{\Delta p^{-2}(f_2^2+f_4)^2 + \Delta p^2(g_1g_2-g_3g_4)^2}\,. \tag{6.34g}$$

The structure of the dynamics in the y direction is very simple. It is a Gaussian distribution with the width Δw_y. As found previously in Sec. 6.1.2 (*Refocusing directions*), the coefficient g_5 vanishes at the instant of recollision. This means that in the y direction, the wave packet refocuses to the initial width $\Delta w_y = 1/\Delta p$.

6.1.3 Results and discussion

With the analytical expression for the probability density ρ, wave packets can be plotted and the reaction probability of recollision reactions can be calculated. For a comparison, it is useful to consider a nonspreading Gaussian wave packet with constant spatial widths Δw which moves in the z direction with velocity u:

$$\rho_{ref} = \left(\sqrt{\pi}\Delta w\right)^{-3} \exp \frac{x^2 + y^2 + (z - ut)^2}{\Delta w^2} \,. \tag{6.35}$$

With a target fixed at the origin, the following reaction probability is found:

$$\tilde{N}_{ref} = \int_{-\infty}^{\infty} \sigma u \rho_{ref}(\vec{x} = 0) dt = \frac{\sigma}{\pi \Delta w^2} \,. \tag{6.36}$$

Later on, results will be related to the yield $N_{ref} \equiv \tilde{N}_{ref}(\Delta w = 1)$ of a reference wave packet with spatial widths of $\Delta w = 1$.

The reaction rate of a laser-driven electron has been calculated in Sec. 4.2.3 and was found to be

$$\dot{N} = \sigma \frac{c}{\sqrt{1 - \left[1 + \frac{1}{2c^4} A_2(\varphi)^2\right]^{-2}}} \rho \,. \tag{6.37}$$

This expression can be integrated numerically to yield the total reaction probability $N = \int \dot{N} dt$.

In the following, the parameters for the laser wave length and the parameter for the pulse length are chosen to be $\lambda = 800$ nm and $l = 6$, respectively. The corresponding laser pulse shape is depicted in Fig. 6.2 according to Eq. (6.7a).

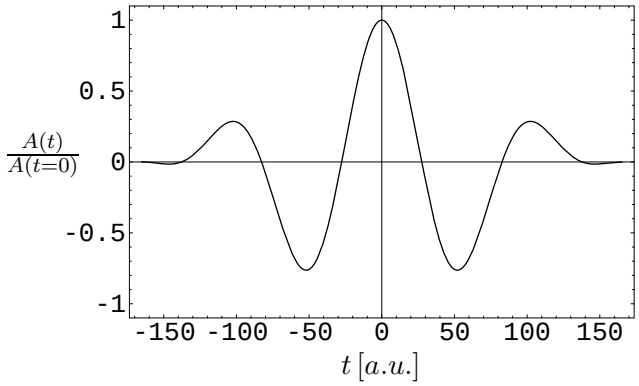

Figure 6.2: The time-dependence of the laser pulse at the origin is shown with the amplitude normalized to one. The shape is given by Eq. (6.7a) (with the parameter $l = 6$).

The strength of the magnetic field B is related to the time t_C. The order of magnitude required can be estimated by the time $t = 3\pi/B$ needed by an electron to travel one and a half loops in a constant magnetic field. This would roughly correspond to the trajectory shown in Fig. 5.1(a). For example, $t_C = 4000$ a.u. corresponds to a magnetic field of the order $B \approx 600$ T. Magnetic fields of this strength with the required rotational symmetry can be created [99, 100], however, the time scale of these pulses are in the microsecond regime, whereas such pulses would require lengths of only 100 fs for refocusing. Short magnetic field pulses in the picosecond regime have been

created with relativistically moving electron bunches [101, 102] with field strengths in the lower Tesla-regime. However, such an implementation would require the electrons to approach from different sides simultaneously to account for the rotational symmetry of the induced electric field (see Sec. 5.1). The first results presented are obtained for magnetic fields with similar length $t_C = 500000$ a.u. and the corresponding strength $B \sim 4.5$ T. Figure 6.3(a) shows the reaction probability, where the plotted energy range covers the relativistic regime up to 1 GeV. The reaction rate reached for $\Delta p_0 = 0.1$ a.u.

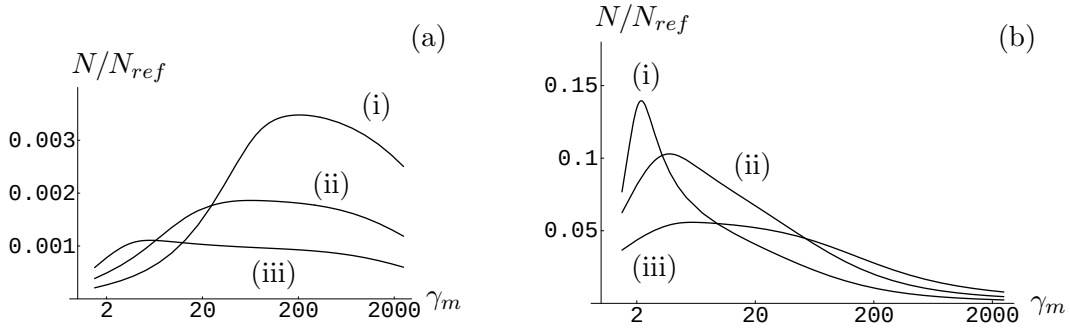

Figure 6.3: The reaction probability is plotted for different parameters. The resulting values N are related to the reaction probability N_{ref} corresponding to a Gaussian wave packet with spatial widths of one atomic unit. Part (a) shows the dependence on the maximum energy for a long magnetic field pulse with $t_C = 500000$ a.u. and the initial momentum widths (i) $\Delta p_0 = 0.1$ a.u., (ii) $\Delta p_0 = 0.25$ a.u. and (iii) $\Delta p_0 = 0.5$ a.u. The energy of 1 GeV corresponds to $\gamma_m = 2000$ which is reached at the laser intensity of roughly $10^{22}\mathrm{W/cm}^2$. The results for a short pulse with $t_C = 4000$ a.u. are depicted in (b). The initial momentum widths are chosen to be (i) $\Delta p_0 = 1$ a.u., (ii) $\Delta p_0 = 0.5$ a.u. and (iii) $\Delta p_0 = 0.25$ a.u.

and $\gamma_m = 200$ corresponds to the yield of a Gaussian wave packet with spatial widths of $\Delta x_{1,2} \approx 17$ a.u., which is of the order of the initial widths with $\Delta x_{1,2} = 1/\Delta p_0 = 10$ a.u. More efficient refocusing can be achieved by means of shorter magnetic field pulses as shown in Fig. 6.3(b). The time between the pulses $t_C = 4000$ a.u. allows for yields that are by roughly two orders of magnitude higher.

Figure 6.4 shows the wave packets for different laser intensities as they return to the core. The orientations of the density distributions also represent the directions of motion because the orientation of the magnetic field has been chosen such that these directions are equal.

The time-dependent current density at the origin corresponding to the wave packets of Fig. 6.4 is shown in Fig. 6.5. As seen in the plots for the probability density where the wave packets become shorter for higher energies, i.e., the collision times of the wave packet decrease. Although the maximum current density increases, the total current decreases as seen in Fig. 6.3.

The yield N strongly depends on the initial wave packet widths. On the one hand, the minimal widths of refocusing are limited by the initial widths but on the other hand, smaller widths imply faster wave packet spreading due to greater widths Δp_0 in momentum space. Since refocusing works for two dimensions only, rapid spreading in the third direction reduces the reaction probability. There is a value for the initial momentum width which maximizes the total yield as seen in Fig. 6.6.

There is a dependence of the yield on the time between the laser pulses t_C as already

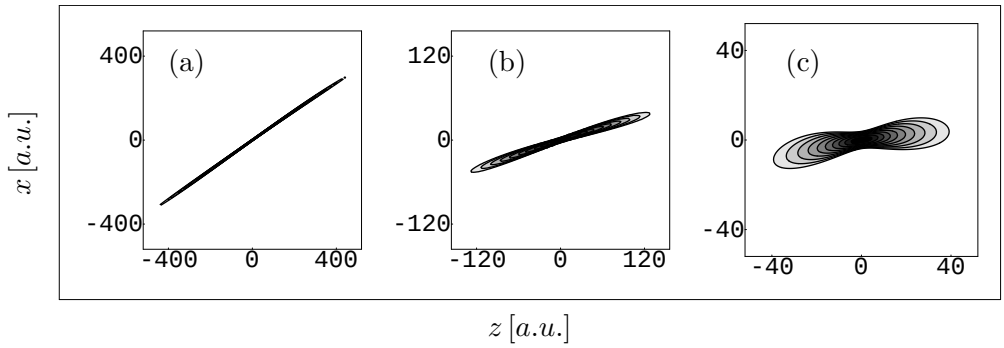

Figure 6.4: The plots show distributions of the probability densities (logarithmic scale over the range of four orders of the Euler number e) for different energies [(a) $\gamma_m = 5$, (b) $\gamma_m = 20$, (c) $\gamma_m = 80$] and $t_C = 4000$ a.u. at the instant when the maximum returns to the origin. The initial width in momentum space is $\Delta p_0 = 0.5$ a.u. which corresponds to spatial initial widths of $\Delta x = 2$ a.u. The orientations of the longest extensions of the wave packets coincide with the directions of motion.

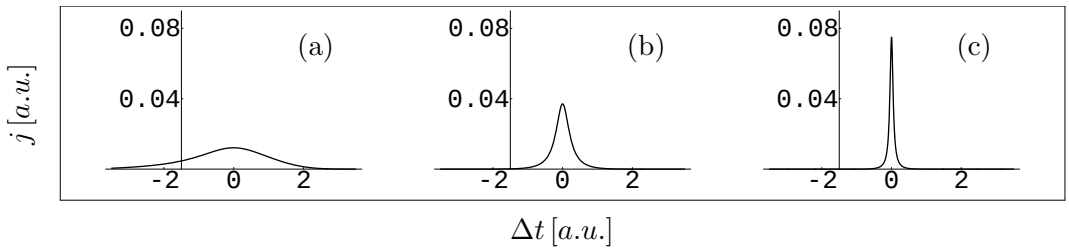

Figure 6.5: The diagrams show the time-dependent current densities of the returning wave packets at the origin for different energies [(a) $\gamma_m = 5$, (b) $\gamma_m = 20$, (c) $\gamma_m = 80$]. $\Delta t = 0$ denotes the time when the maximum reaches the origin. For higher laser intensities the maxima of the current densities increase, whereas the collision times become shorter. The surface of the distribution which is proportional to the reaction probability decreases for higher energies [see Fig. 6.3(b)].

seen from the difference for the two cases in Fig 6.3. The probability density only refocuses in two dimensions, i.e., one-dimensional wave packet spreading still occurs whose effect on the yield can obviously be influenced by the time of evolution as shown in Fig. 6.7. Shorter times give better results and require higher magnetic fields. If the momentum reversal occurs immediately after the first laser pulse, i.e., for $t_C = 0$, the yield of a nonspreading Gaussian wave packet which keeps its initial widths $\tilde{N}_{ref}(\Delta p = 0.5)/N_{ref} = 0.25$ is almost reached for lower collision energies.

The previous analysis is based on the short laser pulses shown in Fig. 6.2. Longer laser pulses imply the disadvantage that there is more time for spreading in the broadening direction, because both the laser pulses and the time delay after the magnetic field pulse according to Eq. (6.27) are longer. Thus, the yield is expected to decrease as shown in Fig. 6.8 for pulses five times as long as previously.

The angle δ_m for the direction of the magnetic field direction given by Eq. (6.24) has been deduced from the wave packet maximum which yields the highest current density. Although outer parts with lower current densities are of less importance, the total reaction probability might be optimized by a slightly different choice of δ. The

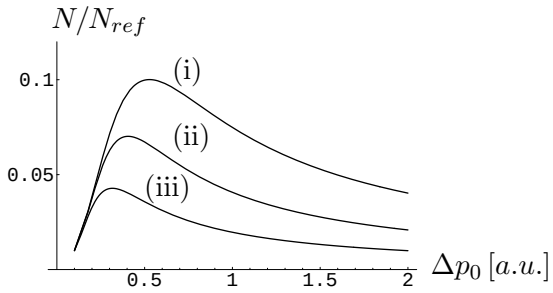

Figure 6.6: The yield N/N_{ref} is plotted versus the initial width in momentum space with $t_C = 4000$ a.u. Large widths enable small widths in coordinate space but also imply faster spreading. Depending on the energy [(i) $\gamma_m = 5$, (ii) $\gamma_m = 20$, (iii) $\gamma_m = 80$] there is an optimum value which maximizes the reaction probability.

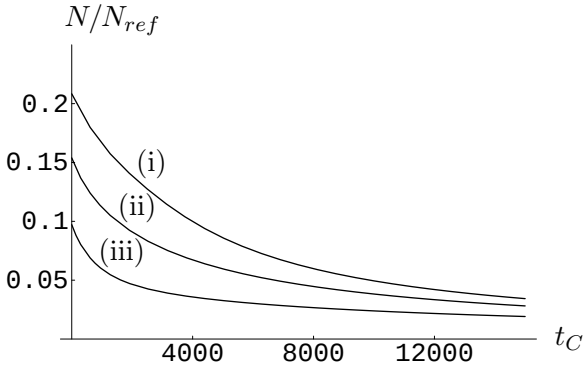

Figure 6.7: The total reaction probability is plotted versus the time between the laser pulses. A magnetic field of the order $B = 600$ T and $B = 150$ T corresponds to $t_C = 4000$ a.u. and $t_C = 15000$ a.u., respectively, i.e., with stronger magnetic fields the yield increases. Energies are chosen to be (i) $\gamma_m = 5$, (ii) $\gamma_m = 20$ and (iii) $\gamma_m = 80$.

dependence of the yield on deviating angles is shown in Fig. 6.9. It is seen that the angle δ_m actually agrees with the position of the maxima of the curves, i.e., the analysis of the wave packet maximum is shown to be sufficient.

Fig. 6.10 shows the current densities of the wave packet for the axis $\hat{n}$ perpendicular to the velocity and the y direction for the relevant time interval of recollision. Slight deviations of the magnetic field direction have strong effects on the position n of the maximum current density because the orientation of the wave packet changes. Obviously, high yields are achieved if the current density is concentrated on the axis $n = 0$ as for $\delta = \delta_m$.

The best choice for the magnetic field direction is determined by Eq. (6.24). It depends on the laser intensity and the time t_C between the laser pulses. The dependence is shown in Fig. 6.11.

Spin effects have not been considered here. However, slight deviations of the electron trajectories which may occur for high energies can be eliminated if the electron spins are aligned in a way that they point into the magnetic field direction of the laser pulses [72].

Finally, two effects should be considered which can disturb the recollision process if it is applied to a gas sample. First, the coulomb interactions of the electrons in the

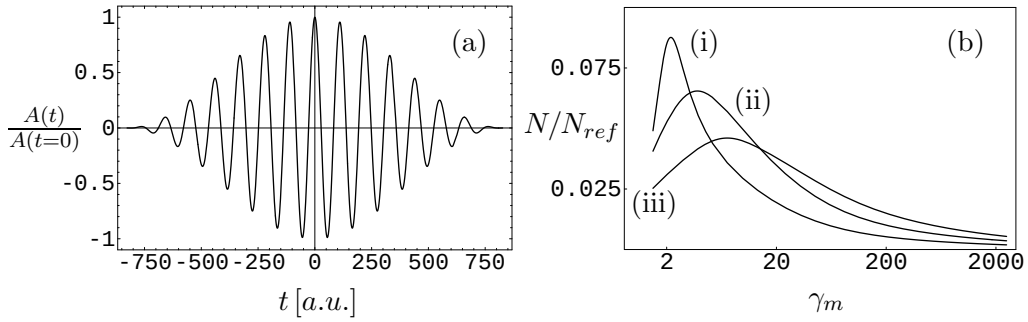

Figure 6.8: The total reaction probability depending on γ_m is plotted in (b) for a laser pulse shown in (a) (see Eq. (6.7) with $l = 30$) which is five times as long as the one used previously (see Fig. 6.2). A comparison with Fig. 6.3(b) shows that the yield is reduced by a factor of less than two. The initial widths are chosen to be (i) $\Delta p = 1$ a.u., (ii) $\Delta p = 0.5$ a.u. and (iii) $\Delta p = 0.25$ a.u.

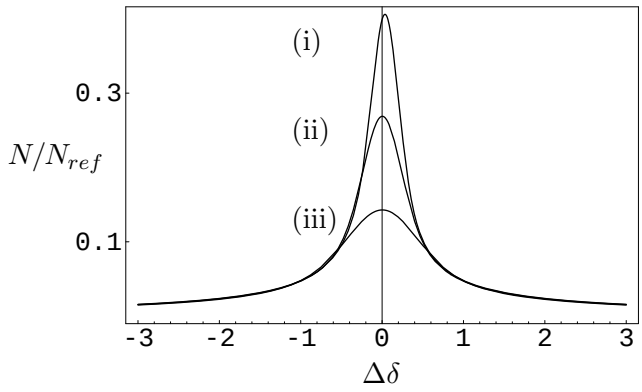

Figure 6.9: The yield strongly depends on the magnetic field direction. Shown is the behavior for angles deviating from the value δ_m which has been determined analytically [see Eq. (6.24)]. The energy is given by (i) $\gamma_m = 5$, (ii) $\gamma_m = 20$ and (iii) $\gamma_m = 80$.

ionized gas and second, the initial thermal velocity of the atoms.

In order to keep the deviations due to Coulomb interactions small, the process needs to be fast enough such that the electron positions are not altered too much. Otherwise recollisions are inhibited. Especially the time between the two laser pulses can be long if the magnetic fields are not sufficiently strong and short. To estimate the magnitude of the magnetic field strength required to keep the deviations small enough to enable recollisions, consider the distance Δr which an electron travels in a Coulomb potential of a singly charged core during the time interval between the laser pulses t_C. The initial distance r_0 is taken to be the mean distance between particles in a gas. For $\Delta r \ll r_0$ the Coulomb problem ($\ddot{r} = -r^{-2}$) is solved by the equation:

$$\Delta r = \frac{t^2}{2r_0^2}\,. \tag{6.38}$$

With the time interval $t_C = 4000$ a.u. corresponding to a magnetic field pulse of the order $B \approx 600$ T and the mean distance of $r_0 = 2000$ a.u. which corresponds to the particle density of about 10^{15} cm^{-3}, a shift of $\Delta r = 2$ a.u. is found. This means, if wave packets are refocused to widths of a few atomic units in a gas with the above density,

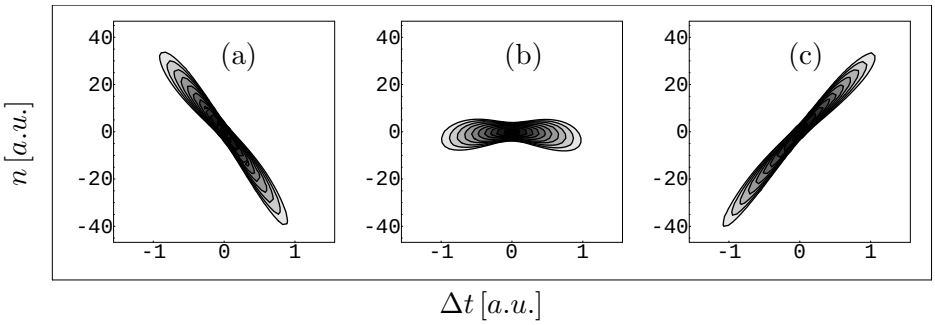

Figure 6.10: The current density (logarithmic scale) of the direction perpendicular to the velocity and the y direction (denoted by n) is plotted as a function of time. $\Delta t = 0$ is the time when the maximum is found at the origin. If the angle δ which defines the magnetic field direction deviates from δ_m [(a) $\delta - \delta_m \hat{=} -1$, (b) $\delta = \delta_m$, (c) $\delta - \delta_m \hat{=} 1$], high density parts of the wave packet miss the point of recollision $n = 0$. For this example, the energy is $\gamma_m = 20$.

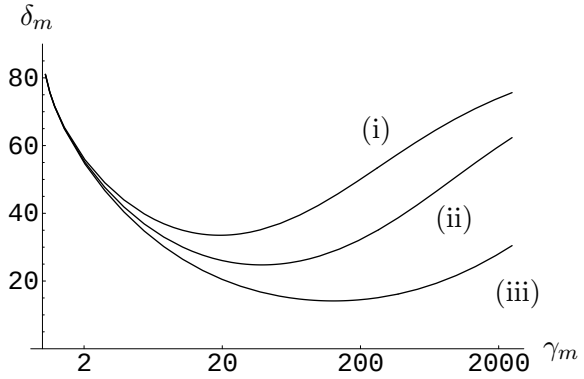

Figure 6.11: The optimal angle δ_m which defines the magnetic field direction is plotted versus the maximum γ-factor. δ_m denotes the angle between the magnetic field and the laser propagation direction. Different time intervals between the laser pulses have been chosen [(i) $t_C = 1600$ a.u., (ii) $t_C = 4000$ a.u., (iii) $t_C = 15000$ a.u.].

extremely strong and short magnetic fields are required to keep Coulomb interactions small.

The motion of the core due to thermal kinetic energy might also play a role for the long times of the recollision process. From the kinetic energy in thermal equilibrium $\frac{1}{2}Mv^2 = \frac{3}{2}k_BT$ (with Boltzmann's constant k_B), the mean velocity of hydrogen atoms at room temperature are $v = 10^{-3}$ a.u. The distance Δs which a proton can travel during the time from ionization to recollision $t_P = 2t_1 + t_C$ is of the order of $\Delta s \approx 10$ a.u. for the electron energy of $\gamma_m = 80$ and the time of $t_C = 4000$ a.u. Generally, the distance Δs can always be reduced by heavier atoms or lower temperatures. For instance, the temperature of liquid helium reduces the value of Δs by a factor of almost ten. Note that the effect of the thermal initial velocity of the bound system is different for electrons, because first, they are subject to the refocusing dynamics, i.e., except for the broadening-direction, they return to their initial position and secondly they move relativistically. Therefore, the deviations of the electron and the core do not cancel.

The Coulomb interactions become important because of the long time t_C which is

needed for the momentum reversal by the magnetic field. If this part of the recollision process is omitted as in the scheme of Sec. 4.2, the deviations become much smaller. Furthermore, in this case, the wave packets are not refocused and the deviations are much smaller than the widths of the wave packets. The same argument holds for the effects due to the initial thermal motion. Consequently, these effects are not important for that scheme.

6.2 Refocused recollisions with harmonic potentials

The mechanism of refocusing by a harmonic potential which has been introduced in Sec. 5.2 can also be incorporated into the double pulse recollision scheme (see Fig. 6.12). Refocusing is initiated after the first laser pulse as for the case of magnetic refocusing, such that the wave packet is small again when it is driven to the core by the counterpropagating pulse.

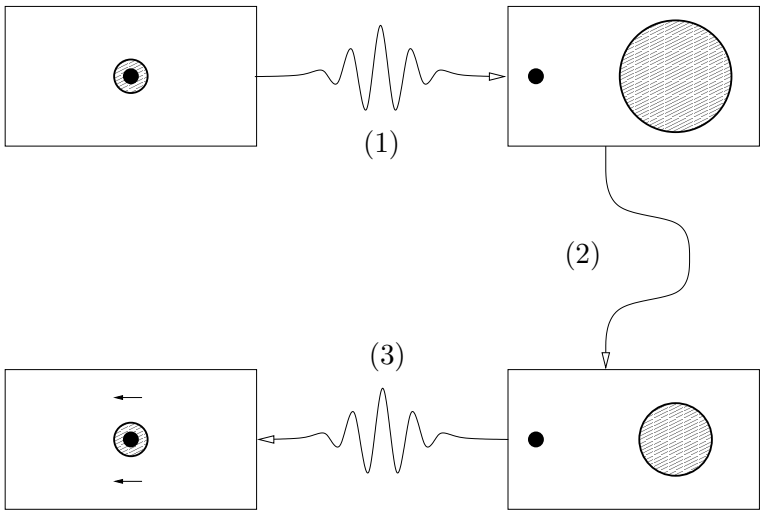

Figure 6.12: An atom is ionized by the first intense laser pulse (1). Then, a harmonic potential is employed (2) which reverses the spreading dynamics. Finally, the electron is driven back to the core by the second intense laser pulse (3). Recollisions occur when the electron reaches its maximum kinetic energy.

The analysis is carried out quantum mechanically. The parts where the electron is driven away and back to the core are described by means of the Klein-Gordon equation, whereas refocusing is initiated by a nonrelativistic process which can be described by the Schrödinger equation.

6.2.1 Relativistic wave solution

The electron dynamics of the first laser pulse which drives the electron away from the core is described by the relativistic wave function given by Eq. (A.13). The initial momenta are considered to quadratic order which allows for an analytical treatment. Since the wave packet which will be constructed later on only contains solutions of a small range of initial momenta, this simplification is sufficient. The same procedure

has also been carried out in Sec. 2.2. The solution then reads

$$\phi_\pm(\vec{x},t) = (2\pi)^{-3/2} \exp i \left[-c^2 t + \vec{p}_0 \cdot \vec{x} - \frac{1}{2}\vec{p}_0^{\,2} t + \frac{p_x}{\omega c}\left(1 \pm \frac{p_z}{c}\right) \int A \, d\varphi \right. \\ \left. - \frac{1}{2\omega c^2}\left(1 \pm \frac{p_z}{c} + \frac{p_z^2}{c^2} - \frac{\vec{p}_0^{\,2}}{2c^2}\right) \int A^2 \, d\varphi \right] . \quad (6.39)$$

The negative signs of the terms $\pm p_z$ apply if the laser pulse propagates in the negative z direction. This will be needed later on for the counterpropagating laser pulse. After the laser pulse has passed the electron, the dynamics is nonrelativistic again. This is known from the classical solution [see the expression for the γ-factor (A.9)], but it can as well be shown from the quantum mechanical solution. By means of the energy operator $\hat{E} = \partial/\partial t$, it is seen that relativistic behavior is connected to the time-dependence of the solution. After the pulse has passed, the vector potential in Eq. (6.39) is constant and the only time-dependence is given by the term $(-c^2 + \vec{p}_0^{\,2}/2)t$ in the phase. The initial momentum is nonrelativistic and the dependence on c^2 originates from the rest energy of the electron which does not imply relativistic dynamics.

Since the next step of the recollision model is described by means of nonrelativistic quantum mechanics, it needs to be shown how the solution of the Klein-Gordon equation is related to the wave function of nonrelativistic wave mechanics. To find the connection, the Klein-Gordon equation needs to be reduced to the Schrödinger equation for small kinetic energies. The analysis is carried out for the free Klein-Gordon equation, where interactions can be introduced at any point of the derivation by means of the minimal substitution (6.40b):

$$\ddot{\phi} = c^2 \triangle \phi - c^4 \phi \, , \quad (6.40a)$$

$$\frac{\partial}{\partial t} \to \frac{\partial}{\partial t} + i\Phi \, , \quad \vec{\nabla} \to \vec{\nabla} + \frac{i}{c}\vec{A} . \quad (6.40b)$$

This equation can be rewritten in the following form which contains only first order derivatives with respect to time:

$$i\dot{\Theta} = -\frac{1}{2}\triangle(\Theta + \chi) + c^2 \Theta \, , \quad (6.41a)$$

$$i\dot{\chi} = \frac{1}{2}\triangle(\Theta + \chi) - c^2 \chi \, , \quad (6.41b)$$

$$\Theta \equiv \frac{1}{2}\left(\phi + \frac{i}{c^2}\dot{\phi}\right) , \quad \chi \equiv \frac{1}{2}\left(\phi - \frac{i}{c^2}\dot{\phi}\right) . \quad (6.41c)$$

From these equations, the following relation for χ is found:

$$\left(1 + \frac{i\frac{\partial}{\partial t} - c^2}{2c^2}\right)\chi = \frac{1}{4c^2}\triangle(\Theta + \chi) \, . \quad (6.42)$$

In the nonrelativistic limit, both the kinetic energy operator $i\frac{\partial}{\partial t} - c^2$ (the energy operator minus the rest mass) and the square of the momentum operator $\triangle$ yield small numbers which are small[1] compared to c^2. One then finds

$$\chi \approx 0 \, , \quad (6.43a)$$

$$i\dot{\Theta} = -\frac{1}{2}\triangle\Theta + c^2\Theta \, . \quad (6.43b)$$

[1]The nonrelativistic limit of the Klein-Gordon equation can be carried out systematically in orders of c as shown, e.g., in [81].

Finally, with $\Theta \equiv \exp(-ic^2t)\psi$, Eq. (6.43b) reduces to the Schrödinger equation

$$i\dot{\psi} = -\frac{1}{2}\triangle\psi\,. \tag{6.44}$$

Thus, in the nonrelativistic limit, the wave function of the Klein-Gordon equation ϕ and the Schrödinger equation are related via

$$\phi = \exp(-ic^2t)\psi\,. \tag{6.45}$$

To describe the evolution of the wave function in a harmonic potential which is envisaged to refocus the wave packet, consider the one-dimensional harmonic oscillator propagator (for a derivation see e.g. [93]):

$$D(x',t;x,0) = \sqrt{\frac{\Omega}{2\pi i}}\sin^{-1/2}(\Omega t)\exp i\Omega\frac{(x'^2+x^2)\cos(\Omega t)-2x'x}{2\sin(\Omega t)}\,. \tag{6.46}$$

This propagator describes how the amplitude of the wave function at some point x at time $t=0$ evolves with time. $D(x',t;x,0)$ gives the amplitude at some other point x' at time t. As found in Sec. 5.2, refocusing is achieved for $\Omega t = 3\pi/2$. The propagator is then given by

$$D\left(x',t=\frac{3\pi}{2\Omega};x,0\right) = \sqrt{\frac{\Omega}{2\pi i}}\exp i\Omega\,x'x\,. \tag{6.47}$$

The propagator is applied to $\psi = \exp(ic^2t_1)\phi(\vec{x},t_1)$, where t_1 denotes the time after the first laser pulse. The new wave function is then rewritten in momentum space which will be needed later on. These two steps can be carried out immediately by means of the following equation:

$$\sqrt{\frac{\Omega}{2\pi i}}\int\exp ipx\exp i\Omega xx'dx = (i\Omega)^{-1/2}\int\exp i\frac{pp'}{\Omega}(2\pi)^{-1/2}\exp ip'x'dp'\,. \tag{6.48}$$

The left hand side represents the propagation of a plane wave and the right hand side which is found via the coordinate transformation $\Omega x = p'$, is the solution written as a superposition of plane waves. Furthermore, it needs to be considered that the angular frequencies of the harmonic potentials are not equal for the three dimensions. It will turn out that the angular frequency for the z direction Ω_z is different from the ones for the x and the y direction Ω_{xy}. The harmonic potentials therefore have to be turned on at different times. This means that the parts of the wave function which correspond to the dynamics of the x and the y direction propagate longer (with $A_1 = 0$) until the harmonic potential is turned on. To consider the dynamics of the three directions separately, it must be possible to separate the wave function according to $\psi(\vec{p}_0) = \psi(p_x)\psi(p_y)\psi(p_z)$. This can be done since—in order to enable recollisions—the vector potential will be chosen as in Sec. 4.2 such that the integral $\int_{-\infty}^{\infty}A_1 d\varphi$ vanishes [see Eqs. (4.21)]. Then, the mixed term p_xp_z in Eq. (6.39) does not occur after the first laser pulse anymore. With Eq. (6.48), the wave function in momentum

space after the application of the harmonic potential is found[2]:

$$\tilde{\psi}(\vec{p}\,') = (2\pi i)^{-3/2}(\Omega_{xy}^2\Omega_z)^{-1/2}\exp i\left[\frac{p_x p_x' + p_y p_y'}{\Omega_{xy}} + \frac{p_z p_z'}{\Omega_z}\right.$$
$$\left. -\frac{1}{2}\left(\vec{p}_0^{\,2}t_1 + (p_x^2+p_y^2)\frac{t_d}{2}\right) - \frac{1}{2\omega c^2}\left(1+\frac{p_z}{c}+\frac{p_z^2}{c^2}-\frac{\vec{p}_0^{\,2}}{2c^2}\right)\int_{-\infty}^{\infty} A_1^2\, d\varphi\right]. \quad (6.49)$$

The harmonic potential for the z direction acts longer by the time $t_d = 3\pi(1/\Omega_z - 1/\Omega_{xy})/2$. The potential for the x and the y direction is therefore turned on later by $t_d/2$ and will be turned off early by the same period of time [see Eq. (6.52, later on)].

To arrive at the wave function of the returning electron ϕ_r, the solutions ϕ_- of the electrons in the counterpropagating laser field [see Eq. (6.39)] have to be superimposed according to the momentum distribution (6.49):

$$\phi_r(\vec{x},t) = \exp\left[-ic^2\left(t_1+\frac{3\pi}{2\Omega_z}+t\right)\right]\int \tilde{\psi}(\vec{p}\,',t)[\exp(ic^2t)\phi_-(\vec{p}\,')]d^3p'\,. \quad (6.50)$$

Note that according to Eq. (6.45), the time duration of the whole process needs to be considered in the phase factor to get back to the relativistic wave function of the Klein-Gordon equation. Now, t denotes the time from the beginning of the final process where the electron is driven back. The wave function $\phi_-(\vec{p}\,')$ contains a mixed term $p_x'p_z'$ which complicates the integration. However, for the interesting time when the electron recollides, the integrals can be reduced to three one-dimensional ones. The expression which contains the mixed term can be approximated in the following way:

$$\frac{p_x}{\omega c}\left(1+\frac{p_z}{c}\right)\int A_2\, d\varphi \approx \frac{p_x}{\omega c}\int A_2\, d\varphi\,. \quad (6.51)$$

To enable recollisions, the integral over the vector potential of the second pulse A_2 has to vanish [see again Eqs. (4.21)]. The integral is therefore small during the recollision process and it is sufficient to consider only the leading order term. The mixed term is smaller by a factor of p_z/c. The following expression is then found for the wave function at the time of recollision:

$$\phi_r(\vec{x},t) = (2\pi i)^{-3/2}(\Omega_{xy}^2\Omega_z)^{-1/2}\exp i\left[-c^2\left(t_1+\frac{3\pi}{2\Omega_z}+t\right)\right.$$
$$\left. -\frac{1}{2}\left(\vec{p}_0^{\,2}t_1 + (p_x^2+p_y^2)\frac{t_d}{2}\right) - \frac{1}{2\omega c^2}\left(1+\frac{p_z}{c}+\frac{p_z^2}{c^2}-\frac{\vec{p}_0^{\,2}}{2c^2}\right)\int_{-\infty}^{\infty} A_1^2\, d\varphi\right]$$
$$\times\int (2\pi)^{-3/2}\exp i\left[\vec{p}\,'\cdot\vec{x} - \frac{1}{2}\left(\vec{p}\,'^2 t + (p_x'^2+p_y'^2)\frac{t_d}{2}\right) + \frac{p_x'}{\omega c}\int A_2\, d\varphi\right.$$
$$\left. -\frac{1}{2\omega c^2}\left(1-\frac{p_z'}{c}+\frac{p_z'^2}{c^2}-\frac{\vec{p}\,'^2}{2c^2}\right)\int A_2^2\, d\varphi\right]\exp i\left(\frac{p_x p_x' + p_y p_y'}{\Omega_{xy}} + \frac{p_z p_z'}{\Omega_z}\right)d^3p'\,. \quad (6.52)$$

[2]Since the harmonic potentials do not end at the same times, this wave function contains different times for the different dimensions. This is not problem because the wave function can be considered for each dimension separately.

These Gaussian integrals can be carried out and the following result is found:

$$\begin{aligned}
\phi_r(\vec{x},t) &= (2\pi)^{-3/2}(-i)(\alpha_{xy}^2\alpha_z\Omega_{xy}^2\Omega_z)^{-1/2}\exp i\left[-c^2\left(\alpha_z^{(1)}+\frac{3\pi}{2\Omega_z}+\alpha_z\right)\right] \\
&\times\exp i\left[\frac{\left(x+\frac{1}{\omega c}\int A_2 d\varphi\right)^2}{2\alpha_{xy}}+\frac{y^2}{2\alpha_{xy}}+\frac{\left(z+\frac{1}{2\omega c^3}\int A_2^2 d\varphi\right)^2}{2\alpha_z}\right] \\
&\times\exp i\left[\frac{p_x}{\Omega_{xy}\alpha_{xy}}\left(x+\frac{1}{2\omega_{xy}c}\int A_2 d\varphi\right)+\frac{p_x^2}{2\Omega_{xy}}\left(\frac{1}{\Omega_{xy}\alpha_{xy}}-\Omega_{xy}\alpha_{xy}^{(1)}\right)\right] \\
&\times\exp i\left[\frac{p_y}{\Omega_{xy}\alpha_{xy}}y+\frac{p_y^2}{2\Omega_{xy}}\left(\frac{1}{\Omega_{xy}\alpha_{xy}}-\Omega_{xy}\alpha_{xy}^{(1)}\right)\right] \\
&\times\exp i\left[\frac{p_z}{\Omega_z\alpha_z}\left(z+\frac{1}{2\omega_z c^3}\int A_2^2 d\varphi\right)-\frac{p_z}{2\omega_z c^3}\int_{-\infty}^{\infty}A_1^2 d\varphi+\frac{p_z^2}{2\Omega_z}\left(\frac{1}{\Omega_z\alpha_z}-\Omega_z\alpha_z^{(1)}\right)\right], \\
\alpha_{xy}^{(1)} &\equiv t_1-\frac{1}{2\omega c^4}\int_{-\infty}^{\infty}A_1^2 d\varphi+\frac{t_d}{2}, \quad \alpha_z^{(1)}\equiv t_1+\frac{1}{2\omega c^4}\int_{-\infty}^{\infty}A_1^2 d\varphi, \\
\alpha_{xy} &\equiv t-\frac{1}{2\omega c^4}\int A_2^2 d\varphi+\frac{t_d}{2}, \quad \alpha_z\equiv t+\frac{1}{2\omega c^4}\int A_2^2 d\varphi .
\end{aligned} \tag{6.53}$$

6.2.2 Gaussian superposition

The result of the previous section can now be employed to construct a localized Gaussian wave packet. With Eq. (1.33), the following wave function is found:

$$\begin{aligned}
\Phi(\vec{x},t) &= \pi^{-3/4}(-i)(\alpha_x\alpha_y\alpha_z\Omega_{xy}^2\Omega_z)^{-1/2}\exp i\left[-c^2\left(\alpha_z^{(1)}+\frac{3\pi}{2\Omega_z}+\alpha_z\right)\right] \\
&\times\frac{\exp i\frac{\left(x+\frac{1}{\omega c}\int A_2 d\varphi\right)^2}{2\alpha_{xy}}}{\sqrt{\Delta p^{-1}-i\Delta p\frac{1}{\Omega_{xy}}\left(\frac{1}{\Omega_{xy}\alpha_{xy}}-\Omega_{xy}\alpha_{xy}^{(1)}\right)}}\exp-\frac{\frac{\Delta p}{2}\left[\frac{1}{\Omega_{xy}\alpha_{xy}}\left(x+\frac{1}{\omega c}\int A_2 d\varphi\right)\right]^2}{\Delta p^{-1}-i\Delta p\frac{1}{\Omega_{xy}}\left(\frac{1}{\Omega_{xy}\alpha_{xy}}-\Omega_{xy}\alpha_{xy}^{(1)}\right)} \\
&\times\frac{\exp i\frac{y^2}{2\alpha_{xy}}}{\sqrt{\Delta p^{-1}-i\Delta p\frac{1}{\Omega_{xy}}\left(\frac{1}{\Omega_{xy}\alpha_{xy}}-\Omega_{xy}\alpha_{xy}^{(1)}\right)}}\exp-\frac{\frac{\Delta p}{2}\left[\frac{y}{\Omega_{xy}\alpha_{xy}}\right]^2}{\Delta p^{-1}-i\Delta p\frac{1}{\Omega_{xy}}\left(\frac{1}{\Omega_{xy}\alpha_{xy}}-\Omega_{xy}\alpha_{xy}^{(1)}\right)} \\
&\times\frac{\exp i\frac{\left(z+\frac{1}{2\omega c^3}\int A_2^2 d\varphi\right)^2}{2\alpha_z}}{\sqrt{\Delta p^{-1}-i\Delta p\frac{1}{\Omega_z}\left(\frac{1}{\Omega_z\alpha_z}-\Omega_z\alpha_z^{(1)}\right)}} \\
&\qquad\times\exp-\frac{\frac{\Delta p}{2}\left[\frac{1}{\Omega_z\alpha_z}\left(z+\frac{1}{2\omega c^3}\int A_2^2 d\varphi\right)-\frac{1}{2\omega c^3}\int_{-\infty}^{\infty}A_1^2 d\varphi\right]^2}{\Delta p^{-1}-i\Delta p\frac{1}{\Omega_z}\left(\frac{1}{\Omega_z\alpha_z}-\Omega_z\alpha_z^{(1)}\right)} .
\end{aligned} \tag{6.54}$$

The charge distribution for a Klein-Gordon wave function is given by Eq. (2.50) which can be calculated by means of Eq. (1.34):

$$\begin{aligned}
\Phi(\vec{x},t) &= -|\phi|^2 \mathrm{Im}\frac{\dot{\Phi}}{\Phi c^2} = -|\Phi|^2 \mathrm{Im}\frac{d}{dt}\left(\frac{\ln\Phi}{c^2}\right) = \frac{1+\frac{1}{2c^4}A_2^2}{\sqrt{\pi}^3 \Delta w_{xy}^2 \Delta w_z} \\
&\quad \times \exp - \left[\frac{\left(x+\frac{1}{\omega c}\int A_2 d\varphi\right)^2 + y^2}{\Delta w_{xy}^2} + \frac{\left(z+\frac{1}{2\omega c^3}\int A_2^2 d\varphi - \frac{\Omega_z \alpha_z}{2\omega c^3}\int_{-\infty}^{\infty} A_1^2 d\varphi\right)^2}{\Delta w_z^2} \right] . \\
\Delta w_{xy} &\equiv \sqrt{\Delta p^{-2}(\Omega_{xy}\alpha_{xy})^2 + \Delta p^2 \left(1-\Omega_{xy}^2 \alpha_{xy}\alpha_{xy}^{(1)}\right)^2 \Omega_{xy}^{-2}} , \\
\Delta w_z &\equiv \sqrt{\Delta p^{-2}(\Omega_z \alpha_z)^2 + \Delta p^2 \left(1-\Omega_z^2 \alpha_z \alpha_z^{(1)}\right)^2 \Omega_z^{-2}} .
\end{aligned} \tag{6.55}$$

This rather simple result is obtained with the following approximation:

$$-\mathrm{Im}\frac{d}{dt}\left(\frac{\ln\phi}{c^2}\right) \approx 1 + \frac{1}{2c^4}A_2^2 . \tag{6.56}$$

Further terms are much smaller compared to the leading term in Eq. (6.56). To see this, consider the terms which follow from the density in the z direction Φ_z, i.e. from the last two lines in Eq. (6.54):

$$\begin{aligned}
&-\mathrm{Im}\frac{d}{dt}\left(\frac{\ln\phi_z}{c^2}\right) = \left[\frac{\Omega_z\alpha_z^{(1)}}{2\Delta w_z^2 c^2} + \frac{1}{2\alpha_z^2 c^2}\left(1-\frac{\Delta p^2}{\Delta w_z^2 \Omega_z^2}\right)\left(z+\frac{1}{2\omega c^3}\int A_2^2 d\varphi\right)^2\right] \\
&\times\left(1+\frac{1}{2c^4}A_2^2\right) + \left[-\frac{1}{\alpha_z c} + \frac{\Delta p^2}{\Delta w_z^2 \Omega_z c}\left(\frac{1}{\Omega_z\alpha_z} - \Omega_z\alpha_z^{(1)}\right)\right]\left(z+\frac{1}{2\omega c^3}\int A_2^2 d\varphi\right)\frac{1}{2c^4}A_2^2 \\
&\qquad - \frac{\Delta p^2}{4\Delta w_z^2 \Omega_z c^2}\left(\frac{1}{\Omega_z\alpha_z} - \Omega_z\alpha_z^{(1)}\right)\left(z+\frac{1}{2\omega c^3}\int A_2^2 d\varphi\right)^2 \frac{\Delta\dot{w}_z}{\Delta w_z} .
\end{aligned} \tag{6.57}$$

Due to the Gaussian distribution of the charge density (6.55), the terms $(z+\int A_2^2/(2\omega c^3)d\varphi)$ are of the order Δw_z. The wave packet reaches the minimal value $\Delta w_z = \Delta p^{-1}$ for $\Omega_z\alpha_z = \Omega_z\alpha_z^{(1)} = 1$. Thus, the parameter Ω_z will be chosen correspondingly and the terms $\Omega_z\alpha_z \approx \Omega_z\alpha_z^{(1)}$ are of the order one.

To analyze the magnitude of the term $1/(\Omega_z\alpha_z) - \Omega_z\alpha_z^{(1)}$, it is first expanded about $\alpha_z = \alpha_z^{(1)}$. The evolution of α_z is then considered to linear order in t to arrive at

$$\frac{1}{\Omega_z\alpha_z} - \Omega_z\alpha_z^{(1)} \approx \left(1+\frac{1}{2c^4}A_2^2\right)\frac{t-t_1}{\alpha_z^{(1)}} \sim \frac{\Delta w_z}{\alpha_z^{(1)} c} . \tag{6.58}$$

The maximum time difference $t-t_1$ is only the time the wave packet needs to pass a fixed point. The width of the wave packet in the z direction is given by $\Delta w_z/\gamma$, i.e., it is Lorentz contracted by $\gamma = 1 + A_2^2/(2c^4)$. This is seen if the dependence on z of the Gaussian in the charge density is expanded according to $(z+\int A_2^2/(2\omega c^3)d\varphi) \approx z\gamma$. Since the velocity of the electron is of the order of c, the time needed for the electron to pass is given by[3] $\Delta w_z/(\gamma c)$. Note that the linearizations needed for this argument have sufficient accuracy since the refocused wave packet is very small compared to the

[3]Here, it is explicitely seen that the wave packet it Lorentz contracted by the γ-factor.

wave length of the driving laser field and consequently, the time the wave packet needs to pass a certain point is small, too.

With these order of magnitude estimates, the terms on the right hand side of Eq. (6.57) are shown to be of the order

$$-\operatorname{Im}\frac{d}{dt}\left(\frac{\ln\phi_z}{c^2}\right) \sim \left[\frac{\Delta p^2}{2c^2}+\frac{1}{2c^2}\left(\Omega_z^2-\Delta p^2\right)\right]\left(1+\frac{1}{2c^4}A_2^2\right) + \left[-\frac{\Omega_z}{c\Delta p}+\frac{\Delta p^2}{c^2}\right]\frac{1}{2c^4}A_2^2-\frac{\Delta p}{4c^3}\frac{\Delta\dot{w}_z}{\Delta w_z}\,. \quad (6.59)$$

The relative deviation of the width $\Delta\dot{w}_z/\Delta w$ is a number smaller than one, in particular because the wave packet reaches a minimum at the instant of recollision. Ω_z is a number smaller than the optical laser frequency ω which—for visible light—is much smaller than one. In all, it is seen that the terms of Eq. (6.59) are strongly suppressed at least by a factor c with respect to the leading term given by Eq. (6.56). This analysis has been carried out for the terms corresponding to the density in the z direction. However, the same procedure can be carried out for the remaining terms to show that they are negligible.

Refocused recollisions

It has been shown in Chapter 5.2 that freely spreading wave packets refocus after applying the harmonic potential for a certain time. The time of minimal width has been shown to be reached when the time after the application of the harmonic potential t equals the spreading time t_1 before the potential is applied. Further conditions have been found stating that the product of the angular frequency and the duration of the harmonic potential is given by $\Omega t_C = 3\pi/2$, and second, that $\Omega t_1 = 1$.

The refocusing condition for the laser-driven wave packet is similar. From Eq. (6.54) it is read off that Δw_{xy} and Δw_z reduce to the initial width Δp^{-1} for

$$\Omega_{xy}\alpha_{xy}^{(1)} = \Omega_{xy}\alpha_{xy} = 1\,, \quad (6.60a)$$

$$\Omega_z\alpha_z^{(1)} = \Omega_z\alpha_z = 1\,. \quad (6.60b)$$

Since the expressions $\alpha_{xz}^{(1)}$ and $\alpha_z^{(1)}$ are different [see Eq. (6.53)], the harmonic potentials, i.e. Ω_z and Ω_{xy}, are not equally strong and harmonic potentials have to be turned on for different periods of time. In the derivation, the time difference has been denoted by t_d (see Sec. 6.2.1) which can be determined, now:

$$\begin{aligned} t_d &= \frac{3\pi}{2}\left(\frac{1}{\Omega_z}-\frac{1}{\Omega_{xy}}\right) = \frac{3\pi}{2}\left(\alpha_z^{(1)}-\alpha_{xy}^{(1)}\right)\,, \\ \Rightarrow t_d &= \frac{\frac{3\pi}{2\omega c^4}\int_{-\infty}^{\infty}A_1^2 d\varphi}{1+\frac{3\pi}{4}}\,. \end{aligned} \quad (6.61)$$

From the probability density (6.54), it is seen that recollisions occur at the instant of maximal refocusing if the following recollision conditions are fulfilled:

$$\int_{-\infty}^{\infty}A_1^2 d\varphi_1 = \int A_2^2 d\varphi\,, \quad (6.62a)$$

$$\int A_2 d\varphi = 0\,. \quad (6.62b)$$

These conditions are identical to the ones of the previous recollision models [compare the probability densities (4.20) and (6.33)]. This suggests that the same vector potentials (6.7) for the two laser pulses can be chosen again:

$$A_1(\varphi) \propto \begin{cases} \cos\varphi \cdot \cos^2(\varphi/l) & |\varphi/l| \leq \pi/2 \\ 0 & |\varphi/l| > \pi/2 \end{cases}, \tag{6.63a}$$

$$A_2(\varphi) = \sqrt{2}\, A_1(\varphi)\,, \text{ where } l = 4, 6, 8, \ldots\,. \tag{6.63b}$$

However, it needs to be made sure, that the conditions for maximal refocusing (6.60) are not violated when the recollision conditions (6.62) are fulfilled. If Eq. (6.62a) is inserted into Eqs. (6.60) one finds the condition $t = t_1$. As in the case of magnetic refocusing, this can be achieved despite the different intensities of the two counterpropagating laser pulses if the second pulse is delayed by $\Delta t = \pi l/(2\omega)$ [see Eq. (6.27)]. This result has been derived in Sec. 6.1.2 (*Laser timing*).

In all, it is shown that the three dimensional wave packet refocuses and with the choice of the vector potentials (6.63), it recollides with maximal energy.

6.2.3 Restrictions of ponderomotive refocusing with laser beams

It has been shown in Sec. 5.2.3 how harmonic potentials can be realized with laser beams. However, there are restriction on the oscillator strength which need to be considered.

First, the dynamics must be nonrelativistic for several reasons. If the inertia of the electron increases for high velocities, the effective motion in the ponderomotive potential will become inharmonic which would spoil the mechanism of refocusing. Furthermore, the dynamics in the x, y and z direction would couple because the γ-factor depends on the velocity components of each direction. Therefore, the wave packet could not be refocused independently in the three directions as required.

Another restriction is that the spatial extension of the electron dynamics remains within the range where the ponderomotive potential is linear. It will be seen that these limitations restrict the laser intensity of the refocusing beam to an upper and lower bound.

To keep the dynamics nonrelativistic, the quick oscillations in the laser field need to be slow enough. From Eq. (5.15b) it is seen that the vector potential is restricted to values $A^0/c^2 \lesssim 0.1$ to keep the maximal velocity below 10% of the speed of light. From the ponderomotive potential (5.24), the angular frequencies of the oscillations in the harmonic potential are found to be

$$\Omega_{x,y,z} = \frac{A^0_{x,y,z}}{\sqrt{2}\Delta w_{x,y,z} c}\,, \tag{6.64a}$$

$$\Rightarrow \Omega_{x,y,z} \lesssim \frac{10}{\Delta w_{x,y,z}}\,. \tag{6.64b}$$

If the laser beam is focused to the order of the theoretical limit of the laser wave length ($\Delta w_{x,y,z} \approx 15000$ a.u.) then the maximal angular frequency is $\Omega_m \approx 6.6 \times 10^{-4}$ for the laser wave length of 800 nm.

The amplitude of an oscillation in a harmonic potential p_0/Ω [see e.g. Eq. (5.4b)] depends on the initial momentum. With the notion that a wave packet can be described by an ensemble of classical particles, the maximum extension of a wave packet,

spreading in the harmonic potential, can be estimated with the initial momentum of the order of the wave packet width in momentum space Δp. The initial spatial extension Δw is much smaller and does not need to be considered in this estimate. In order to keep nonlinear terms of the ponderomotive potential small [compare the electric laser field (5.22)], such that the dominating linear terms are always at least by a factor of 10 stronger than the next terms of third order, the amplitude has to fulfill the condition

$$\left(\frac{\Delta p}{\Omega_{x,y,z}}\right)^2 \lesssim 0.1\Delta w_{x,y,z}^2 \,. \tag{6.65}$$

With the relation (6.64b), a minimum for the vector potential is found which depends on the initial momentum width of the wave packet:

$$\frac{1}{c^2}A_{x,y,z}^0 \gtrsim \sqrt{20}\frac{\Delta p}{c} \,. \tag{6.66}$$

For initial widths of $\Delta p = 1$ a.u., one finds $A^0/c^2 \gtrsim 0.03$, which is only by a factor of roughly three smaller than the highest value allowed.

Since $\Omega_z < \Omega_x$ [see Eq. (6.61)], one finds the following two conditions which follow from $\Omega_z \alpha(1) = \Omega_{xy}\alpha_{xy}(1)$, Eq. (6.64a) and the two restrictions (6.64b) and (6.66):

$$\frac{1}{\Omega_z} = t_1 + \frac{1}{2\omega c^4}\int_{-\infty}^{\infty} A_1^2 d\varphi \lesssim \frac{\Delta w_z}{\sqrt{10}\Delta p} \,, \tag{6.67a}$$

$$\frac{1}{\Omega_{xy}} = t_1 + \left(\frac{\frac{3\pi}{4}-1}{\frac{3\pi}{4}+1}\right)\frac{1}{2\omega c^4}\int_{-\infty}^{\infty} A_1^2 d\varphi \gtrsim \frac{\Delta w_{xy}}{10} \,. \tag{6.67b}$$

In principle, the first condition can always be fulfilled by adapting Δw_z, whereas the right hand side of the second condition cannot be arbitrarily small since Δw_{xy} has to be greater than the laser wave length. However, the left hand side is not limited because the time t_1 can always be increased, i.e., one only has to wait for some time t_d after the electron has been separated by the first pulse before the refocusing pulse is applied.

To further analyze this result, consider the laser pulses defined in Eqs. (6.63) which is the same pulse as depicted in Fig. 6.2 of Sec. 6.1.3. The following integral can be evaluated:

$$\int_{-\infty}^{\infty} A_1^2 d\varphi = \frac{3\pi l}{16}(A_1^0)^2 \,, \tag{6.68}$$

where A_1^0 is the maximal vector potential of the first laser pulse. The time t_1 can be calculated from the proper time τ according to $t_1 - \int_{-\infty}^{\infty} A_1^2/(2\omega c^4)d\varphi = \tau = \varphi/\omega$. This relation has been derived in Sec. 2.2.3 [see Eqs. (2.64), (2.66) and (2.67)]. With Eq. (6.68), one then finds

$$t_1 = t_d + \frac{\pi l}{\omega}\left(1 + \frac{3}{32c^4}(A_1^0)^2\right) \,. \tag{6.69}$$

If the maximum vector potential is expressed by the γ-factor at the instant of recollision $\gamma_m = 1 + (A_1^0)^2/(c^4)$, the following results are obtained:

$$\frac{1}{\Omega_z} = t_d + \frac{\pi a}{\omega}\left[1 + \frac{3}{16}(\gamma_m - 1)\right] \,, \tag{6.70a}$$

$$\frac{1}{\Omega_{xy}} = t_d + \frac{\pi a}{\omega}\left[1 + \frac{9\pi}{16(4+3\pi)}(\gamma_m - 1)\right] \,. \tag{6.70b}$$

For $\omega = 0.057$ which corresponds to the laser wave length of 800 nm and with $l = 6$ for a few cycle pulse, this reduces to

$$\frac{1}{\Omega_z} = t_d + 331 + 62(\gamma_m - 1) \lesssim \frac{w_z}{\sqrt{10}\Delta p}\,, \tag{6.71a}$$

$$\frac{1}{\Omega_{xy}} = t_d + 331 + 44(\gamma_m - 1) \gtrsim \frac{w_{xy}}{10}\,. \tag{6.71b}$$

Remember, the smallest values which can be chosen for $\Delta w_{x,y,z}$ are of the order of 15000 a.u. Now, the shortest time required to initiate refocusing which complies with these conditions can be determined. The duration of the refocusing pulse is given by $t_C = 3\pi/(2\Omega_z)$ (see Sec. 5.2.2) which is determined by t_d and γ_m. With Eq. (6.71b), i.e. $1/\Omega_{xy} \gtrsim 1500$, the time t_d can be eliminated and one finds

$$t_C \gtrsim 7000 + 85\gamma_m\,. \tag{6.72}$$

This means that the duration of the refocusing pulse increases linearly with the recollision energy. The required time doubles for $\gamma_m \approx 80$.

6.2.4 Results

To calculate the reaction probability, the current density is need for the short time of recollision. Since the wave packet is refocused, this period is only a small fraction of one atomic unit. Thus, the wave packet shape can be considered to be constant for the time of interest. The charge density (6.55) then reduces to the simple form:

$$\rho(\vec{x},t) = \frac{\Delta p^3}{\sqrt{\pi}^3}\left(1 + \frac{1}{2c^4}A_2^2\right)\exp -\Delta p^2 y^2$$
$$\times \exp -\Delta p^2\left[\left(x + \frac{1}{\omega c}\int A_2 d\varphi\right)^2 + \left[z + \frac{1}{2\omega c^3}\left(\int A_2^2 d\varphi - \int_{-\infty}^{\infty} A_1^2 d\varphi\right)\right]^2\right]. \tag{6.73}$$

This result can be further simplified if the integrals are linearly expanded about the time and the location of recollision:

$$\rho(\vec{x},t) = \frac{\Delta p^3}{\sqrt{\pi}^3}\left(1 + \frac{1}{2c^4}A_2^2\right)\exp -\Delta p^2 y^2$$
$$\times \exp -\Delta p^2\left[\left(x + \frac{1}{c^2}A_2(c(t-t_0)+z)\right)^2 + \left[\left(1 + \frac{1}{2c^4}A_2^2\right)z + \frac{1}{2c^4}A_2^2 c(t-t_0)\right]^2\right]. \tag{6.74}$$

Here, t_0 denotes the instant when the maximum of the wave packet recollides. The motion of the maximum is found by equating the exponent to zero. One then finds:

$$x_m(t) = -\frac{\frac{1}{c^2}A_2}{1 + \frac{1}{2c^4}A_2^2}c(t-t_0)\,, \quad z_m(t) = -\frac{\frac{1}{2c^4}A_2^2}{1 + \frac{1}{2c^4}A_2^2}c(t-t_0)\,. \tag{6.75}$$

With this result, the charge density can be rewritten with new coordinates ($\tilde{x}$, $\tilde{z}$) which represent the position with respect to the maximum:

$$\rho(\vec{x},t) = \frac{\Delta p^3}{\sqrt{\pi}^3}\gamma_m \exp -\Delta p^2\left[\left(\tilde{x} + \frac{1}{c^2}A_2\tilde{z}\right)^2 + y^2 + \gamma_m^2\tilde{z}^2\right], \tag{6.76a}$$

$$\tilde{x} \equiv x + \frac{\frac{1}{c^2}A_2}{\gamma_m}c(t-t_0)\,, \quad \tilde{z} \equiv z + \frac{\frac{1}{2c^4}A_2^2}{\gamma_m}c(t-t_0)\,, \quad \gamma_m = 1 + \frac{1}{2c^4}A_2^2\,. \tag{6.76b}$$

To find the widths $\Delta w_\pm$ of this wave packet in the x-z plane and its orientation, the eigenvalues of the quadratic form in the exponent have to be determined. This quadratic form has the same structure as the one in Eq. (2.20), i.e., the previous results can be employed:

$$\Delta w_\pm = \lambda_\pm^{-1/2}\,, \quad \lambda_\pm = \Delta p^2 \left(\frac{1+\gamma_m^2}{2} \pm \frac{1-\gamma_m^2}{2} \sqrt{1 + \frac{4\frac{1}{c^4}A_2^2}{(\gamma_m^2-1)^2}} \right)\,, \tag{6.77a}$$

$$\tan\alpha = \frac{\frac{1}{c^2}A_2}{\frac{\lambda_-}{\Delta p^2} - 1}\,. \tag{6.77b}$$

The orientation is characterized by the rotation angle α by which the old coordinate system needs to be turned about the y axis such that the quadratic form is diagonal. For relativistic recollision energies $\gamma_m > 10$, these results simplify because the square root in Eq. (6.77a) can be approximated by one. Then, the following result is found:

$$\Delta w_+ = \Delta p^{-1}\,, \quad \Delta w_- = (\gamma_m \Delta p)^{-1}\,, \quad \tan\alpha = \frac{\frac{1}{c^2}A_2}{\gamma_m^2 - 1}\,. \tag{6.78}$$

This means that the wave packet has its initial widths Δp^{-1} whereas it is Lorentz-contracted in the direction of motion by the γ-factor.

Now, the absolute value of the current density is obtained by multiplying the charge density by the velocity which can be derived from Eq. (6.76b). This yields the following expression:

$$\begin{aligned} j(\vec{x},t) = {} & \frac{\Delta p^3}{\sqrt{\pi}^3} \frac{1}{c} A_2 \sqrt{1 + \frac{1}{4c^4}A_2^2} \\ & \times \exp -\Delta p^2 \left[\left(x + \frac{1}{c^2}A_2(ct+z) \right)^2 + y^2 + \left[\left(1 + \frac{1}{2c^4}A_2^2 \right) z + \frac{1}{2c^4}A_2^2 ct \right]^2 \right]\,. \end{aligned} \tag{6.79}$$

The reaction rate of collisions with the nucleus at the origin is given by $\dot{N} = \sigma \cdot j(0,t)$, where σ is the total cross section of some recollision reaction. This expression can be integrated and the following surprisingly simple result for the total reaction probability is obtained:

$$N = \frac{\sigma}{\pi} \Delta p^2\,. \tag{6.80}$$

This is exactly the same yield as for a colliding Gaussian wave packet with the initial, spatial widths of Δp^{-1} [see Eq. (6.36)], i.e., the reaction probability is equal to the one of a nonspreading wave packet keeping its initial widths.

For strongly refocused wave packets, slight deviations of the electron trajectory caused by the electron spin in strong laser fields may be important. As already stated for the scheme with magnetic refocusing, spin effects can be eliminated with a proper alignment of the spins [72].

If this scheme is applied to a gas sample, the same problems occur as for magnetic refocusing. The time needed to initiate refocusing is long such that the electrons are influenced by the Coulomb forces of the charged particles. The order of magnitude estimate for singly charged particles of Sec. 6.1.3 [see Eq. (6.38)] yields a deflection of 8 a.u. for the gas density of $10^{15}\mathrm{cm}^{-3}$ with $t_C = 8000$ a.u. [compare Eq. (6.72)] Furthermore, the distance a proton travels due to its initial thermal energy at room

temperature has been found to be of the same order. It is clear, that these processes limit the reasonable minimal wave packet widths of refocused recollisions in a gas sample.

Summary

In the present work, it has been shown how the dispersive relativistic dynamics of electrons in intense laser fields can be described analytically and how wave packets can be manipulated to enable effective, relativistic recollisions.

The basis for describing laser-driven wave packets was given in the first chapter, where the methods have been established. An analytical approach to phase-space averaging has been developed which allows to represent relativistic wave packets in classical terms. This intuitive method is suitable to describe the spreading dynamics of wave packets. Intrinsic quantum effects such as tunneling or interferences cannot be described in this way, but those effects are often of minor importance as for the applications discussed in this thesis. For cases where classical, analytical solutions are not available, this approach can be implemented numerically to describe wave packets with little computational effort. For each time in question, a limited number of coefficients—21 for the most general case—need to be fixed by solving the classical equations of motion for different initial conditions. In order to find the probability density, a three dimensional integral then needs to be solved numerically. Furthermore, an analytical quantum mechanical wave packet analysis was shown to be feasible for complex solutions of wave equations with constant modulus.

In Chapter 2, this quantum approach was employed to describe free electrons driven by a plane laser wave with arbitrary pulse shape. First, the system was analyzed by solving the Schrödinger equation for nonrelativistic laser intensities. The analysis takes magnetic field effects into account, as the calculation goes beyond the dipole approximation. Simple formulas for the orientation and deformation of laser-driven Gaussian wave packets have been established. In a second calculation, relativistic Volkov solutions have been superimposed to yield the probability density of relativistically driven electrons. As a result, rather simple expressions have been found which allow to extract relativistic effects like Lorentz contraction and time dilation.

The electron dynamics in standing laser waves was analyzed in Chapter 3, where configurations of linear and circular laser polarization were considered. As opposed to propagating laser fields, those setups enable recollisions up to relativistic energies. In the nonrelativistic regime, analytical solutions for classical particles and quantum mechanical wave packets have been found for both configurations, where the wave packet maxima were shown to move on classical trajectories. In this energy regime, both configurations yield similar results for the electron dynamics. For relativistic parameters, the classical equations of motion could be solved for some times of interest allowing for an analysis of the long-term behavior. A quantum mechanical calculation for the weakly relativistic regime was carried out for the case of linear laser polarization revealing some interesting relativistic effects. A fully relativistic wave packet analysis was carried out by means of the analytical phase-space averaging method of Chapter 1.

It turned out that the circular laser polarization is much more stable for high energies than the configuration of linear polarization in which the wave packet is strongly stretched in the laser propagation direction. Furthermore, it has been shown for the circular polarization that due to time dilation, spreading is more and more suppressed for increasing laser intensities.

The novel scheme of two consecutive counterpropagating laser pulses introduced in Chapter 4 enables relativistic recollisions at the highest electron energy accessible in propagating laser fields. The recollision energies in the other schemes with positronium [25] and standing laser fields [27, 19] have been shown to be smaller for some given laser intensity. Due to low repetition rates for currently available high-energy laser systems, the luminosities are rather small compared to conventional accelerators. Correspondingly, probabilities for particle reactions are also small. However, the process of bremsstrahlung with photon energies of the order of 100 MeV was shown to be observable for recollisions of electrons with their parent cesium atoms.

The general problem of wave packet spreading inhibiting effective recollisions has been addressed in Chapter 5, where it was demonstrated that spreading can be reversed. Two approaches—magnetic refocusing and refocusing by a harmonic potential—have been introduced. Magnetic refocusing by means of a short and strong magnetic pulse works for two dimensions, whereas the application of a harmonic potential allows for three-dimensional refocusing. It was shown that the effective potential of a laser beam in the TEM01 mode can be employed to provide the required harmonic potential. Furthermore, an analytic solution for a possible magnetic field configuration which is suitable for magnetic refocusing were given.

In Chapter 6, the concepts of refocusing were implemented in the recollision scheme with two consecutive laser pulses in which refocusing is initiated after the electron is separated. For magnetic refocusing, it was shown that efficient, relativistic recollisions in the range of 100 MeV could be obtained for magnetic field pulses of currently available intensities and pulse lengths. The efficiency could be further increased by means of stronger and shorter magnetic field pulses. However, the experimental realization of the strong and short magnetic fields needed, especially with the required symmetry of the induced electric fields, appears challenging today. The study of the scheme where refocusing is achieved by means of harmonic potentials shows that the wave packet contracts in all three dimensions. The reaction probability is found to be equal to that of a wave packet with the initial width, i.e., the effect of spreading is completely eliminated in this case. However, recollisions of such small wave packets require very high precision during the entire process and it is therefore a demanding task to implement this scheme experimentally.

In all, analytical methods based on either classical or quantum mechanics have been established. These can be applied to relativistic quantum systems to describe the dispersion of wave packets which, for instance, is important for determining reaction probabilities of laser-driven collisions. In this thesis, the methods have been applied to various systems where intuitive understanding of relativistic wave packet dynamics is gained from the analytical treatment. If problems cannot be solved analytically, the classical approach provides a fast numerical method to describe wave packet dynamics. Furthermore, a novel relativistic recollision scheme has been introduced allowing for the highest collision energies reachable in propagating laser fields. This scheme has then been combined with two different techniques of refocusing electron wave packets. As a result, two schemes are establish which give rise to efficient relativistic recollisions.

A future development would be to consider the deviations for strongly focused laser pulses from the plane wave approximation and the consequences for the recollision schemes considered here. This is important since the laser intensities depend on the size of the focus which—in order to reach maximal laser intensities—can become as small as the laser wave length. The analysis could be carried out by means of the numerical implementation of the classical method established in Sec. 1.1.

Furthermore, it would be interesting to see whether the classical, relativistic Monte-Carlo approach of phase-space averaging could be generalized to a semi-classical method by extending the classical particle states by some quantum mechanical phase information. This would allow for a description of interferences in laser-driven systems which is, for instance, relevant for scattering processes. The relativistic recollision schemes discussed here might then be applied to monitor the dynamics of atoms, molecules or clusters after the impact of an intense laser pulse by analyzing the electron probability distribution after the returning electrons have scattered.

Appendix A

Relativistic dynamics of laser-driven particles

A.1 Classical particles

The relativistic problem of a classical, charged particle in a propagating, plane laser field can be solved analytically. An elegant way is to employ the Hamilton-Jacobi method [103]. First, the Hamiltonian of a relativistic particle in an electromagnetic field, characterized by the scalar potential Φ and the vector potential $\vec{A}$, is needed. It is equal to the energy of the particle [104]. For an electron it reads

$$H = c\sqrt{\left(\vec{p} + \frac{1}{c}\vec{A}\right)^2 + c^2} + \Phi\,. \tag{A.1}$$

Then with the momentum $\vec{p} = \partial S/\partial\vec{x}$, the Hamilton-Jacobi equation is given by:

$$\frac{\partial S}{\partial t} + H\left(\vec{x}, \frac{\partial S}{\partial \vec{x}}, t\right) = 0\,, \tag{A.2}$$

where S is the generating function of the canonical transformation. For this Hamiltonian, this can be rewritten in an explicitly covariant form:

$$\left(\frac{\partial S}{\partial x^\mu} + \frac{1}{c}A_\mu\right)\left(\frac{\partial S}{\partial x_\mu} + \frac{1}{c}A^\mu\right) = c^2\,. \tag{A.3}$$

Since the vector potential is a plane wave, it depends only on the phase $\varphi = k_\nu x^\nu$, i.e. $A^\mu = A^\mu(k_\nu x^\nu)$. Furthermore, it is assumed to be given in the Lorentz gauge $\nabla_\mu A^\mu = k_\mu A^{\mu\prime} = 0$ and the vector potential is chosen in way that the condition $k_\mu A^\mu = 0$ is fulfilled.[1] The wave equation for the laser field reads $\Box A^\mu = 0$ in the Lorentz gauge and therefore one finds $k_\mu k^\mu = 0$. Now, the solution for a free particle with the four-momentum p_0^μ can be generalized by an additional term F which only depends on the laser phase:

$$S = -p_0^\mu x_\mu + F(k_\mu x^\mu)\,. \tag{A.4}$$

[1] If this condition does not hold, the vector potential can be transformed with the gauge transformation $A^\mu \to A^\mu + \nabla^\mu(f_\nu x^\nu) = A^\mu + f^\mu$. With a proper choice for the vector f^μ, one finds $k_\mu A^\mu + k_\mu f^\mu = 0$.

The vector potential is assumed to be zero, initially, and thus, the ansatz reduces to the solution of a free particle for which the scalar $p_{0\mu}p_0^\mu$ is equal to the rest energy c^2. In all, the ansatz yields the following solution to the Hamilton-Jacobi equation (A.3):

$$S = -p_0^\mu x_\mu + (p_0^\mu k_\mu)^{-1}\left(-\frac{1}{c}\int p_0^\mu A_\mu d\varphi + \frac{1}{2c^2}\int A_\mu A^\mu d\varphi\right). \tag{A.5}$$

According to the Hamilton-Jacobi formalism, the derivatives $\partial S/\partial\vec{p}_0$ are equal to some constants which can be chosen according to the initial conditions. Thus, the equations of motion are determined. The canonical momenta are obtained by differentiating S with respect to the coordinates x, y and z.

The equations of motion will now be deduced explicitly for the case that the laser wave is polarized in the x direction and propagates in the z direction. Then $p_0^\mu k_\mu$ reduces to $(p_0^0 - p_{z_0})\omega/c$ and it is convenient to consider $\kappa \equiv p_0^0 - p_{z_0}$ as an independent variable rather than p_{z_0}. Consequently, p_{z_0} needs to be replaced. From $p_{0\mu}p_0^\mu = c^2$, one finds

$$p_{z_0} = p_0^0 - \kappa\,, \quad p_0^0 = \frac{\kappa + (p_0^0 + p_{z_0})}{2} = \frac{\kappa}{2} + \frac{c^2 + p_{x_0}^2 + p_{y_0}^2}{2\kappa}\,. \tag{A.6}$$

Furthermore, the time t can be replaced by means of the laser phase $\varphi = \omega(t - z/c)$. Then the generating function (A.5) reduces to the following form:

$$S = p_{x_0}x + p_{y_0}y - \kappa z - c\left(\frac{\kappa}{2} + \frac{c^2 + p_{x_0}^2 + p_{y_0}^2}{2\kappa}\right)\frac{\varphi}{\omega} + \frac{1}{\omega\kappa}\left(\int p_{x_0}A d\varphi - \frac{1}{2c}\int A^2 d\varphi\right). \tag{A.7}$$

The derivatives of S with respect to the p_{x_0}, p_{y_0} and κ set equal to zero yields the following equations of motion:

$$x = \frac{p_{x_0}c}{\kappa\omega}\varphi - \frac{1}{\kappa\omega}\int A(\varphi)d\varphi\,, \tag{A.8a}$$

$$y = \frac{p_{y_0}c}{\kappa\omega}\varphi\,, \tag{A.8b}$$

$$z = \frac{c}{2\omega}\left(\frac{c^2 + p_{x_0}^2 + p_{y_0}^2}{\kappa^2} - 1\right)\varphi - \frac{p_{x_0}}{\kappa^2\omega}\int A(\varphi)d\varphi + \frac{1}{2\kappa^2\omega c}\int A^2(\varphi)d\varphi\,. \tag{A.8c}$$

Here, the initial position is chosen to be the origin, which is not a restriction as the problem is translationally invariant.

The energy of the electron is derived according to $E = H = -\partial S/\partial t$. Expressed by the relativistic γ-factor, it is given by

$$\gamma = \frac{\kappa}{2c} + \frac{c^2 + p_{x_0}^2 + p_{y_0}^2}{2\kappa c} - \frac{p_{x_0}}{\kappa c^2}A + \frac{1}{2\kappa c^3}A^2 = \frac{p_0^0}{c} - \frac{p_{x_0}}{(p_0^0 - p_{z_0})c^2}A + \frac{1}{2(p_0^0 - p_{z_0})c^3}A^2\,. \tag{A.9}$$

A.2 Quantum dynamics of spinless particles

The problem of a charged particle driven by a plane laser wave can also be solved quantum mechanically. The solutions are known as *Volkov* states. Here, the solution of the Klein-Gordon equation is derived describing the dynamics of spinless particles. Corresponding solutions to the Dirac equation are, e.g., found in [105].

The Klein-Gordon equation for an electron in an electromagnetic field is given by

$$\left(\frac{\partial}{\partial x^\mu}+\frac{1}{c}A_\mu\right)\left(\frac{\partial}{\partial x_\mu}+\frac{1}{c}A^\mu\right)\phi+c^2\phi=0\,. \tag{A.10}$$

With the same conditions as in the classical case, i.e., if the vector potential depends only on the laser phase φ and the Lorentz gauge holds ($k_\mu A^\mu=0$), this equation can be solved by the free solution which is extended by some function $F(\varphi)$:

$$\phi=(2\pi)^{-3/2}\exp i[-p_0^\mu x_\mu+F(\varphi)]\,. \tag{A.11}$$

The initial four-momentum is given by p_0^μ, because the vector potential is equal to zero at the beginning and the result reduces to the free solution. It turns out, that the exponent in (A.11) is proportional to the classical solution given in Eq. (A.5). The result reads:

$$\phi=(2\pi)^{-3/2}\exp i\left[-p_0^\mu x_\mu+(p_0^\mu k_\mu)^{-1}\left(-\frac{1}{c}\int p_0^\mu A_\mu d\varphi+\frac{1}{2c^2}\int A_\mu A^\mu d\varphi\right)\right]\,. \tag{A.12}$$

For the case, the laser fields propagate in the z direction and the vector potential points in the x direction, the result reduces to

$$\phi=(2\pi)^{-3/2}\exp i\left[-p_0^\mu x_\mu+(p_0^\mu k_\mu)^{-1}\left(\frac{p_{x_0}}{c}\int A\,d\varphi-\frac{1}{2c^2}\int A^2\,d\varphi\right)\right]\,. \tag{A.13}$$

Appendix B

Atomic units

For calculations, it is often useful to work with units being adapted to an appropriate scale. For example, in atomic physics, numbers can be related to typical values occurring in hydrogen atoms. Furthermore, it is helpful to drop some constants which keeps expressions somewhat simpler. Finally, with the corresponding table, the constants can be restored and any result can be converted to other units again.

Atomic units (a.u.) are obtained by employing Gaussian units to describe electrodynamics and additionally equating Planck's constant $\hbar$, the electron mass m and the unit charge e to unity. Since Gaussian units comprise three independent units (length, time and mass), the missing constants can be uniquely restored. With $\hbar = m = e = 1$, any expression given in atomic units is dimensionless, but any Gaussian unit can be expressed by a product of the factors $\hbar$, m and e. These combinations often have intuitive interpretations in terms of atomic properties. This means, with the simplification of dropping the three constants, any expression is transformed to an atomic scale. Table B.1 shows the relevant units, how they are expressed as a combination of the three constants, their interpretations and their values in regular SI units.

For example, to restore the units of some expression of energy given in atomic units which is proportional to some frequency ω, it has to be multiplied by $\hbar$ to get back to Gaussian units (energy $= [me^4/\hbar^2]$), because the units of ω are given by $[\omega] = \text{time}^{-1} = [me^4/\hbar^3]$. If an explicit number is given in atomic units, it can be multiplied by the corresponding entry of the right column to yield the result in SI units.[1]

The speed of light is connected to the fine structure constant via $\alpha = e^2/(\hbar c)$ (Gaussian units). Thus, in atomic units it is given by $c = 137.04$.

To convert the electric field E in atomic units of a sinusoidal laser wave to laser intensities I in SI units, the following formula is helpful:

$$I[\mathrm{W/cm^2}] = 3.51 \times 10^{16} E^2[\text{a.u.}]\,. \tag{B.1}$$

[1] To convert complete formulas from Gaussian to SI units, see [104].

unit	1 a.u. expressed by $\hbar$, m and e	interpretation	value in SI units
length	$\frac{\hbar^2}{me^2}$	radius of first Bohr orbit	5.292×10^{-11} m
time	$\frac{\hbar^3}{me^4}$	the time needed for $(2\pi)^{-1}$ revolutions of the electron in the first Bohr orbit	2.419×10^{-17} s
mass	m	mass of the electron	9.109×10^{-31} kg
charge	e	unit charge	1.602×10^{-19} C
velocity	$\frac{e^2}{\hbar}$	classical speed of the electron in the first Bohr orbit	2.188×10^{5} m/s
energy	$\frac{me^4}{\hbar^2}$	twice the ionization energy of hydrogen	27.21 eV
momentum	$\frac{me^2}{\hbar}$	classical momentum in the first Bohr orbit	1.993×10^{-24} kg m/s
angular momentum	$\hbar$	smallest quantum of angular momentum	1.055×10^{-34} Js
electric field (E)	$\frac{m^2e^5}{\hbar^4}$	nuclear field strength at the first Bohr orbit	5.142×10^{11} v/m
magnetic flux density (B)	$\frac{m^2e^5}{\hbar^4}$		1.715×10^{3} T

Table B.1: This table is helpful for dealing with atomic units (a.u.). In the first column, the units are listed. The constants $\hbar$, m and e can be restored by means of the second column which converts expressions from atomic to Gaussian units. The entries of the third column state the meaning of one atomic unit, while the corresponding values in SI units are listed in the fourth column.

Bibliography

[1] W. Becker et. al., Adv. At. Mol. Opt. Phys. **48**, 35 (2002)

[2] A. L'Huillier, K. Schäfer and K. Kulander, J. Phys. B **24**, 3315 (1991)

[3] D. Milosevic and F. Ehlotzky, Adv. At. Mol. Opt. Phys. **49**, 373 (2003)

[4] C. Joachain, M. Dörr and N. Kylstra, Adv. At. Mol. Opt. Phys. **42**, 225 (2000)

[5] M. Protopapas, C. H. Keitel and P. Knight, Rep. Prog. Phys. **60**, 389 (1997)

[6] Y. I. Salamin et. al., Phys. Rep. **427**, 41 (2006)

[7] F. Ehlotzky, A. Jaron and J. Kaminski, Phys. Rep. **297**, 63 (1998)

[8] F. H. M. Faisal and A. Becker, Laser Phys. **7**, 684 (1997)

[9] W. Becker et. al., Phys. Rev. A **56**, 645 (1997)

[10] C. Spielmann et. al., Science **278**, 661 (1997)

[11] Z. Chang et. al., Phys. Rev. Lett. **79**, 2967 (1997)

[12] M. Lein, Phys. Rev. Lett. **94**, 053004 (2005)

[13] S. Baker et. al., Science **312**, 424 (2006)

[14] H. Niikura et. al., Nature **421**, 826 (2003)

[15] J. Itatani et. al., Nature **432**, 867 (2004)

[16] P. M. Paul et. al., Science **292**, 1689 (2001)

[17] M. Hentschel et. al., Nature **414**, 509 (2001)

[18] A. Scrinzi et. al., J. Phys. B **39**, R1 (2006)

[19] N. Milosevic, P. B. Corkum and T. Brabec, Phys. Rev. Lett. **92**, 013002 (2004)

[20] K. Z. Hatsagortsyan, C. Müller and C. H. Keitel, Phys. Rev. D **74**, 074017 (2006)

[21] R. Fischer, A. Staudt and C. H. Keitel, Comp. Phys. Com. **157**, 139 (2004)

[22] G. R. Mocken and C. H. Keitel, J. Phys. B **37**, L275 (2004)

[23] C. C. Chirila et. al., Phys. Rev. Lett. **93**, 243603 (2004)

[24] R. Fischer, M. Lein and C. H. Keitel, Phys. Rev. Lett. **97**, 143901 (2006)

[25] B. Henrich, K. Z. Hatsagortsyan, C. H. Keitel, Phys. Rev. Lett. **93**, 013601 (2004)

[26] K. Z. Hatsagortsyan, C. Müller and C. H. Keitel, Europhys. Lett. **76**, 29 (2006)

[27] N. Kylstra et. al., Phys. Rev. Lett. **85**, 1835 (2000)

[28] V. D. Taranukhin, J. Opt. Soc. Am. B **19**, 1132 (2002)

[29] J. de Aldana and L. Roso, J. Opt. Soc. Am. B **19**, 1467 (2002)

[30] M. Klaiber, K. Z. Hatsagortsyan and C. H. Keitel, **74**, 051803(R) (2006)

[31] G. Mourou, C. Barty and M. Perry, Phys. Today **51**, 22 (1998)

[32] S. Bahk et. al., Opt. Lett. **29**, 2837 (2004)

[33] T. E. Cowan et. al., Nucl. Instrum. Methods Phys. Res. A **455**, 130 (2000)

[34] K. Nakashima, H. Takabe, Phys. Plasmas **9**, 1505 (2002)

[35] S. S. Bulanov, Phys. Rev. E. **69**, 036408 (2004)

[36] P. Golovinski, M. Dolgopolov and V. Khlebostroev, J. Nonlinear Opt. Phys. & Mater. **5**, 139 (1996)

[37] K. W. D. Ledingham et. al., Phys. Rev. Lett. **84**, 899 (2000)

[38] T. E. Cowan et. al., Phys. Rev. Lett. **84**, 903 (2000)

[39] G. A. Mourou, T. Tajima and S. V. Bulanov, Rev. Mod. Phys. **78**, 309 (2006)

[40] S. P. Hatchett, Phys. Plasmas **5**, 2076 (2000)

[41] M. Allen et. al., Phys. Rev. Lett. **93**, 265004 (2004)

[42] A. Maksimchuk et. al., Phys. Rev. Lett. **84**, 4108 (2000)

[43] H. Schwoerer et. al., Nature **439**, 445 (2006)

[44] A. Modena et. al., Nature **377**, 606 (1995)

[45] A. Pukhov and J. Meyer-ter-Vehn, Appl. Phys. B **74**, 355 (2002)

[46] J. Faure et. al., Nature **431**, 541 (2004)

[47] W. P. Leemans et. al., Nature Phys. **2**, 696 (2006)

[48] T. Ditmire et. al., Nature **398**, 489 (1999)

[49] T. J. Bürvenich, J. Evers and C. H. Keitel, Phys. Rev. C **74**, 044601 (2006)

[50] M. Kress et. al., Nature Phys. **2**, 327 (2006)

[51] H. Witte et. al., Opt. Expr. **13**, 4903 (2005)

[52] D. Strickland and G. Mourou, Opt. Commun. **56**, 219 (1985)

[53] A. Dubeis et. al., Opt. Commun. **88**, 437 (1992)

[54] T. Tajima and G. Mourou, Phys. Rev. ST AB **5**, 031301 (2002)

[55] A. Tarasevitch et. al., Phys. Rev. Lett. **98**, 103902 (2007)

[56] S. Gordienco et. al., Phys. Rev. Lett. **94**, 103903 (2005)

[57] N. J. Kylstra, A. M. Ermolaev and C. J. Joachain, J. Phys. B **30**, L449 (1997)

[58] U. W. Rathe et. al., J. Phys. B **30**, L531 (1997)

[59] U. W. Rathe, P. Sanders and P. L. Knight, Parallel Comput. **25**, 525 (1999)

[60] J. W. Braun, Q. Su, R. Grobe, Phys. Rev. A **59**, 604 (1999)

[61] G. R. Mocken and C. H. Keitel, J. Comp. Phys. **199**, 558 (2004)

[62] Y. I. Salamin, G. R. Mocken and C. H. Keitel, Phys. Rev. ST AB **5**, 101301 (2002)

[63] A. D. Bandrauk and H. Z. Lu, Phys. Rev. A **73**, 013412 (2006)

[64] A. Staudt, J. Prager and C. H. Keitel, Europhys. Lett. **62**, 691 (2003)

[65] J. San Roman, L. Roso and H. Reiss, J. Phys. B **33**, 1869 (2000)

[66] J. San Roman, L. Plaja and L. Roso, Phys. Rev. A **64**, 063402 (2001)

[67] M. Verschl and C. H. Keitel, Laser Physics **15**, 529 (2005)

[68] M. Verschl and C. H. Keitel, Phys. Rev. ST AB **10**, 024001 (2007)

[69] M. Verschl and C. H. Keitel, J. Phys. B **40**, F69 (2007)

[70] M. Verschl and C. H. Keitel, Europhys. Lett **77**, 64004 (2007)

[71] M. W. Walser and C. H. Keitel, J. Phys. B **33**, L221 (2000)

[72] J. San Roman, L. Roso and L. Plaja, J. Phys. B **37**, 435 (2004)

[73] S.-I. Chu and R.Y. Yin, J. Opt. Soc. Am. B **4**, 720 (1987)

[74] G. A. Kyrala, J. Opt. Soc. Am. B **4**, 731 (1987)

[75] M. Gajda et. al., Phys. Rev. A **46**, 1638 (1992)

[76] C. H. Keitel, J. Phys. B **29**, L873 (1996)

[77] H. Schmitz, K. Bouke and H.-J. Kull, Phys. Rev. A **57**, 467 (1998)

[78] S. X. Hu and A. F. Starace, Phys. Rev. E **73**, 066502 (2006)

[79] J. G. Leopold and I. C. Percival, Phys. Rev. Lett. **41**, 944 (1978)

[80] J. G. Leopold and I. C. Percival, J. Phys. B **12**, 709 (1979)

[81] J. D. Bjørken and S. D. Drell, *Relativistic quantum mechanics* (McGraw Hill, New York, 1998)

[82] Y. I. Salamin, G. R. Mocken and C. H. Keitel, Phys. Rev. E **67**, 016501 (2003)

[83] X. M. Tong and S. I. Chu, Phys. Rev. A **58**, R2656 (1998)

[84] J. T. Mendonca, Phys. Rev. A **28**, 3592 (1984)

[85] Z.-M. Sheng et. al., Phys. Rev. Lett. **88**, 055004 (2002)

[86] H. Schwoerer et. al., Phys. Rev. Lett. **96**, 014802 (2006)

[87] http://www.clf.rl.ac.uk/Facilities/AstraWeb/AstraGeminiHome.htm

[88] Q. Su, B. A. Smetanko and R. Grobe, Opt. Expr. **2**, 277 (1998)

[89] Mathematica®5.2

[90] H. A. Bethe and E. E. Salpeter, *Quantum mechanics of one- and two-electron atoms* (Plenum Press, New York, 1977)

[91] H. W. Koch and J. W. Motz, Rev. Mod. Phys. **31**, 920 (1959)

[92] A. I. Achiezer and W. B. Berestetskii, *Quantum electrodynamics* (Interscience Publ., New York, 1965)

[93] B. Holstein, *Topics in advanced quantum mechanics* (Addison-Wesley, Redwood City, CA, 1992)

[94] J. L. Chaloupka and D. D. Meyerhofer, Phys. Rev. Lett. **83**, 4538 (1999)

[95] D. Leibfried et. al., Rev. Mod. Phys. **75**, 281 (2003)

[96] R. J. Cook, D.G. Shankland and A. L. Wells, Phys. Rev. A **31**, 564 (1985)

[97] Q. Kong et. al. Phys. Rev. E **69**, 056502 (2004)

[98] J. Eichler and H.-J. Eichler, *Laser* (Springer, Heidelberg, 2002)

[99] S. Takeyama, T. Osada and N. Miura, Physica B **346**, 576 (2004)

[100] Y. Matsuda, Rev. Sci. Instrum. **73**, 4288 (2002)

[101] C. Back et. al., Science **285**, 864 (1999)

[102] C. Back et. al., Phys. Rev. Lett. **81**, 3251 (1998)

[103] L. D. Landau and E. M. Lifschitz, *The classical theory of fields* (Pergamon Press, Oxford, 1971), p. 112

[104] J. D. Jackson, *Classical electrodynamics* (Wiley, New York, 1999)

[105] V. B. Berestetskii, E. M. Lifshitz and L. P. Pitaevskii *Quantum Electrodynamics* (Butterworth-Heinemann, Oxford, 2004), p. 148

Danksagung

Mein Dank gilt allen, die in irgendeiner Form zum Gelingen dieser Arbeit beigetragen haben. Insbesondere möchte ich mich bedanken bei

- Herrn Prof. Dr. Christoph H. Keitel für die Aufnahme am Institut, die Betreuung meiner Arbeit und die Möglichkeit eigene Ideen umsetzen zu können,
- Carsten Müller für hilfreiche Diskussionen und Anregungen,
- Peter Brunner für die Betreuung der Rechner,
- Lucia, Adriana, Carsten und Benedikt für das Korrekturlesen dieser Arbeit,
- David für seine bereitwillige Hilfe bei sprachlichen Angelegenheiten,
- all meinen Kollegen für die sehr angenehme Arbeitsatmosphäre,
- meinen Eltern für jegliche Unterstützung während meiner gesamten Ausbildung.